Thesis Report

Electric Aircraft Design Including an In-the-loop Propeller Design Model with Regenerative Mode

Frank Scholtens

Delft University of Technology

TU Delft Delft University of Technology

Challenge the future

Thesis Report

Electric Aircraft Design Including an In-the-loop Propeller Design Model with Regenerative Mode

by

Frank Scholtens 4359224

in partial fulfillment of the requirements for the degree of

Master of Science
in Aerospace Engineering

at the Delft University of Technology,

Tuesday 29th June, 2021
Delft

cover image taken from https://www.pipistrel-ca.com/alpha_electro.html, on 30-05-2020

TU Delft Delft University of Technology

Preface

This thesis research work about the research of regenerative aircraft design marks the end of my time at the faculty of Aerospace Engineering at Delft University of Technology.

The challenging times we are living in today ask for a drastic change in the way we live. Not only should we care more about the amount of fossil fuel used in the aviation industry, but also the environment as a whole. With this work, I hope that all-electric flight is a step closer to reality.

This work has been my greatest challenge so far, and not only because of the effect and time it took to complete the work, but also due to the corona-virus pandemic that started when I only started one month with my work. Although this definitely made my time working on this thesis not easier, I could always rely on some people. First of all, I would like to thank Tomas Sinnige and Maurice Hoogreef, my daily supervisors, for quickly adapting to the new situation and making sure I could still continue my work. But also my parents on which I could rely for good advice. And of course, also my roommates, who were also suddenly stuck at home and with whom I suddenly spend a lot more time than I anticipated when I started this thesis work.

F. Scholtens
Delft, June 2021

Abstract

With the increase in environmental awareness, the need for reducing the emission of (greenhouse-)gasses from the aviation industry has become more present. It is known that propellers can produce thrust more efficiently than jet engines. Moreover, when these propellers are powered by electric motors, using electric energy coming from batteries, no gasses or other particles are emitted at all during an aircraft mission. Therefore, the interest in the development of (full-)electric aircraft has increased in the past year. However, one major disadvantage is present when storing the energy in batteries. Only a very limited amount of energy can be stored per unit of weight, compared to the nowadays mostly used energy storage: kerosene. Therefore, for aircraft that require high amounts of energy, the battery can become very heavy.

To make the aircraft as energy efficient as possible, during the descent of the aircraft the excess energy available during this flight phase can be harvested. The idea is that this harvested energy reduces the mission energy requirement resulting in lighter aircraft, which is proven to be not always the case in this research. However, no research has been done yet on the combination of the initial sizing of an aircraft, combined with the potential energy harvesting, the regeneration mode, during the descent. Furthermore, no research has been done on in-the-loop propeller aircraft design for regenerative propulsion. Moreover, the operating conditions for the propulsive and regenerative case pose significantly different requirements on the propeller design. Therefore, during this research, it is investigated how the regenerative mode influences the aircraft sizing and propeller geometry when this regenerative mode is already taken into account during the initial sizing of the aircraft.

To do this, first an aircraft sizing tool, based on a modified conceptual aircraft design method, and a propeller analysis methods, based on the blade element momentum method, have been created and validated. This tool is able to perform the initial sizing of a full-electric aircraft, while also optimising a propeller geometry for the sized aircraft. With this tool, different descent strategies, propeller airfoils and mission types have been simulated to find their effect on the aircraft- and propeller design.

From the descent analysis, it is found that by flying a steep descent, with a descent angle of 8.2°, up to 1.5% of the mission energy can be regenerated for a mission with $75NM$ range. However, due to the large negative thrust during the descent, the propeller solidity also has to increase by up to 200%, compared to the baseline mission. This increased solidity has a negative effect on the propeller efficiency during the cruise, where the cruise efficiency can be up to 5 percentage point lower than the baseline mission cruise efficiency. Moreover, the steeper descent results in a longer cruise flight, while the cruise efficiency also reduces. This means that more energy is used during the cruise flight than can be regenerated during the descent. In turn, this results in that the aircraft becomes heavier when designed for steep, regenerating, descent strategies. To minimize the mission energy usage, it is found that a descent at minimum airframe drag should be performed, while also minimizing the descent angle. However, at these low descent angles, no energy regeneration is possible.

The increased solidity required for the steep descent strategies can be reduced by approximately 20% when reducing the propeller airfoil camber, as found from the propeller airfoil analysis. When the propeller geometry design is constrained by the descent, reducing the airfoil camber leads to the same generated negative thrust for a lower solidity. This lower solidity is also increasing the cruise and climb performance, resulting in lower aircraft mass for the reduced propeller airfoil camber, when the aircraft is designed for a steep descent. However, the mass weight of the aircraft is only a few percentage of the total aircraft mass.

From the design mission profile analysis, it was found that for some specific flight cases the regeneration mode does positively influence the aircraft weight when the regeneration mode is taken into account during the initial design of the aircraft. When flying airport flight patterns, the steeper descent can result in a shorter cruise phase (reduced length of the downwind leg), resulting in a shorter total range of the flight pattern mission. When the range is also reduced due to the steeper descent, the aircraft mission energy can be reduced by up to 7.7%, compared to the baseline mission. However, this reduced energy requirement is mainly due to the reduced range. This reduced range while using a steep descent can be the result of a flight pattern mission. Furthermore, when a steep descent is required by external factors, such as reduced ground noise exposure, the regenerative mode can regenerate up to 2.3% mission energy, compared to when the steep descent is performed with air-brakes, and thus no energy is regenerated. This results in that for the exact same mission profile, for a $75NM$ mission $2.3MJ$ (which is 2.9% mission energy) less energy is needed due to the regeneration.

Finally, a short 'trainer' mission is analysed, where the climb, cruise and descent phase are performed multiple times in a row on one full battery charge. This results in a propeller design more optimised for the climb and descent phase, however also for this mission type (where the traffic patterns are not used), the regenerative mode does increase the total mission energy compared to when a more shallow descent strategy is chosen.

Combing the three analyses, some final conclusions can be made. It is found that when the descent strategy can be freely chosen and the total aircraft range is fixed, it will always be more energy efficient to perform a shallow descent, at a low descent angle, at the minimum airframe drag speed, than to perform a steep descent in which energy can be regenerated. Furthermore, due to the steep descent, the in-the-loop propeller design shows that the solidity needs to increase to be able to produce the negative thrust. However, when a steep descent has to be performed, it is more beneficial to regenerate the excess energy than to dump this excess energy in the air using air-brakes. Similar, for a steep descent it might be more energy efficient to reduce the propeller airfoil camber, since the negative thrust that is produced during the steep descent is constraining the propeller solidity. The reduced airfoil camber reduces the solidity, causing an increase in cruise efficiency. Also, when due to the steeper descent also the cruise range can be shortened, shortening the total range, this results in a lower energy requirement of the aircraft. Thus, although the regenerative mode does not always reduce the mission energy requirement, for some specific mission it can be beneficial to use the regenerative mode to harvest energy while in-flight.

Contents

Preface iii

Abstract v

Nomenclature xi

1 Introduction 1
- 1.1 Previous Performed and State-of-the-Art Research . . . 2
  - 1.1.1 Recent Research on Regenerative Propellers . . . 3
  - 1.1.2 Recent Research on Electric Aircraft Design . . . 3
- 1.2 Research Objective . . . 4
- 1.3 Thesis Scope . . . 6

2 Theoretical Background 7
- 2.1 Theoretical Background . . . 7
  - 2.1.1 Aircraft Sizing . . . 7
  - 2.1.2 Propeller Analysis . . . 8
  - 2.1.3 Energy Harvesting . . . 10
- 2.2 Current Aircraft Design Models . . . 10
- 2.3 Propeller Operations . . . 11

3 Aircraft and Propeller Analysis Model 13
- 3.1 Aircraft Sizing Model . . . 14
  - 3.1.1 Constraint Analysis . . . 14
  - 3.1.2 Mission Analysis . . . 15
  - 3.1.3 Weight Estimation . . . 20
- 3.2 Propeller Performance Model . . . 21
  - 3.2.1 Analysis Model . . . 22
  - 3.2.2 Performance Data Acquisition . . . 23
  - 3.2.3 Response Surface Fit Model . . . 24
  - 3.2.4 Propeller Design and Optimisation . . . 25

4 Model Validation 29
- 4.1 Aircraft Sizing Model . . . 29
  - 4.1.1 Drag Polar Estimation . . . 33
  - 4.1.2 Reference Mission Profile . . . 36
  - 4.1.3 Reference Propeller . . . 37
  - 4.1.4 Mission Performance . . . 38
- 4.2 Propeller Performance Model . . . 46
- 4.3 Regenerative Flight Model . . . 49

5 Baseline Mission Definition **51**

6 Descent Strategy Analysis **55**
6.1 Simulation Case Studies . . . 55
6.1.1 Fixed Flight Speed, Variable Rate of Descent and Descent Angle . . . 56
6.1.2 Fixed Rate of Descent, Variable Flight Speed and Descent Angle . . . 56
6.1.3 Fixed Descent Angle, Variable Rate of Descent and Flight Speed . . . 57
6.2 Simulation Results . . . 57
6.2.1 Variable RPM, Fixed Pitch . . . 57
6.2.2 Variable RPM, Variable Pitch . . . 68
6.3 Discussion . . . 71
6.3.1 Optimal Descent Strategy . . . 72
6.3.2 Fixed Pitch versus Variable Pitch . . . 74
6.3.3 Propeller Geometry Optimisation . . . 76

7 Propeller Airfoil Camber Analysis **79**
7.1 Simulation Case Studies . . . 79
7.1.1 Airfoil Drag Polars . . . 80
7.2 Simulation Results . . . 80
7.2.1 Shallow descent . . . 81
7.2.2 Steep descent . . . 82
7.3 Discussion . . . 90

8 Design Mission Type Analysis **91**
8.1 Simulation Case Studies . . . 91
8.1.1 Final Descent Pattern Analysis . . . 91
8.1.2 Steep Descent Without Regeneration . . . 92
8.1.3 Short Mission Analysis . . . 93
8.2 Simulation Results . . . 94
8.2.1 Final Descent Pattern Analysis . . . 94
8.2.2 Steep Descent without Regeneration . . . 96
8.2.3 Short Mission Analysis . . . 97
8.3 Discussion . . . 101
8.3.1 Design Mission Profile . . . 102
8.3.2 Off-design Descent Performance . . . 102

9 Conclusion **107**

10 Recommendations **109**

Bibliography **111**

A Appendix A: Detailed Descent Analysis Results **115**
A.1 vR - Fixed Flight Speed . . . 116
A.2 vR - Fixed Rate of Descent . . . 119
A.3 vR - Fixed Descent Angle . . . 122
A.4 vRvP - Fixed Airspeed . . . 125
A.5 vRvP - Fixed Rate of Descent . . . 128
A.6 vRvP - Fixed Descent Angle . . . 131

B Appendix B: Detailed Propeller Analysis Results **135**
B.1 vR - Shallow Descent . . . 136
B.2 vR - Steep Descent . . . 139
B.3 vRvP - Shallow Descent . . . 142
B.4 vRvP - Steep Descent . . . 145

C Appendix C: Detailed Mission Analysis Results **149**
C.1 Final Traffic Pattern Descent . . . 150
C.2 Regen on vs. off . . . 153
C.3 Long vs. Short Mission . . . 156

D Appendix D: Simulation Results Using the New Optimisation Function **159**
D.1 Baseline Mission . . . 160
D.2 Steep Descent Mission . . . 161
D.3 Fixed Descent Angle, Reduced Flight Speed Descent . . . 162

Nomenclature

Abbreviations

AoA	Angle of Attack
BEM	Blade Element Momentum
CFD	Computational Fluid Dynamics
CST	Class Shape-Transformation
ISA	International Standard Atmosphere
MIL	Minimum Induced Loss
MTOW	Maximum Take Off Weight
OEI	One Engine Inoperative
OEM	Operational Empty Weight
PREE	Payload Range Energy Efficiency
RoD	Rate of Descent
RPM	Revolutions per Second
SE	Specific Energy
SoC	State of Charge
SP	Specific Power
SQP	Sequential Quadratic Programming
TLAR	Top Level Aircraft Requirement
TOM	Take Off Mass
vR	Variable RPM, Fixed Pitch Propeller
vRvP	Variable RPM, Variable Pitch Propeller

Roman symbols

A	Area $[m^2]$
AR	Aspect Ratio $[-]$
c	Chord Length $[m]$
c	Climb Descent $[m/s]$
C_D	3D Drag Coefficient $[-]$
C_d	2D Drag Coefficient $[-]$
C_L	3D Lift Coefficient $[-]$
C_l	2D Lift Coefficient $[-]$
C_P	Power Coefficient $[-]$
C_Q	Torque Coefficient $[-]$
C_T	Thrust Coefficient $[-]$
D	Drag $[N]$
E	Energy $[J]$
e	Oswald Factor $[-]$
e_v	Span Efficiency Factor $[-]$
J	Advance Ratio $[-]$
L	Lift $[N]$
M	Mass $[kg]$
N	Number of Blades $[-]$
P	Power $[W]$
P_c	Power Coefficient $[-]$
Q	Torque $[Nm]$
q	Dynamic Pressure $[N/m^2]$
R	Radius $[m]$
R	Range $[m]$
R	Resultant Force $[N]$
Re	Reynolds Number $[-]$
S	Surface Area $[m^2]$

T	Thrust $[N]$
T_c	Thrust Coefficient $[-]$
V	Velocity $[m/s]$
W	Weight $[N]$

Greek symbols

α	Angle of Attack $[rad]$
η	Efficiency [-]
Λ	Sweep $[rad]$
ρ	Air Density $[kg/m^3]$
σ	Propeller Solidity $[-]$
Θ	Aircraft Pitch Angle $[rad]$
Θ	Propeller Pitch Angle $[rad]$

Subscripts

∞	Free-stream Conditions
ax	Axial
bat	Battery
cl	Climb
cr	Cruise
de	Descent
eff	Effective
EM	Electrical Machine
f	fuselage
min	Minimum
n	nacelle
OEM	Operational Empty Mass
p	propulsive
r	Radial
s	Shaft
TO	Take Off
UC	undercarriage
w	Main Wing

1

Introduction

The increased awareness of the environment as seen in the past years asks for improved aircraft efficiency. This will result in the reduction of the emission of greenhouse gasses. However, to be able to drastically reduce the emission of greenhouse gasses during the flight, some large changes to the current aircraft designs are needed.

Currently, most commercial aircraft are propelled by kerosene burning jet engines [1]. These jet engines burn fuel to rapidly accelerate the air, which results in a thrust force. Although propulsion by propellers is known to be more efficient, due to the lower kinetic energy in the accelerated air that is lost for propeller propulsion compared to the jet engines [2]. Propellers are currently not widely used for large commercial aircraft, mainly due to the lower cruise speed a propeller aircraft can fly at, compared to aircraft that use jet engines. This results in longer flight times for propeller aircraft. On smaller, general aviation, aircraft more use is made of propellers, since the flight speed is of less importance for these aircraft. The fact that propellers are less mechanically complex makes that propeller aircraft are generally cheaper to design, fly and maintain [2]. The need to reduce the environmental impact of flying can encourage the change from jet engines to propeller driven aircraft, also for larger commercial aircraft as for instance in the new developments made by the engine manufacturers *CFM* and *GE* [1].

Furthermore, recent developments in battery technology have made it possible to use electric engines, instead of the conventional, fuel burning, engines to power the aircraft. The large benefit of these electric engines is that no (greenhouse-)gasses are emitted during the flight, which is beneficial for the environment. However, the storage of the energy for electric machines is still causing technological challenges. Battery technology is still in development and batteries can currently not store enough energy per kilogram to be able to be used for propulsive purposes on large scale aircraft.

For smaller aircraft batteries can now be used, in combination with an electric machine and a propeller to power the aircraft. Since the energy requirement is lower for these types of aircraft, all the energy can be stored in the battery, while the battery mass is not becoming too large. However, also on these aircraft the limited energy that can be stored in the batteries is still a limiting factor, which results in a low range and flight time for currently existing full-electric

[1] https://www.cfmaeroengines.com/press-articles/ge-aviation-and-safran-launch-advanced-technology-demonstration-program-for-sustainable-engines-extend-cfm-partnership-to2050/, taken on 25-06-2021.

aircraft [3]. Therefore, battery powered aircraft are still not widely seen and only a few full-electric aircraft are currently flying. Nonetheless, since it is expected that the battery technology will soon become mature enough for wide use within the aviation industry [4], several electric aircraft are now being designed and prototypes are being made [5]. Unfortunately, also for these aircraft, the range and flight time will be lower than for the currently conventional fuel burning aircraft. Therefore, new techniques are being explored to extend the range of a full-electric aircraft without increasing the energy requirement of the aircraft.

Since the working of the electric machines can easily be switched from a power delivering device to a power generating device, this can be used to charge the battery while in-flight [6, 7]. To do this, the propeller of the aircraft needs to work like a wind-turbine, so it has to deliver shaft power to the electric machine, which can then be used to charge the battery while in-flight. Since power is extracted from the air during this regenerative flight, the so-called 'regeneration mode' can only be used during flight phases where excess energy is available, which are the descent and landing phases. This regenerated energy is then expected to lead to a reduced energy requirement for the complete mission. This can result in a lower required battery mass, which might reduce the weight of the complete aircraft when the aircraft is designed for this reduced battery mass, or an increased range for the same aircraft design and mass.

Within this thesis work, the influence of the regenerative mode on the aircraft- and propeller design and the corresponding energy consumption of these new designs is researched. The aim is to find how the aircraft design and the propeller geometry are influenced by the regenerative mode when incorporated during the initial sizing of the aircraft. As mentioned, the regenerated energy can result in reduced energy requirement of the mission, resulting in a weight reduction of the sized aircraft.

To do this, an existing sizing tool for electric aircraft was expanded to include the regenerative flight phase and in-the-loop propeller design. First, a brief introduction and background around the topics of propeller and aircraft design are given in chapter 2. The models are described in chapter 3, and the validation of the models is shown in chapter 4. After the validation, a baseline mission is defined in chapter 5 from which the different analyses can be performed. The effect of the descent strategy on the aircraft sizing and propeller geometry is investigated and discussed in chapter 6. Furthermore, the propeller design is analysed in chapter 7, as well as the chosen design mission profile in chapter 8. Finally, conclusions are drawn and presented in chapter 9 and recommendation for future research are given in chapter 10.

1.1. Previous Performed and State-of-the-Art Research

Although currently no aircraft has been designed and built with the regenerative mode taken into account during the design phase, research related to in-flight energy regeneration has been performed both in the field of propeller aerodynamics, as well as in the field of aircraft design. Furthermore, one aircraft that is built as a full-electric general aviation aircraft has been retrofitted with a regenerative system, showing that it is feasible to use the in-flight energy regenerating system.

1.1.1. Recent Research on Regenerative Propellers

Both propellers and wind turbines have been thoroughly researched to maximise their performance [8–10]. However, research on a propeller that is being used as a wind turbine or a wind turbine being used as a propeller is done less frequent.

Recently, Sinnige et al. [11, 12] performed a wind-tunnel experiment where a (propulsive-)propeller has been placed in energy-harvesting conditions. This research has shown that it can both be theoretically calculated that propellers are able to regenerate power, as well as it has been experimentally shown. However, since the propellers are not designed to work in the regenerative mode, where the local angle of attack on the blade is negative, the efficiency during the regenerative operation is very low, about 10% harvesting efficiency. Furthermore, the numerical prediction model of the propeller in regenerative conditions does under-predict the amount of power and thrust on the propeller, compared to what is measured during the wind-tunnel experiment. Although it has been shown that it is possible to use propellers designed for thrust generation to harvest energy, it is also shown that the prediction of the performance is still challenging.

Based on the research of Sinnige et al. [11], a thesis work has created by van Neerven [13]. It was studied how a regenerating propeller should be designed for a complete aircraft mission, where the aircraft design is fixed and the propeller geometry is optimised for different cruise lengths. This shows that the most (relative) mission energy can be saved, compared to the non-regenerative mission, for a short mission. It was calculated that for short missions up to 4.1% energy can be saved for regenerative missions. It does make sense that the most relative energy is saved for the short cruise mission since the regenerative mode makes up a relatively longer part for this short cruise mission. Furthermore, during the design of the propeller, the aircraft design is not optimised for the regenerative propeller. Thus, the effect of the regenerative mode on the aircraft design is not investigated.

1.1.2. Recent Research on Electric Aircraft Design

Also on the aircraft design side, recently research has been performed. Existing aircraft design methods rely on conventional, fuel-based, aircraft which burn fuel throughout the mission and thus getting lighter. However, full-electric aircraft do not burn any fuel, and thus have a constant aircraft weight throughout the whole mission.

This results in that the conventional aircraft design methods, for instance, the design method by Torenbeek [14], cannot directly be used to design a full-electric aircraft. De Vries et al. [15] modified this design method, such that the method is also suitable to perform the initial sizing of an (hybrid-)electric aircraft. Instead of using the Bréguet range [16] equation and fuel-fractions to determine the range of the aircraft, and the corresponding fuel weight, the full aircraft mission is step-wise simulated, where the energy consumption per flight phase is calculated, from which the aircraft weight can be determined.

Currently, only one full-electric aircraft has been designed, build and certified, the *Pipistrel Velis*

Electro[2], which is a design iteration of the *Pipistrel Alpha Electro* aircraft, which was, in turn, the electrified version of the fuel-based version of this aircraft. This aircraft shows the potential uses cases of current existing full-electric aircraft, where this aircraft is designed as a trainer aircraft.

Besides the theoretical research that has been performed on regenerative flight, the regenerative mode has also already been shown to work on an actual full-electric aircraft. Erzen et al. [17] retrofitted the *Pipistrel Alpha Electro* with a propeller design for regeneration of energy to investigate the performance benefits when an aircraft is regenerating energy using an optimised propeller compared to a propeller that is designed for a conventional, non-regenerative, aircraft. From the experiment, it was found that using the propeller that is designed to regenerate energy during the descent phase, the aircraft can fly up to 27% more flight patterns. The optimised propeller for regenerative mode is shown in figure 1.1. First, on the left, the original cruise optimised propeller is shown, where it can be seen that the solidity of the propeller is relatively low, compared to the most right propeller. This most right propeller is the propeller optimised for regenerative flight and features a higher solidity. This indicates that a propeller designed with the regenerative mode in mind requires a larger solidity to be able to harvest energy while keeping the diameter of the propeller constant. Moreover, the camber at the root of the propeller blades has been reduced to be able to have higher regenerative performance.

The increased number of flight patterns flown with the optimised propeller for the specific flight pattern mission hints towards the benefits of the regenerative mode, even though the aircraft design is not designed with the regenerative mode in mind. It is therefore of interest to see for which flight missions the regenerative mode is indeed reducing the total mission energy requirement. Furthermore, it is of interest how the aircraft sizing and design would change when the regenerative mode would be incorporated during the initial sizing of the aircraft.

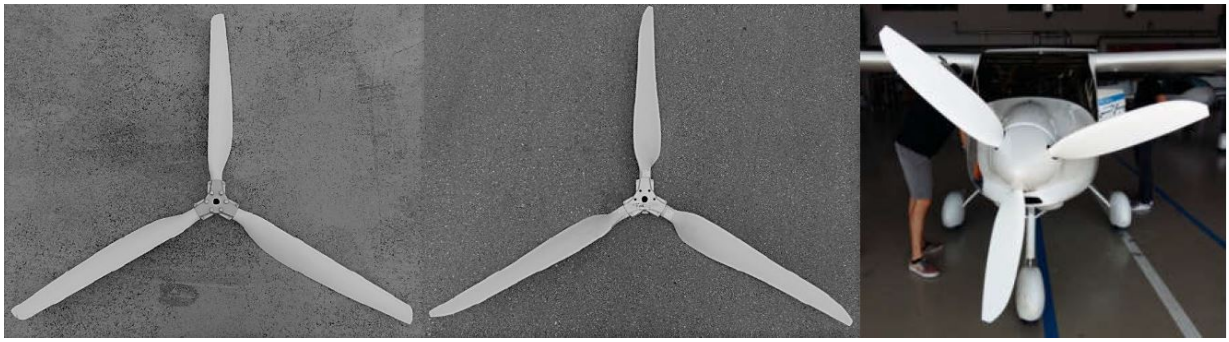

Figure 1.1: Propeller design for the Alpha Electro of Pipistrel, from left to right: AS-D, EA-001 and EA-002 [17].

1.2. Research Objective

In this chapter, a short introduction is given into the theoretical background and current research around the topic of regenerative aircraft and propeller design. Although research regarding regenerative propellers has been performed, both in a wind-tunnel experiment and during experimental flights, the combination of simultaneous aircraft design and (regenerative) propeller

[2] https://www.pipistrel-aircraft.com/aircraft/electric-flight/velis-electro-easa-tc/

design has not been conducted yet. Therefore, is it currently not known how the regenerative mode influences the propeller- and aircraft design when the regenerative mode is taken into account during the initial design of the aircraft. Furthermore, the possible reduction in mission energy requirement when an aircraft is designed with the regeneration mode is therefore also not known. This reduced mission energy can then lead to improved aircraft performance, resulting in longer possible cruise distance or endurance.

Moreover, usually the aircraft and propeller are designed separately. For the initial sizing of the aircraft, an assumed efficiency of the propeller is used for the different flight phases. However, due to the large differences in the operating condition of the propeller between the propulsive and regenerative mode, and therefore the large difference in optimal design for these two conditions, it is unknown how the propeller geometry should look like when designing an aircraft that is also able to fly in the regenerative mode. Therefore, not only the aircraft is designed during the sizing loop, but also an in-the-loop propeller design will be performed, such that the propeller will give the optimal performance (i.e. highest efficiency), both for the propulsive flight and the regenerative flight.

The current state-of-the-art research does not combine the aircraft design with propeller design for full electric aircraft, with the regenerative mode included. To research this topic, the following research objective has been formulated:

> The objective of this research project is to study the effects on mission energy and aircraft- and propeller design for the initial sizing of regenerative flight by creating an in-the-loop propeller design within the aircraft design process.

To reach this research objective, the following research question has been formulated:

> What is the effect of regenerative flight on the aircraft mission energy and aircraft design for small full-electric aircraft?

It is expected that the regenerative flight will harvest in-flight energy, resulting in that the battery will charge during this flight phase. This harvested energy will then cause that the overall mission energy usage will be reduced, resulting in either an extended range for a given aircraft, or an aircraft weight reduction when the aircraft is designed for a given range. To find out if this is true, the research question has been split up into three sub-questions:

1. How is the energy regeneration influenced by the chosen descent strategy and how does this influence the overall mission energy requirement and aircraft- and propeller design?
2. How does the in-the-loop propeller design influence the aircraft design and the mission energy requirement?
3. What is the influence of different mission types on the mission energy requirements?

1.3. Thesis Scope

During the research it is not feasible to research all details of the regenerative aircraft design, therefore the scope of the thesis is given to indicate which parts of the design will be taken into account, and more importantly, what is not taken into account during the research.

First, a full-electric sizing method is created, in which the mass distribution of the different components are estimated using statistical methods. Furthermore, as explained before, the propeller design is also added to this sizing method. However, this design is only based on its aerodynamic properties. The structural integrity, manufacturability and noise emissions are not taken into account during the design of the propeller.

For the regenerative model, only the energy generated by the propeller is influencing the design of the aircraft. Thus, how the produced in-flight energy changes the energy requirements for the mission, resulting in changing battery masses, which in turn can influence the weight of the other components. During the regenerative mode, the wake of the propeller changes with respect to the propulsive case. Since this wake slows down the local velocity of the air this can influence wings or control surfaces that are located in the wake of the regenerating propeller. The local effects of this wake on the lifting surfaces that are in this wake are not taken into account. So, for example, the change in the lift-to-drag ratio of the main wing due to the change in the wake is not included. Furthermore, the change in the wake can have an effect on the horizontal stabilizer of the aircraft, resulting in adverse stability of the aircraft. However, since the stability and control of the aircraft are not calculated in the sizing method, this effect is not taken into account during the sizing.

Finally, the variable pitch propeller does add complexity and weight to the propeller installation systems. However, for simplicity it is assumed that both the fixed pitch propellers and variable pitch propellers do have the same relations for the installation weight, meaning that the variable pitch propeller does not impose extra weight on the installation weight. Therefore, the aircraft with a variable pitch propeller will have a slight underestimation of the installation weight of the propeller system.

2

Theoretical Background

Before diving deep into the thesis work, first some theoretical background and an outline of the thesis is given. This will give an insight into the theoretical work that is already existing and the research work that is already been done around the topic of regenerative propellers, initial (full-)electric aircraft sizing methods and the integration of regenerative mode on electric aircraft. Furthermore, the research objectives for the thesis are given as well as the scope of the work that is being done.

2.1. Theoretical Background

To place the thesis work into perspective, and to give an idea on what theories and methods the thesis is based, a short theoretical background of the used theories and methods are given. First, the background of aircraft sizing methods is being presented, after which the propeller analysis methods are shown. Finally, some details around in-flight energy harvesting are given.

2.1.1. Aircraft Sizing

The first ever aircraft built, the Wright Flyer, was designed by trial and error [18]. The main purpose of this aircraft was to show that heavier-than-air flight would be a feasible method of transportation. Nowadays, it is not possible to just build an aircraft by trial and error anymore, due to the complex systems aircraft have become and the enormous amount of money involved in aircraft design [19]. Therefore, before building an aircraft, the design and performance of the aircraft are needed to be known. This will result that when the aircraft has been built, the aircraft will be able to perform the intended mission.

For the initial sizing and design of an aircraft, aircraft sizing methods have been developed that are able to predict the aircraft mass from only a few top level aircraft requirements ($TLARs$). Examples of these methods are the methods as created by, for example, Torenbeek [14], Raymer [20] or Roskam [21]. These methods are based on statistical analysis and equations, derived from already existing aircraft. Therefore, these methods work especially well when the aircraft that is to be designed has large similarities with already existing aircraft. For a new type of aircraft, such as full-electric aircraft, these methods are less suitable. Furthermore, as technology improves, the prescribed relations can become outdated due to, for instance, better materials and manufacturing techniques, improving the aircraft weight.

These methods give estimations of the aircraft mass, with a subdivision into the payload mass, fuel mass and operational empty mass (OEM). This is also known as the Class-I weight estimation. These weight estimations are the first step in the conceptual design of an aircraft. Using these estimations a first idea of the size and mass distribution of the aircraft is obtained.

For a more detailed design of the to be designed aircraft, the Class-II sizing is performed. During this design phase, the weight of the separate components are determined, as well as their location on the aircraft to determine the centre of gravity and subsequently the stability and controllability of the aircraft. This requires more knowledge about the different components however, such as the dimensions or aerodynamic performance of these components. Therefore, this analysis can only be performed when the conceptual design of the aircraft is already performed.

After the Class-II sizing is done, and an idea of the weight of all the separate components is created, the detailed design of the aircraft can be started. In this phase all the components are worked out in detail and the aircraft as a whole is designed.

These aircraft design methods were created when the demand for the reduction of greenhouse gasses was not significant yet. Therefore, these methods do not incorporate the use of alternative fuel sources, such as the energy stored in batteries or hydrogen. Thus, some modifications are needed to these design methods to make them suitable for the sizing of a full-electric aircraft, as will be explained in chapter 3.

2.1.2. Propeller Analysis

In the field of aerodynamic propeller analysis, numerous methods are available to compute the performance of a given propeller design. Some examples of these methods are: the Actuator Disk theory, Blade Element Momentum (BEM) Theory, Lifting Line Theory Or Computational Fluid Dynamics (CFD). Where the first mentioned model is the lowest fidelity analysis method, and the latter is the highest, most detailed, analysis method.

The first, and lowest fidelity, analysis model, the actuator disk theory as based on the work of Rankine and Froude [8, 22, 23], is able to predict the axial induction of the propeller for a given thrust setting, from which it can compute the power losses associated with the axial induction. Therefore, this theory is only useful for top level assumptions, when no details about the propeller design are known. The BEM theory does split the propeller blade up into separate elements, solving the local aerodynamic performance of the elements, after which the elements are integrated again to calculate the performance of the whole propeller [24, 25]. This does of course take more computational power than the actuator disk theory, but gives also more information on the propeller performance, such as the power required to produce thrust and the rotational speed of the propeller.

Figures 2.1 and 2.2 show a cross-section of a propeller blade, with the local forces on the cross-section indicated. Since both the propulsive and regenerative modes are considered, the propulsive mode of a propeller is associated with positive thrust, resulting from a positive local angle of attack, while in the regenerative mode the angle of attack is negative. This negative

angle of attack results in negative thrust and torque. This negative torque is then applied to the electric machine, resulting in in-flight power delivery to the battery.

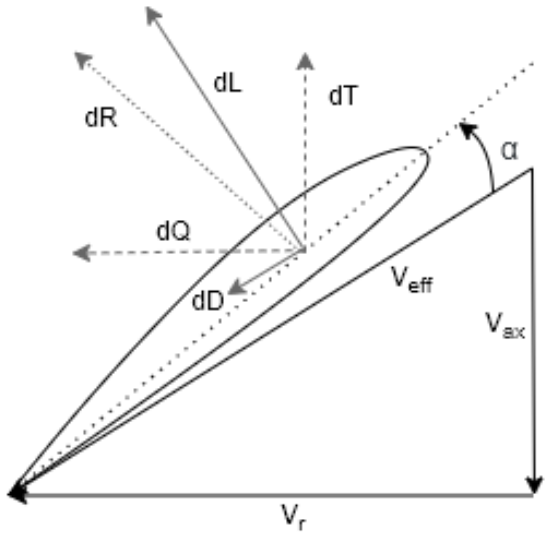

Figure 2.1: Loads on a blade section in propulsive mode.

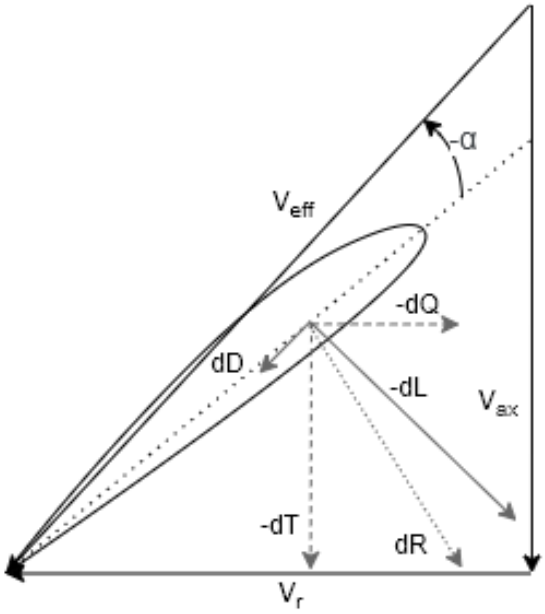

Figure 2.2: Loads on a blade section in regenerative mode.

For the regenerative part of the propeller analysis, a different definition of the propeller efficiency is used. During the propulsive part of the operations of the propeller, the ratio between the power added to the free-stream velocity and the shaft power is used to calculate the efficiency. For the regenerative case, the wind-power that passes through the propeller, compared to how much of this energy is converted by the propeller to rotational power is used. This results in two different efficiency definitions of the propeller for the two cases, as shown in equations (2.1) and (2.2).

$$\eta_{prop} = \frac{TV_\infty}{P_{shaft}} = \frac{C_T}{C_P} J \qquad (2.1)$$

$$\eta_{regen} = \frac{P_{shaft}}{qV_\infty A_{disk}} \qquad (2.2)$$

If also the influence of the wake of the propeller on the performance is taken into account, the lifting line theory can be used, this method does not only solve the local aerodynamic properties on the propeller blades, but does also take the propeller wake into account. This results in more information on the propeller performance, with also higher accuracy, but again at the cost of higher required computational power. The last method to find the propeller performance is to solve the aerodynamic properties using a CFD solver. This method calculates the whole aerodynamic field around the propeller, giving the most details about the flow field of the air around the propeller. However, the drawback of this method is that is very computationally expensive.

2.1.3. Energy Harvesting

This thesis work focuses on the in-flight regeneration of energy for a full-electric aircraft. However, excess energy must be available to perform this in-flight regeneration of energy. The energy of a flying aircraft that can be harvested consists of two main parts: the kinetic energy and the potential energy. For general aviation aircraft, the flight speed is usually relatively small, meaning that only a little of the kinetic energy can be used during the regeneration phase since this regeneration will slow down the aircraft even more. Thus, the most energy that can be regenerated comes from the potential energy. During the descent of a 'normal' aircraft, an aircraft without the regeneration mode, the power setting is reduced and a gentle descent is started. During this descent, the potential energy of the aircraft is converted to kinetic energy. To keep the airspeed during the descent at the desired level either the descent angle can be reduced or additional drag can be created, by for instance using the flaps of the aircraft.

For a regenerative aircraft, the excess (potential) energy that is present during the descent phase is not tried to be dissipated into the air, and thus removed from the aircraft system, but the excess energy is converted to electric energy and stored in the batteries. To do this the propeller of the aircraft is used as a wind turbine. However, wind turbine rotor geometries, made for energy production, have very different requirements than propellers designed for propulsive purposes. This results in that power harvesting rotors usually have large rotor diameters, with negatively cambered airfoils [26]. These contradicting design requirements for propulsive and regenerative cases can lead to differences in the propeller design compared to the case where only the propulsive condition is considered.

2.2. Current Aircraft Design Models

As stated before, the classical aircraft design methods, (e.g. Torenbeek [14]) are not able to perform the initial sizing of a full-electric aircraft. However, since they serve as a basis for design methods for full-electric, a short introduction to these methods is given.

The Class-I aircraft sizing method consists of two steps: the constraint analysis and the mission analysis. First, from the input parameters, a wing- and power loading diagram is created. Each constraint associated with the flight manoeuvres the aircraft is required to be able to perform is plotted in this diagram. After this is done, the feasible design phase is found and a design point is chosen. This design point consists of the weight-to-power ratio and the weight-to-wing-surface-area ratio.

Using this design point, and an initial guess on the aircraft weight, the installed power and the wing surface area can be determined. Using this information, the mission analysis can be performed. From the fact that fuel is burned during the flight, the weight fractions of each flight phase are determined, where the fractions represent how much of the fuel weight is used during the phase, and the total required fuel mass for the mission is determined. From the Bréguet equation, and the given flight conditions: the flight speed and altitude, the flight range of the aircraft can be determined. However, since a full-electric aircraft does not burn fuel during the flight, which reduced the aircraft weight, this relation cannot be used.

Finally, the operational empty mass (OEM) of the aircraft is estimated using statistical relations. Adding the weights of the payload, the OEM and the fuel weight, the total aircraft weight is determined, as shown in equation (2.3). This updated total aircraft weight is then used to update the initial guess on the installed power and wing area, which are used to perform the analysis again. After the aircraft weight has converged, the initial sizing loop is done.

$$W_{TO} = W_{payload} + W_{fuel} + W_{OEM} \tag{2.3}$$

For a more detailed weight breakdown of the aircraft, the Class-II weight estimation can be used. For this estimation, the OEM of the aircraft is split up into the different components of the aircraft, such as the wings, fuselage and engines. During this stage of the weight estimation also the snowball-effect of aircraft design becomes apparent. For instance, an increase in estimated engine weight results in an increase in the required wing surface area. This increased wing surface area is heavier, resulting in a higher thrust requirement, which in return results in a heavier engine weight again and the whole drive-train needs to increase in size. Therefore, an initial increase of $1kg$ in one component, can lead to a multiple kilogram increase of the complete aircraft design.

2.3. Propeller Operations

For the described aircraft sizing method, the propeller design is not taken into account. However, since the regenerative mode is expected to have a large influence on the propeller operating conditions, some background in the propeller operations is given. The geometry of the propeller blades consists of the chord-length distribution, as well as the span-wise twist distribution. Using this chord distribution, the solidity of the propeller can be determined, using equation (2.4)

$$\sigma = \frac{Nc}{\pi R} \tag{2.4}$$

From the calculated propeller blade geometry, in combination with the propeller characteristics, such as the propeller diameter, the number of blades and the airfoil, the performance of the propeller can be determined for each flight condition and propeller operating condition, where the operating conditions consist of the rotational speed of the propeller, the RPM, and the blade pitch setting.

Depending on the type of propeller, the RPM, the (collective) pitch or both the RPM and pitch can be varied during the flight. These settings will, in combination with the flight condition, determine the performance of the propeller, where the performance consists of the thrust delivered by the propeller and the shaft power that is needed to deliver this thrust. Or, in the regenerative mode, the power that is delivered to the shaft by the propeller.

The propeller with a variable RPM, but with a fixed pitch (vR) can only be varied in rotational speed to change the performance for a given flight condition. An example of such a propeller is

given in figure 2.3. To achieve this variation in RPM, either the engine needs to be able to work at different rotational speeds, or gearboxes are needed. Since electric engines are well known for their large operational RPM range while keeping a high efficiency [27], usually these engines can be directly connected to the propeller without gearboxes. The change in propeller RPM is then a direct effect of a change in the electric machine RPM. Therefore, it can be assumed that propellers driven by electric machines always have a variable RPM.

On the other end, a propeller with a fixed RPM, but with variable pitch is possible, as shown in figure 2.4. For these propellers, the rotational speed is kept constant, but the pitch is varied to determine the performance. This results in higher propeller efficiency for a larger operating range than the fixed pitch propeller [28]. The system to make the propeller blades able to vary the pitch setting in-flight does add weight and complexity.

Finally, a combination of the variable RPM and variable pitch ($vRvP$) is possible, where both the rotational speed and pitch settings of the blades can be adjusted. In this way, not only the operating conditions can be set to achieve the correct power and thrust setting, but the propeller efficiency can be maximised for this thrust setting.

Figure 2.3: Picture of a fixed pitch propeller[2].

Figure 2.4: Picture of a variable pitch propeller[3].

[2]taken from https://hartzellprop.com/how-do-fixed-pitch-propellers-work/, on 02-06-2020
[3]taken from https://www.wikiwand.com/en/Variable-pitch_propeller, on 02-06-2020

3

Aircraft and Propeller Analysis Model

In order to be able to answer the research question, to find the effect of regenerative flight on the aircraft mission energy and aircraft design for small full-electric aircraft, a tool is created in which different full-electric aircraft with regeneration mode can be modelled. After the validation of this tool, the results will give an insight into how differences in the top level aircraft requirements will influence the performance and design of the aircraft.

The tool that is chosen is an iterative Class-I aircraft sizing method, but with a detailed breakdown of the weight of the different components. The details of the aircraft sizing model are explained in section 3.1. This method consists of a constraint analysis and a mission analysis. The constraint analysis selects a design point of the aircraft such that the power-to-weight ratio is sufficient to perform predetermined flight manoeuvres, while the mission analysis sizes the aircraft such that enough (battery-)energy is present during the whole prescribed mission of the aircraft. Moreover, to this Class-I aircraft sizing also a propeller design method is added. This design method is performed before the mission analysis and will update the propeller design of the aircraft, to make sure the propeller is designed for the current estimated mass and thrust requirements of the aircraft. In this way, a matching propeller is designed for the specific sized aircraft. The propeller analysis and design methods are explained in section 3.2

Since the propeller design method is expected to be the most time-intensive part of the simulation, the amount of times a propeller have to be designed within the iteration loop is minimized. Therefore, for each propeller design, first the take off mass (TOM) is iterated until a consistent mass is found. After this is done, a new constraint analysis is performed and a new propeller is designed for the updated TOM and thrust requirements. This results in two iterations loops within the tool, as schematically shown in figure 3.1. The inner loop creates a consistent aircraft design for the currently designed propeller geometry, while the outer iteration loop will also design a matching propeller geometry for the current TOM and thrust requirements within the iteration. When both loops have converged to a

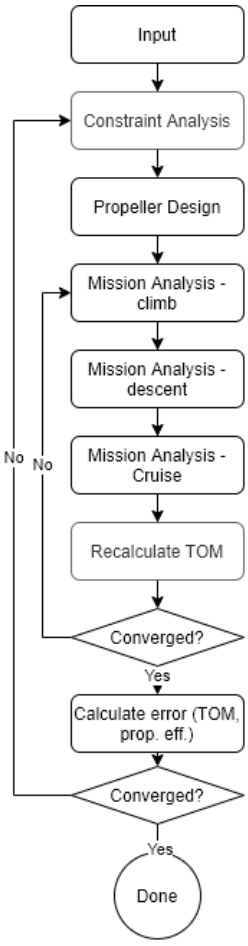

Figure 3.1: Schematic overview of the iterative process to size the aircraft.

consistent design, both the propeller and TOM of the aircraft are used for the performance analysis of the sized aircraft.

3.1. Aircraft Sizing Model

The tool that is used to analyse the performance for regenerative aircraft, is based on a method created by de Vries et al. [15]. This method is made to perform the initial sizing of hybrid-electric aircraft including aero-propulsive interaction models. Since in this analysis a full-electric aircraft with regeneration mode is considered, this tool serves as a good basis to extend, such that it is also usable for the analysis of full-electric aircraft with regeneration mode.

This preliminary sizing tool is based on the Class-I aircraft sizing method. Therefore, it is able to calculate the basic take off mass (TOM) of the aircraft given only a few basic input parameters, such as the aerodynamic properties from the drag polar, the design mission profile and propulsive performance throughout the mission. Also, the constraint manoeuvres are required, where each constraint indicates what the minimal performance of the manoeuvre should be. In this tool, analysis methods are added, such that also a first estimation on the breakdown of the operational empty mass (OEM) is created, which is the same breakdown as used for the Class-II weight estimation.

3.1.1. Constraint Analysis

From the constraint analysis, the design wing- and power loading are determined. To do this, for each flight manoeuvre the feasible combinations of the wing- and power loading are determined. Combining the feasible regions of each flight manoeuvre, the total feasible design space of the aircraft is found. For the design of the full-electric aircraft it is chosen to design the aircraft for maximum feasible wing loading, or in other words, minimum wing surface area.

The constraint analysis of the method as created by de Vries et al. [15] is used for this analysis, since the regenerative mode does not influence the constraint analysis. The constraint analysis creates a wing- and power loading diagram for each component of the drive-train separately. Within this wing- and power loading diagram the feasible design space is indicated. This space indicates where the aircraft has enough power to perform the given manoeuvres, and the wing surface is sufficiently large to perform the manoeuvres. The wing- and power loading diagram for each separate component will make sure that each component is sized according to its own power loading and none of the components are oversized with respect to the required power output of that component. An example of the power loading diagram for each component is given in figure 3.2. Here the wing- and power loading diagram is given for the shaft power where the constraints for stall speed, cruise speed and take off are indicated. The grey area shows the feasible design space, where the black dot is the selected design point of the to be sized aircraft.

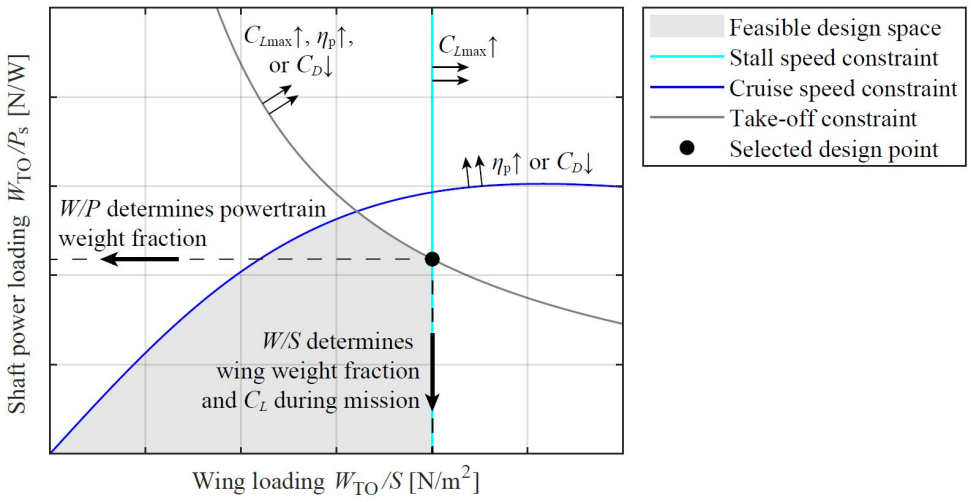

Figure 3.2: Indicative graph of the constraint diagram as created by the sizing loop [29].

Four constraints are analysed for the sizing of the full-electric aircraft with regenerative mode, where the minimal performance requirements the aircraft should be able to achieve is taken from the small-aircraft regulations, the CS-23 specifications [1].

From these constraint manoeuvres, the power loading diagram is created and the design point is determined. The constraints are the cruise-, landing-, take off- and rate of climb at sea level conditions. Since a single engine, single propeller aircraft is considered, no constraints with respect to one engine inoperative (OEI) are taken into account. In case of an engine failure the total power train is considered to be inoperative and no propulsive thrust can be produced anymore.

3.1.2. Mission Analysis

During the mission analysis each flight phase is separately analysed to determine the energy used during the respective flight phase. In contrast to the constraint analysis, the mission analysis needed to be updated to incorporate the regenerative flight mode in the analysis, compared to the method as provided by de Vries et al. [15].

For this analysis only the climb, cruise and descent phases are simulated for the flight mission. The loiter and diversion flight phases are not directly taken into account for the mission analyses, but a minimum state of charge of the battery is used to make sure enough reserve energy is left after the nominal mission to perform diversion or loiter actions, and the battery life is maximised by not discharging the battery completely for each mission. The take off and landing are also included in the mission energy, however the energy consumption during these two phases is taken from energy fractions. An overview of the aircraft mission is given in figure 3.3. The solid

[1] https://www.easa.europa.eu/certification-specifications/cs-23-normal-utility-aerobatic-and-commuter-aeroplanes

line indicates the nominal part of the mission, which includes the take off, climb, cruise, descent and landing phases. The dashed lines are indicated the reserve phases, which are not analysed in the mission analysis.

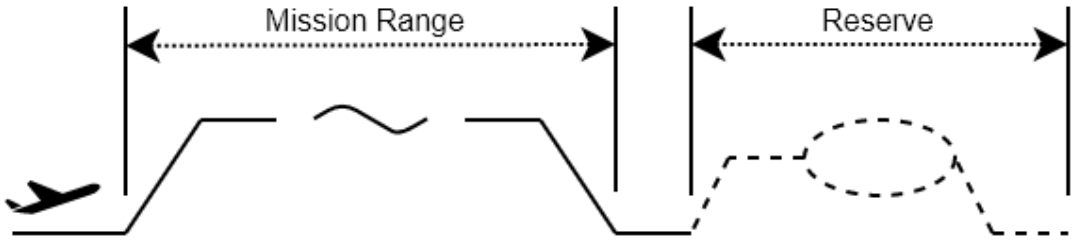

Figure 3.3: Schematic overview of the aircraft mission and the different flight phases

Climb

The first flight phase that is analysed is the climb phase. The climb phase of the mission starts directly after the take off of the aircraft, with the take off speed as the initial speed at an altitude of $0m$, i.e. the International Standard Atmosphere (ISA) sea level conditions. The climb phase ends when the desired cruise altitude and -speed are reached.

The original analysis method used a constant dM/dh climb, in which the aircraft both accelerates and climbs simultaneously to the desired climb and cruise speed. For small general aviation aircraft this is not a common method to perform the climb phase, as can for instance be seen in the flight manual of a full-electric aircraft: the *Pipistrel Alpha Electro* [2]. Most small aircraft will climb at a constant speed, after which it will accelerate to cruise speed once the cruise altitude is reached. Furthermore, since different aircraft input parameters are used for the performance mission analysis, this climb strategy means that each sized aircraft will have a slightly different climb phase. Since different climb strategies are not part of the analysis, the climb phase is standardised for each sized aircraft. The climb phase is changed to a constant climb angle climb while also maintaining a constant flight speed during this climb.

To perform this constant climb angle climb, first the aircraft accelerates to the optimal climb speed, the minimum power required speed, directly after take off, while maintaining a constant altitude equal to the take off altitude. After the climb speed is reached, the aircraft starts climbing at a constant speed to the cruise altitude at a predetermined climb angle. Thus the climb is performed in steady and symmetric flight conditions. When the cruise altitude is reached, the aircraft levels off again to fly at a constant altitude, while it accelerates to the correct cruise speed.

To calculate the details of this flight phase it is assumed the climb is performed in steady and symmetric flight conditions. The lift coefficient of the whole aircraft is determined where the lift coefficient is dependent on the climb angle of the aircraft, as shown in equation (3.1). Using this lift coefficient and the drag polar of the aircraft, also the drag of the aircraft during the climb phase can be determined, depicted in equation (3.2). Then, the thrust that should be produced

[2] https://www.pipistrel-aircraft.com/aircraft/electric-flight/alpha-electro/

by the aircraft to overcome this drag and produce enough thrust force to perform the climb can be calculated as shown in equation (3.3). All the considered forces during the climb are shown in the free-body diagram, as given in figure 3.4. The angle of attack of the aircraft is not taken into account during simulations of the aircraft, and therefore assumed to be equal to zero for all flight conditions, resulting in that the pitch angle and the flight path angle of the aircraft are equal. Furthermore, it is assumed that the thrust vector is aligned with the body axis of the aircraft.

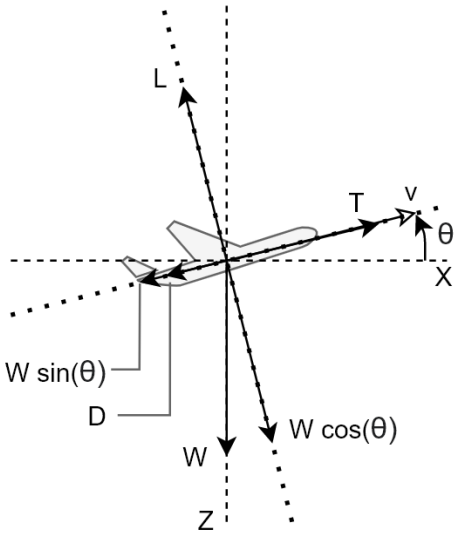

Figure 3.4: Schematic free body diagram of an aircraft during the climb phase, assuming steady and symmetric flight conditions.

$$C_L = \frac{W}{S_w q} \cos \Theta \tag{3.1}$$

$$D = q S_w C_D \tag{3.2}$$

$$T = D + W \sin \Theta \tag{3.3}$$

This thrust force, combined with the speed and altitude of the aircraft is used to determine the propeller efficiency of the propeller, as elaborated on in section 3.2. This efficiency is, in combination with the propulsive power as shown in equation (3.4), used to determine the shaft power of the aircraft, shown in equation (3.5). Also, the electrical machine efficiency and the battery efficiency are used to determine the actual power the battery has to deliver to perform this climb, given in equations (3.6) and (3.7). In contrary to the propeller efficiency, these two efficiencies are assumed to be constant.

$$P_p = T v \tag{3.4}$$

$$P_s = P_p/\eta_p \tag{3.5}$$

$$P_{em} = P_s/\eta_{em} \tag{3.6}$$

$$P_{bat} = P_{em}/\eta_{bat} \tag{3.7}$$

To calculate the performance of this flight phase, the total climb is discretized in small time steps, of $15s$ each. During each time step the thrust, power, and other performance characteristics of the aircraft and propeller are calculated. With integration among other performance parameters, the energy usage, distance flown, acceleration and rate of climb are calculated.

Cruise

During the cruise phase, the aircraft flies at a constant altitude and constant speed. Since the considered aircraft is a full-electric aircraft and no fuel is burned, the weight does not change during the flight mission. Therefore, the lift and thrust produced by the aircraft are also constant during the cruise phase.

This makes the cruise phase a relatively easy phase to analyse, since the flight conditions will be equal throughout the whole cruise phase. The cruise flight performance is calculated analogue to the climb phase though, although the climb angle is equal to zero for the cruise phase, and the cruise flight does not have to be discretized into small time steps, but rather into one large time step which is integrated, due to the constant flight conditions.

Descent

The descent phase of the flight is the part where the actual regenerative mode of the aircraft can be used to regenerate energy, since at this flight phase excess energy might be available that can be harvested. Therefore, the amount of energy that is harvested during the mission is modelled in the descent phase. However, also for the descent phase the original method used a constant dM/dh descent approach. For a better comparable method, this is changed to a constant rate of descent at a constant flight speed descent approach. Both the rate of descent and flight speed are predetermined and fixed for the complete descent. It is assumed that the descent phase starts when the exact distance to reach the total mission range that is left to be flown, has to be used to slow down and descent the aircraft. The first part of the descent phase is used to slow down the aircraft to the given descent speed. After this speed is reached, the descent is started with a constant rate of descent and keeping this flight speed constant, again the steady and symmetric flight conditions are assumed for this flight phase. As well as that the angle of attack of the aircraft is still neglected, resulting in that the flight path angle and the pitch angle of the aircraft are equal. When the aircraft reaches an altitude of $0m$ again, the descent phase is finished and the landing starts.

Analogue to the climb phase, also for the descent phase first the required thrust to fly at the given rate of descent and flight speed is determined. The same relations as used in the climb phase are used to calculate this descent thrust. However, since regenerative flight is possible, also negative thrust is allowed in the descent flight, as shown in figure 3.5. Here the same assumptions are used as for the climb phase, thus the angle of attack of the aircraft is not taken into account, resulting in that the aircraft pitch angle and the flight path angle are considered to be equal to each other. Also, the thrust vector is again aligned with the body axis. When the weight force along the longitudinal axis of the aircraft has become larger than the drag force, the thrust force has to become negative to keep the aircraft at the prescribed (fixed) descent flight speed and rate of descent. For the descent analysis, it is needed that the propeller is able to produce the negative thrust as required. For a propeller geometry that is not able to produce the required negative thrust, the geometry of the propeller is updated in the next iteration of the outer loop of the sizing tool to make sure the required negative thrust as calculated from the descent strategy can be achieved, as will be further explained in section 3.2.4. When for this negative thrust also the shaft power of the propeller becomes negative, the electric machine is producing energy, instead of consuming energy. In this case, the aircraft is in the regenerative flight mode. The regeneration of energy is thus a result of the negative thrust which is produced by the propeller, where the (negative) thrust of the propeller is determined by the described descent trajectory. Whether or not the aircraft is thus regenerating energy is depending on the chosen descent strategy.

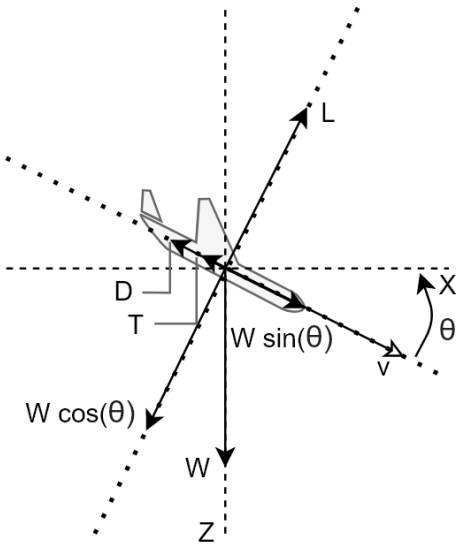

Figure 3.5: Schematic free body diagram of an aircraft during the descent phase.

The (negative) thrust force, combined with the flight conditions is then used to determine the propeller efficiency (in case of positive thrust) or harvesting efficiency (for negative thrust) using the propeller performance model, as described in section 3.2. This efficiency is then used to determine the power that is required by or given to the electric machines and battery of aircraft. The same discretization as for the climb phase is used to integrate the aircraft performance parameters.

Take Off and Landing

The take off and landing phases are not simulated within the model, however both manoeuvres can consume a significant amount of energy. Since the simulation of these two flight phases is not in the scope of the aircraft sizing model, the energy consumption is estimated using energy fractions. For the complete take off procedure, it is assumed that 2.6% battery capacity is needed [30]. In other words, if the battery is fully charged, after the take off at the start of the climb, 97.4% of the battery energy is still available. Within this 2.6% battery energy also all the procedures that are taking place before the take off are considered, such as start-up and taxi to the runway.

Similar to the take off energy fraction, also the energy consumption of the landing phase is modelled using energy fraction. Since during the landing procedure the thrust and power requirement is much lower than during the take off, the complete landing phase is assumed to consume 1.6% battery consumption [30]. Also for the landing, this fraction includes all the procedures from touch-down to shutdown. During the landing also excess energy is available, however since it is assumed no kinetic energy is harvested during the descent, it is assumed no energy is harvested during the landing procedure.

The energy fractions are taken as a percentage of the total battery capacity, which means that the energy consumption of the take off and landing is scaled with respect to the battery capacity. Since heavier aircraft are expected to have more battery energy available, these aircraft are also calculated to use more energy during the take off and landing.

3.1.3. Weight Estimation

After the constraint- and mission analysis it is known how much power and energy is needed such that the constraint flight manoeuvres and the mission can be performed. Using this energy and power requirement, the weight of the battery and electric machines can be determined using the given specific energy and specific power on the pack-level of these components.

Two battery weights can be determined, one such that the battery contains the exact amount of energy required for the mission and one that gives the battery the exact amount of maximum power that can be delivered, as required by the flight manoeuvres. These relations are respectively given in equations (3.8) and (3.9). The battery weight is then determined as the maximum of these two weights, such that always enough energy and power are available. The electric machine weight is calculated in the same manner, however for this case only the power is considered, as shown in equation (3.10). For both the battery and electric machine, the specific power- and energy density on the pack level is used, such that the calculated weights do also include all the overhead weight of these components.

$$M_{bat} = \frac{E_{mission}}{SE_{bat}} \tag{3.8}$$

$$M_{bat} = \frac{P_{bat}}{SP_{bat}} \tag{3.9}$$

$$M_{EM} = \frac{P_{EM}}{SP_{EM}} \tag{3.10}$$

For the other components of the aircraft which make up the OEM of the aircraft, the statistical method from Torenbeek is used [14]. This method splits up the OEM in different components, for which the weight is determined for each component. This method describes the statistical prediction of different components. The components that are taken into account for the sizing of the electric aircraft are:

- Main wing
- Tail wing (Horizontal and vertical)
- Tail boom
- Fuselage structure (including front-mounted engine cover)
- Undercarriage
- Surface controls
- Miscellaneous (instruments, cables, electronics, seats etc.)
- Propeller
- Propeller installation

The total OEM can then be found by taking the sum of all the individual component weights. Combined with the given payload weight and the calculated weight for the battery and electric machines, the total aircraft mass is determined, as shown in equation (3.11). This mass is the take off mass (TOM) of the aircraft, and will be constant for the complete mission, since no fuel is burned, and thus no mass is emitted during the mission.

$$M_{TO} = M_{OEM} + M_{Payload} + M_{Battery} + M_{EM} \tag{3.11}$$

3.2. Propeller Performance Model

In the original preliminary aircraft sizing method no propeller performance model is present for an aircraft with a single propulsor. Only a constant propeller efficiency for each flight phase is used as a fixed input. However, for a more accurate performance estimation, the propeller performance for the correct thrust setting and flight conditions should be calculated. Especially since these flight conditions can differ between multiple iterations, which also results in different obtained propeller efficiencies. Therefore, a propeller model integrated into the sizing model should result in more accurate and consistent results.

Moreover, to see the effect of the propeller on the regenerative performance of the aircraft, it is needed to know what the performance is of the propeller in this regenerative mode. Therefore, a propeller model which is also able to calculate the regenerative performance of the propeller is added to the sizing model. This propeller model is able to calculate the efficiency and operating condition of the propeller at each thrust, both positive and negative, setting and flight condition.

Finally, since it is not known which propeller blade designs for both propulsive and regenerative regimes are performing the most efficient, not only an analysis model is made, but also a propeller blade design algorithm. This design algorithm creates a blade geometry such that the time-weighted efficiency of the propeller is optimised, as will be elaborated on in section 3.2.4.

3.2.1. Analysis Model

The analysis model that is used to calculate the propeller performance is the Blade Element Momentum (BEM) method. This method is able to calculate the performance of a given geometry for a given operating condition. The BEM model that is used, is a *Python* integration of the *XROTOR* [3] graded momentum formulation as created by Willemsen [31] in his thesis work.

This model is a low fidelity model to calculate the performance of the propeller based on its geometry and operating- and flight conditions. This is done by first dividing the propeller blade into different elements. The angle of attack (AoA) and lift- and drag coefficient is then calculated on each blade element. To do this, use is made of the lift- and drag polars of the local airfoil. These lift- and drag polars are created using the program *RFOIL*, an adaptation of *XFOIL* [4] to account for the effects of the rotational aerodynamics on airfoils. This program calculates the two-dimensional performance of the airfoil for a range of angles of attack. Since the lift and drag coefficient are dependent on the local Reynolds (Re) number, the same airfoil is analysed multiple times for different Reynolds numbers, between which can be interpolated to find the approximate lift- and drag coefficient for a given AoA and Re number.

Since propellers operate mostly with fully turbulent boundary layers, due to their rotational speed [31], the airfoils are calculated with a forced boundary layer transition at 5% of the chord. Resulting in that the calculated airfoil polar is also calculated for fully turbulent boundary layers. Furthermore, an exponential factor of $N = 9$ is used, where N is referring to the e^N method which is used in *RFOIL*.

After the polars are determined, two correction factors are applied in the propeller analysis. First, the Prandtl-Glauert correction is applied, to correct for compressibility effects occurring on the propeller blade. Furthermore, due to the rotation of the propeller blades, the two-dimensional lift and drag polars as created by *RFOIL* do not correctly estimate the stall AoA of the airfoils in a rotational frame of reference. Therefore, the correction factor of Snel et al. [32] is used to correct for three-dimensional rotational effects. This correction model simulates the delay of stall of the airfoils, which is caused by the Coriolis effect.

Finally, when the correct C_l and C_d values are found, all the blade elements are combined, resulting in the total thrust and torque on the propeller blade. Since it is assumed that the

[3] http://web.mit.edu/drela/Public/web/xrotor/
[4] https://web.mit.edu/drela/Public/web/xfoil/

propeller blades are working independently, the thrust and torque are multiplied by the total number of blades on the propeller to find the total thrust and torque produced by the propeller.

For the propulsive case, a positive thrust force is found, which is used to propel the aircraft. However, for the regenerative case a negative torque is needed to generate energy. This negative torque can only be produced when the thrust is also negative. In this mode, the thrust acts as an extra drag force on the aircraft.

3.2.2. Performance Data Acquisition

This BEM model is able to predict the performance of a propeller design for one single flight- and operating condition per analysis. However, during the convergence of the aircraft it is not yet known what the exact flight conditions of the aircraft and the operating conditions of the propeller will be. Furthermore, due to the relative long computational time of the BEM model for a single analysis, it is beneficial to minimize the amount of operating points that have to be calculated with this model.

To solve this, a propeller performance database is created for each propeller geometry. Different databases can be created for each propeller geometry depending on the thrust setting mode: variable RPM (vR) or variable RPM & pitch ($vRvP$).

For the thrust setting mode of variable RPM only, vR, a data point is created for each unique combination of flight speed, discretized in steps of $10m/s$, and advance ratio, discretized in steps of $1/3$. Due to the low altitude that general aviation aircraft are flying in, it is chosen that the performance difference due to altitude is neglected in the propeller performance calculation. All the performance parameters are calculated for sea level altitudes as defined in the ISA conditions. The resulting propeller performance that is calculated, is saved using the thrust, power and torque coefficient in a database as shown in table 3.1. Using these coefficients the actual thrust, power and efficiency of the propeller at that operating condition can be determined.

Table 3.1: Example of propeller performance database for one flight speed and geometry

Advance Ratio, J	Pitch Angle, Θ	C_T	C_P	C_Q
⋮	⋮	⋮	⋮	⋮

Within the sizing loop, instead of a known propeller operating condition the resulting thrust requirement of the propeller is known. Therefore, to find the correct operating condition which results in the correct thrust production, the database is used.

When the performance of the propeller is needed, and the databases for the propeller geometry have been generated, the performance parameters are first interpolated between the flight conditions, such that one set of performance parameters is created which is valid for that specific flight condition. For example: when the performance of the propeller is needed at a flight speed of $33m/s$, the propeller databases of $30m/s$ and $40m/s$ are linearly interpolated to create the new performance data set, valid for $33m/s$.

The aircraft convergence loop requires the efficiency of the propeller at a given thrust force

produced by the propeller. However, since the thrust force is an output of the BEM model, it can not be seen upfront which propeller operating conditions correspond to this thrust setting. Therefore, from the performance database for the current flight conditions, the propeller operating condition is determined by interpolation which results in the correct thrust force produced by the propeller. With this propeller operating condition, the performance of the propeller can be determined which results in the correct thrust produced at the correct flight condition. A block diagram is given in figure 3.6 which shows the process to find the correct propeller efficiency for a given thrust force.

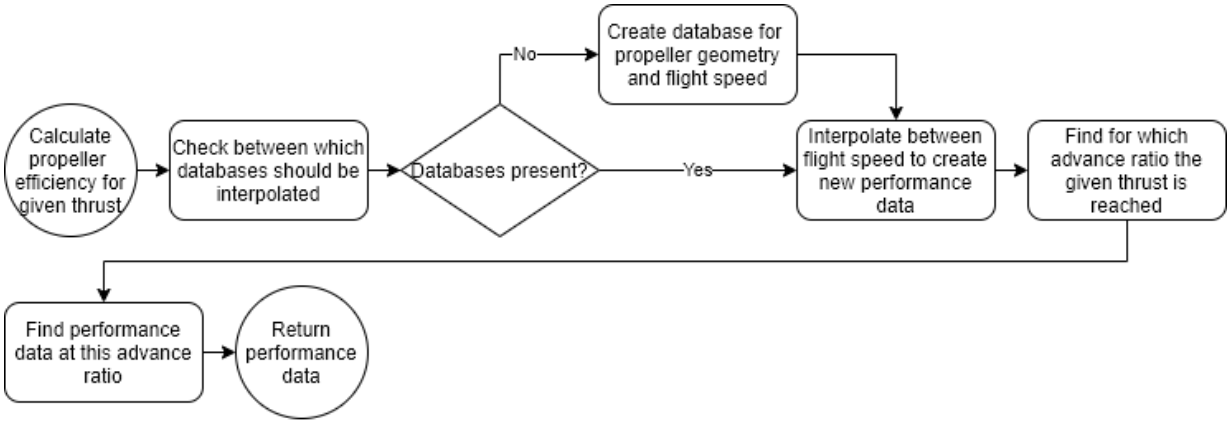

Figure 3.6: Block diagram showing the process to find the correct propeller performance for a given thrust force and flight condition with a variable RPM thrust setting.

3.2.3. Response Surface Fit Model

For the variable RPM mode (vR), only one operating condition corresponds to the correct required thrust as given for a given flight condition. However, for the thrust setting with a variable RPM & pitch setting ($vRvP$), multiple combinations of RPM and pitch setting result in the correct produced thrust. All these possible combinations do however have not the same propeller efficiency, so one combination of RPM and pitch should be chosen for the highest efficiency to produce the required thrust. To solve this issue, first an interpolated surface of the thrust produced for all the calculated RPM and pitch settings is produced, using linear interpolation. Also these calculated points are saved in a database, as shown in table 3.1. The pitch is discretized in steps of 1°.

From this interpolated surface, the response surface, for every 0.5° of pitch setting, the RPM setting is found that results in the correct produced thrust. This results in a list of combinations of RPM and pitch settings that give the correct produced thrust. Then, each of these combinations is analysed to find the propeller efficiency of this specific setting. After this is done, the combination of RPM and pitch setting that results in the highest efficiency is chosen as the operating condition of the propeller. The block diagram illustrating this process is given in figure 3.7.

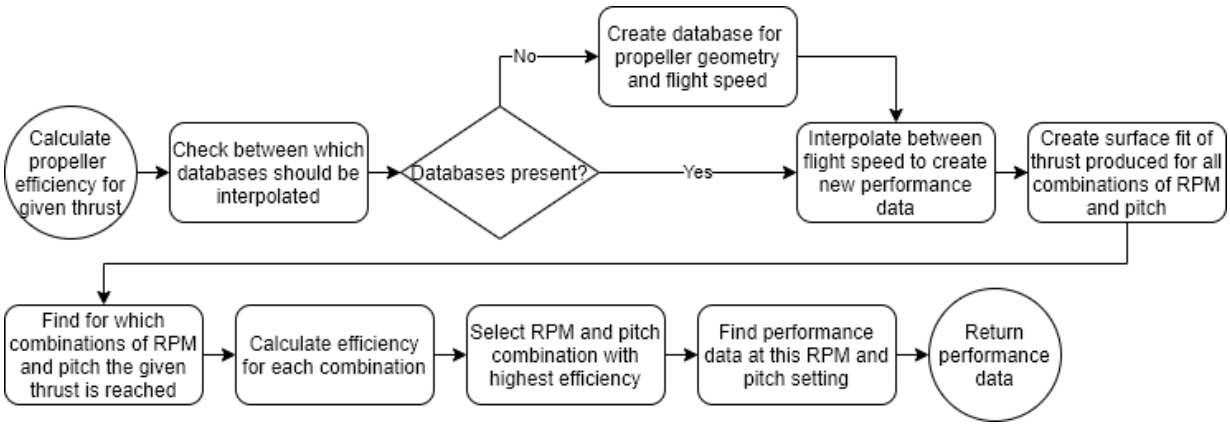

Figure 3.7: Block diagram showing the process to find the correct propeller performance for a given thrust force and flight condition with variable RPM and pitch thrust setting.

3.2.4. Propeller Design and Optimisation

Not only the performance of an existing geometry is calculated during the iterative process, but also new geometries are determined, such that the efficiency of the propeller is to be maximised throughout the mission of the aircraft. Also, by changing and optimizing the propeller geometry for the specific design mission, the influence of the mission and the regenerative part of the mission on the propeller geometry can be found. This will increase the insight into how the in-the-loop propeller design will affect the propeller design, and how this influences the complete aircraft sizing.

Two methods are used to determine and update the propeller geometry. The first method is the Minimum Induced Loss (MIL) design method. This method designs the propeller geometry for a single flight condition, such that for the given required thrust the induced losses on the propeller are minimised.

The advantage of this method is that it is very fast and does not need a starting, reference, geometry to determine the MIL design. However, the drawback of this method is that the propeller geometry will only be designed for one flight- and operating condition. Therefore, all the other operating conditions might have very unfavourable performance in terms of efficiency or thrust produced by the propeller. Furthermore, as the name suggests, this method does only take induced losses into account and not the profile losses on the airfoils. Therefore, the designed propeller might not be optimal for the designed operating condition.

Design by Optimisation

To take multiple flight- and operating conditions, and the different profile losses during these conditions into account during the design of the propeller geometry, use is made of a *Sequential Quadratic Programming* (SQP) optimisation algorithm. The goal of this algorithm is to minimize an objective function, while staying within the feasible region, determined by a set of bounds and constraints. For the propeller optimisation, this means that the average mission efficiency of the propeller is calculated, which is formalized in the objective function, such that a higher

efficiency will lead to a reduction in the objection function.

To do this optimization, the current propeller geometry has to be parameterised into a set of parameters. This set of parameters can then be analysed by the optimizer algorithm, and adjusted to minimize the objective function. For the propeller geometry it is chosen to use the Class-Shape-Transformation (CST) coefficients, based on the Bernstein polynomials [33, 34] for the parametrisation of the propeller geometry. These CST coefficients are able to describe the shape of the chord- and twist distribution with a limited amount of parameters. For the chord distribution the parametrisation is performed with six coefficients, while the twist distribution is parameterised with four coefficients. This is beneficial, since a lower number of parameters leads to less required function evaluations, and usually also less computational time needed. The design vector for the optimisation function in equation (3.12). For the first iteration of the aircraft sizing tool, no propeller geometry is known yet. Therefore, for the first iteration of the sizing tool a MIL design is used, where the design is created for the takeoff conditions. Only after this geometry is known, this can be optimised for the given aircraft constraints and mission profile.

$$\overline{\mathbf{x}} = \langle CST_{chord_1}, CST_{chord_2}, \dots, CST_{chord_6}, CST_{twist_1}, \dots, CST_{twist_4} \rangle \tag{3.12}$$

In figure 3.8 a chord distribution and a twist distribution for an arbitrary propeller geometry are given, with also the underlying shapes as determined from the CST coefficients shown. Adding the individual shapes results in the final chord or twist distribution. In this way, only a limited number of coefficients can be used to determine the full chord and twist distribution of a propeller blade.

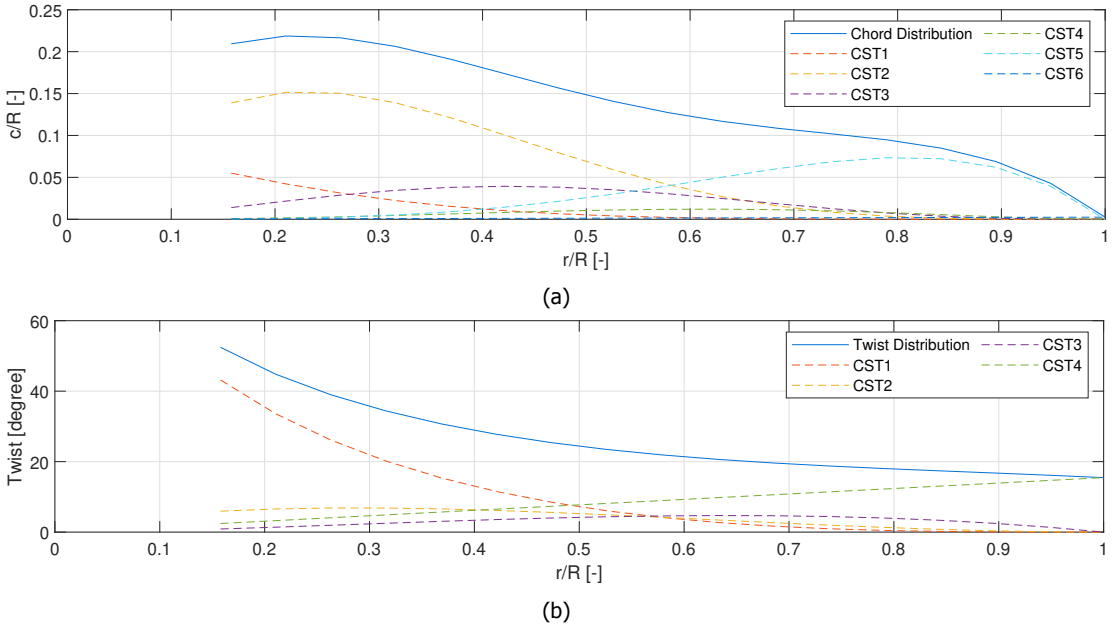

Figure 3.8: Example (arbitrary) propeller blade chord (a) and twist (b) distribution indicating how the CST coefficients can be used to generate the distributions.

The optimisation needs an objective function to optimise the known propeller geometry. To determine the objective function of the optimisation, it has to be known if the current battery weight is determined by the power requirements of the constraint manoeuvres or the energy requirements of the flight mission. In the first case, a single flight- and operating condition determines the weight of the battery, since the peak power delivered by the battery determines the total weight of the battery. Therefore, to reduce the battery weight and thus the total weight of the aircraft, it is beneficial to increase the propeller efficiency of the propeller in this specific flight condition.

In the latter case, the energy stored in the battery is determining the battery weight. To reduce this battery weight, the energy used in the mission should be reduced. Since the energy used in the mission is a function of power delivered and time, where time is fixed for a given mission, the only way to reduce the energy usage is by reducing the power that has to be delivered to the propeller. Since the required thrust is calculated in the mission, the power reduction can only be done by increasing the efficiency of the propeller.

To make sure the total energy during the mission is minimised in this case, both the climb, cruise and descent are taken into account. Each flight phase is then weighted according to the time the aircraft is operating in this flight phase, as shown in equation (3.13). In this way the (weighted) average efficiency is maximised, with the idea in mind that this minimises the mission energy requirement, reducing the battery weight.

$$\min_{\bar{\mathbf{x}}} \quad f(\bar{\mathbf{x}}) = 1 - \left(\frac{t_{cl}\eta_{cl}(\bar{\mathbf{x}}) + t_{cr}\eta_{cr}(\bar{\mathbf{x}}) + t_{de}\eta_{de}(\bar{\mathbf{x}})}{t_{tot}} \right) \tag{3.13}$$

In both cases, where the battery is limited by power and energy requirements, the propeller has to be able to produce the required power also in all the other flight manoeuvres and phases. Therefore, during the optimisation constraints are set on the minimal maximum thrust the propeller is able to produce for each manoeuvre and flight phase. So, thrust as produced for each flight phase should be between the calculated minimum thrust and maximum thrust that can be produced by the propeller geometry at the respective flight conditions, as shown in equations (3.14) to (3.19). The same is true for the four constraint manoeuvres as analysed in the constraint analysis. In this way, the newly optimised propeller geometry will be able to fulfil the complete mission requirements of the aircraft.

$$g_1(\bar{\mathbf{x}}) \leq T_{min_{cl}}(\bar{\mathbf{x}}) - T_{cl} \tag{3.14}$$

$$g_2(\bar{\mathbf{x}}) \leq T_{cl} - T_{max_{cl}}(\bar{\mathbf{x}}) \tag{3.15}$$

$$g_3(\bar{\mathbf{x}}) \leq T_{min_{cr}}(\bar{\mathbf{x}}) - T_{cr} \tag{3.16}$$

$$g_4(\bar{\mathbf{x}}) \leq T_{cr} - T_{max_{cr}}(\bar{\mathbf{x}}) \tag{3.17}$$

$$g_5(\overline{\mathbf{x}}) \leq T_{min_{de}}(\overline{\mathbf{x}}) - T_{de} \tag{3.18}$$

$$g_6(\overline{\mathbf{x}}) \leq T_{de} - T_{max_{de}}(\overline{\mathbf{x}}) \tag{3.19}$$

$$0 \leq \overline{\mathbf{x}} \leq 1 \tag{3.20}$$

On the propeller geometry, the chord and twist distribution, no constraints are set. Only bounds on the design vector are set, where the individual coefficients of the design vector should remain between zero and one, as shown in equation (3.20). The optimisation algorithm only optimises the propeller geometry for aerodynamic properties. Factors such as the structural integrity or noise emission are not taken into account for the optimisation procedures. This could lead to mechanically infeasible designs, such as a tip chord approaching zero length. However, since at the tip no lift is produced anyway, this should not impose any problems for the aerodynamic optimisation. However, it should be noted that it might be possible that the most aerodynamic optimal propellers as designed, might not be able to be used on actual aircraft.

4

Model Validation

To check the validity of the created sizing model, propeller performance model and regenerative flight model, the models are checked against experimental data. If the models are correctly implemented and represent the correct physical phenomena, the results should show high similarity between the simulated and the experimental data.

For the sizing model, the simulation is compared with the full-electric *Pipistrel Alpha Electro* aircraft, the simulation details and a comparison is the real aircraft is given in section 4.1. This aircraft is the first full-electric general aviation aircraft. Since the focus of this thesis and the sizing model is also on full-electric general aviation aircraft, this aircraft is found suitable to check the validity of the sizing tool. Also a flight test has been performed with this aircraft that included the regeneration of energy during the descent phase. These experiments are used for the validation of the regenerative flight model, shown in section 4.3. Although this aircraft is not designed with this regenerative mode in mind, the flight data should be representative for a generalised regenerative flight model, since the flight mode will be performed similarly.

A previous wind-tunnel experiment has been performed at the *TU Delft* [11, 12] with a propeller operating in regenerative conditions. This provided the validation data for comparison with the propeller model. The same propeller geometry, as used in the wind-tunnel experiment, is modelled in the propeller performance model and simulated for the same operating points. Also here, it is expected that, when the model is correct, a high similarity between the simulated data and the experimental wind-tunnel data is found. These results are presented in section 4.2.

4.1. Aircraft Sizing Model

The aircraft sizing model will be validated using the *Pipistrel Alpha Electro* [1]. This aircraft is a full-electric aircraft, focused on flight school operations. The aircraft is an adaptation of the conventional, fuel based-engine, version. Therefore, the baseline aircraft was not intended to be used as a full-electric aircraft. However, since this is the first full-electric general aviation aircraft that has been made commercially available, it is found to be suitable for validation of the aircraft sizing model. The validation is done by using the described sizing tool to model the mission profile of this aircraft. The resulting weight estimation is then compared to the actual

[1] https://www.pipistrel-aircraft.com/aircraft/electric-flight/alpha-electro/

weight of the aircraft. The aircraft is a 2-seater trainer, so it is focused on performing training flights with high powered climbs and a short cruise flight. A drawing of the aircraft is given in figure 4.1 and the full details of the aircraft are given in table 4.1.

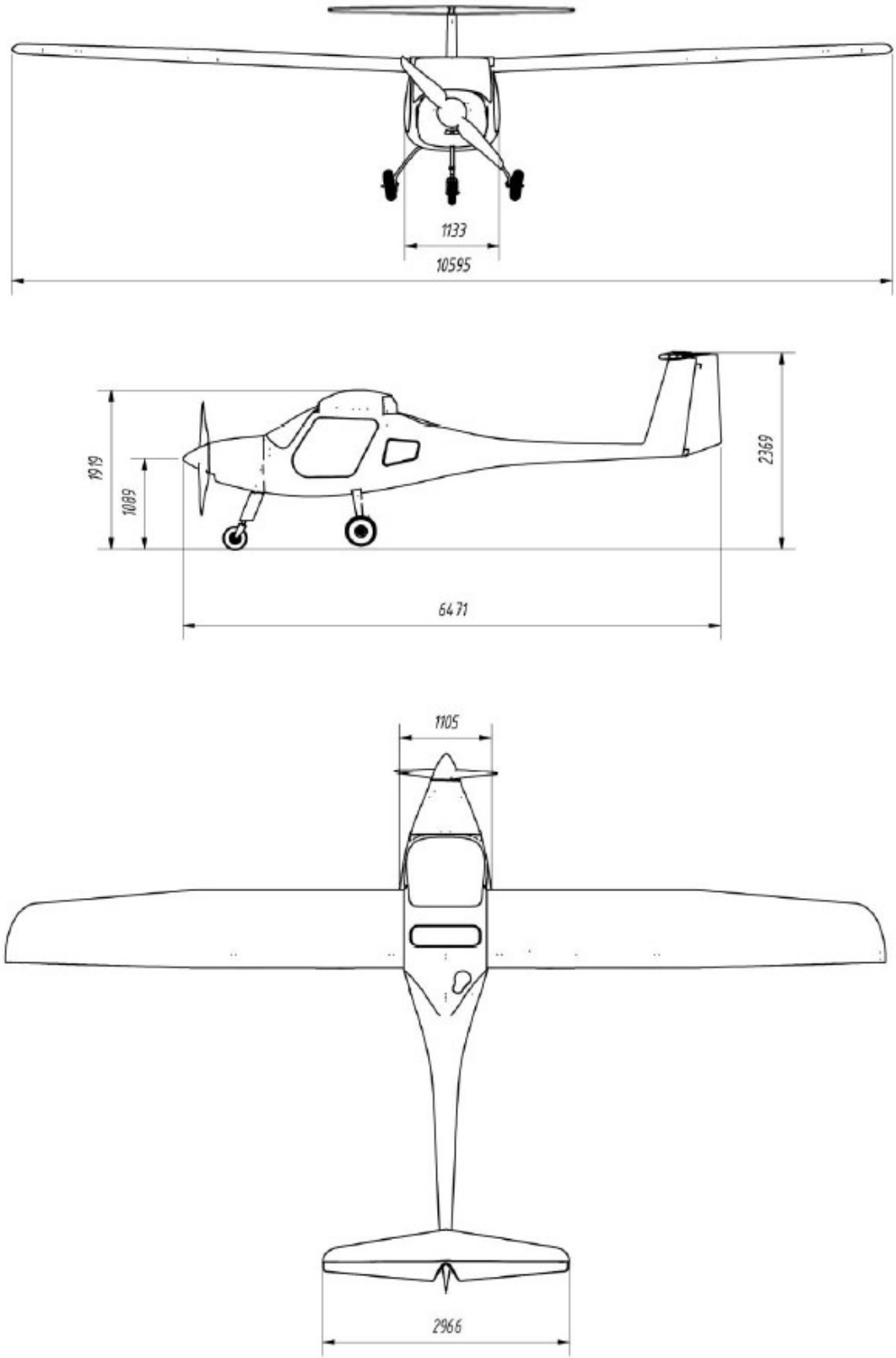

Figure 4.1: Overview of the front, side and top view of the *Pipistrel Alpha Electro* [35].

Table 4.1: Parameters to model the Pipistrel Alpha Electo using the aircraft sizing tool[2]. All values are valid for the clean configuration at sea level, unless specified otherwise.

Paramater	Value	Unit
Wing		
Aspect Ratio	11.8	–
Sweep	0	°
Taper Ratio	1	-
Wing Area	9.51	m^2
Airframe		
Maximum load factor	4	g
Minimum safety factor	1.875	–
Speeds		
Never exceed	135	kts
stall	45	kts
stall, full flaps	38	kts
cruise	75	kts
Propeller		
Radius	0.9	m
Blades	3	–
max. RPM	2650	$1/min$
min. RPM	750	$1/min$
Performance		
Range	75	NM
TO field length	225	m
Rate of Climb	1220	ft/min
max. L/D	15 : 1	–
Weights		
Payload	182	kg
TOM	550	kg
Battery and Electric Motor		
Bat. Capacity	21	kWh
Bat. Specific Energy	198	Wh/kg
Bat. Specific Power	566	W/kg
EM. Power	60	kW
EM. Specific Power	3	kW/kg
Dimensions		
Aircraft length	6.5	m
Fuselage length	3.1	m
Fuselage width	1.1	m
Fuselage height	1.1	m

The technical data will give a start point to model the *Pipistrel Alpha Electro* using the sizing tool. However, the design mission profile used during the design of this aircraft is not given by the manufacturer and has therefore to be estimated. Also the drag polar of the aircraft is not provided. This has also to be estimated using a statistical method. It is chosen to use the drag estimation of Torenbeek [14], since also the weight estimation of the aircraft is based on the same design method.

When all the top level requirements and the mission of the *Pipistrel* have been found, the sizing tool is used to calculate the TOM of the aircraft given these requirements. The resulting simulated aircraft is then to be compared with the real aircraft to see how close the sizing tool is able to predict the sizing and performance of a to be designed aircraft.

4.1.1. Drag Polar Estimation

Unfortunately the drag polar of the *Pipistrel Alpha Electro* is not provided in the technical data by *Pipistrel*. However, with the specifications that are given, an estimation of the drag polar can be made.

The drag polar is assumed to be in the form of a two-term asymmetric parabolic polar, consisting of the minimum drag coefficient and the induced lift drag, as shown in equation (4.1).

$$C_D = C_{D_{min}} + \frac{(C_L - C_{L_{minD}})^2}{\pi A R e_v} \tag{4.1}$$

For the *Pipistrel Alpha Electro* the aspect ratio, AR, is given. However, the span efficiency factor, e_v, the minimum drag component, $C_{D_{min}}$, and the lift coefficient at minimum drag, $C_{L_{minD}}$, are unknown. Some points on the drag polar can be estimated by the performance data provided by *Pipistrel*. Combined with statistical methods as created by Torenbeek [14], an estimation of the drag polar of the aircraft is made.

It is known that the maximum glide ratio, C_L/C_D, is equal to 15 at an aircraft mass of $550kg$ and is reached in the clean configuration of the aircraft, i.e. the flaps are retracted. Furthermore, it is known that this glide ratio is reached at a speed of $64kts$. Therefore, using the basic lift and drag equations, as given in equations (4.2) and (4.3) and assuming this condition is reached in horizontal, steady and symmetric flight, the lift- and drag coefficient can be calculated at this flight condition.

$$L = \frac{1}{2}\rho V^2 S C_L \tag{4.2}$$

.

$$D = \frac{1}{2}\rho V^2 S C_D \tag{4.3}$$

[2]taken from https://www.pipistrel-aircraft.com/aircraft/electric-flight/alpha-electro/

This results in a lift coefficient at the maximum glide ratio of 0.854, while the drag coefficient is equal to 0.057. Since this point is obtained in the clean configuration, it is known that this point should be on the drag polar. However, this is the only point on the drag polar that can be calculated, while at least three points are needed to make an estimate of all the variables in the formulation of the assumed drag polar.

To be able to have an estimation of the drag polar, the statistical method of Torenbeek [14] is used. This method is used to estimate the zero-lift drag coefficient, C_{D_0}. Although the zero-lift drag coefficient is not exactly equal to the minimum drag coefficient, for this statistical estimation it is assumed that the values are equal to each other. Similar, the span efficiency factor is found by calculating the Oswald factor, e, using the empirical methods as described by Niţă and Scholz [36]. Again, these two factors are not the same, but they are assumed to be equal to be able to make an estimation on the complete drag polar.

Zero lift drag coefficient

For the estimation of the zero lift drag some assumptions have to be made based on the geometry of the *Pipistrel Alpha Electro*, first the wing is assumed to have zero sweep and is cantilevered at the root of the wing, resulting in a wing correction factor of $r_w = 1$. The root thickness of the airfoil is assumed to be 15%, resulting in that $t_c = 0.15$. For the wing surface, it is chosen to use the reference value from the Pipistrel Alpha Electro, as can be found in table 4.1. Using these values, the drag area of the wing can be calculated using equation (4.4).

$$(C_D S)_W = 0.0054 r_w \left(1 + 3 t_c \cos^2(\Lambda)\right) S_w \tag{4.4}$$

The fuselage dimensions are measured from technical drawings from the pilot operating handbook [35], resulting in the dimensions as given in table 4.1. With these dimensions, the drag area of the fuselage is also estimated, as shown in equation (4.5).

$$(C_D S)_f = 0.0031 r_f l_f \left(b_f + h_f\right) \tag{4.5}$$

The drag from the nacelle, which is in this case the engine cover in front of the fuselage, is found to be equal to that if a piston engine would be installed, since the original *Pipistrel Alpha* was designed with a piston engine, mounted on the front of the fuselage. Therefore, the drag of the nacelle is calculated using the fuselage dimensions, as can be seen in equation (4.6).

$$(C_D S)_n = 0.015 b_f h_f \tag{4.6}$$

The Reynolds number correction, to account for the effect of turbulent skin friction drag and miscellaneous drag, for the complete aircraft is found by calculating the Reynolds number for the complete aircraft. This Reynolds number can then be used to find the Reynolds number correction factor, as shown in equation (4.7).

$$r_{Re} = 47 Re_f^{-0.2} \tag{4.7}$$

Finally, the undercarriage is not retractable, but is streamlined due to the installed fairings. This results in a correction factor for the undercarriage of $r_{UC} = 1.25$. The drag of the tailplane is estimated to add approximately 24% to the zero lift drag coefficient, resulting in a tailplane correction factor of $r_t = 1.24$ [14]. Combined with all the separate drag area calculations for the wing, fuselage and nacelle, the zero lift drag times the wing area of the complete aircraft is calculated using equation (4.8). This value is divided by the reference wing area, to find the final zero-lift drag.

$$C_{D_0} S = r_{Re} r_{UC} \left(r_t \left((C_D S)_W + (C_D S)_f \right) + (C_D S)_n \right) \tag{4.8}$$

Oswald factor

Following, the Oswald factor is calculated using the statistical method from Niţă and Scholz [36]. First, based on a function dependent on the sweep of the aircraft and the aspect ratio of the main wing a theoretical Oswald factor for the main wing is calculated.

$$f(\Lambda) = 0.0524\Lambda^4 - 0.15\Lambda^3 + 0.1659\Lambda^2 - 0.0706\Lambda + 0.0119 \tag{4.9}$$

$$e_{theo} = \frac{1}{1 + f(\Lambda) AR} \tag{4.10}$$

Three correction factors are applied to correct for the compressibility effects, the zero lift drag and the presence of a fuselage in the middle of the wing. The compressibility effects are neglected though, due to the low speed nature of general aviation aircraft and the low associated cruise Mach numbers. Therefore, the compressibility effect correction factor is equal to one, $k_{e_M} = 1$. Furthermore, for general aviation aircraft the correction factor based on the zero lift drag is found to be equal to $k_{e_{D_0}} = 0.804$ [36]. Finally, the correction factor for the fuselage is computed using equation (4.11). Here, the diameter of the fuselage is assumed to be equal to the width of the fuselage.

$$k_{e_F} = 1 - 2(d_f / b)^2 \tag{4.11}$$

Using the three correction factors, the final Oswald factor is calculated using equation (4.12).

$$e = e_{theo} k_{e_F} k_{e_{D_0}} k_{e_M} \tag{4.12}$$

The minimum drag coefficient (from the zero lift drag coefficient) and the span efficiency factor (from the Oswald factor) are calculated using the statistical methods. The asymmetric term, the

lift coefficient at minimum drag, can be now be found using the point on the drag polar found from the maximum glide ratio. This results in the found terms for a two-term parabolic drag polar, as given in table 4.2. Plotting this drag polar results in the figure as given in figure 4.2.

Table 4.2: Parameters for the estimated two-term parabolic drag polar of the *Pipistrel Alpha Electro*.

Parameter	Value	Unit
$C_{D_{min}}$	0.031	–
e_v	0.66	–
$C_{L_{minD}}$	0.05	–

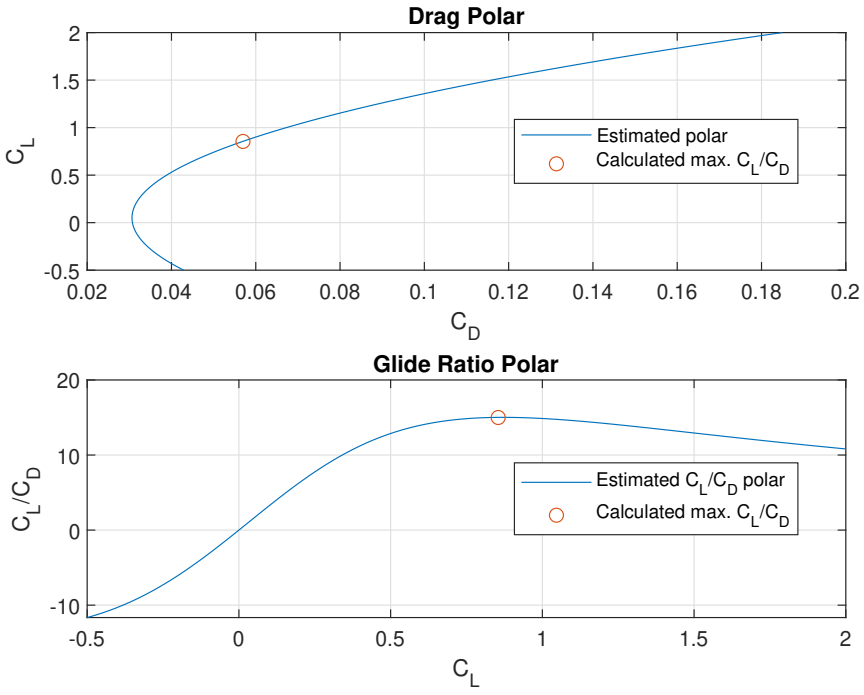

Figure 4.2: Estimated drag polar and glide ratio of the *Pipistrel Alpha Electro*

4.1.2. Reference Mission Profile

The *Pipistrel Alpha Electro* is designed for a short mission, with high powered climbs to be able to carry out a typical training mission. During these type of missions, multiple starts and landings are performed. However, a cross-country cruise is also possible with this aircraft. For the sizing of the aircraft this longer cruise range is used, since this long range cruise will be driving the battery energy requirement, and therefore the battery weight of the aircraft.

The flight range of the aircraft is dependent on the cruise altitude and speed. However, the manufacturer of the aircraft gives a cruise range of $75NM$, which is equal to $138.9km$ for a

typical cross country mission [2]. Therefore, the aircraft will also be sized for this range. This type of cruise is performed at $75kts$, or $38.5m/s$, and is assumed to be the true airspeed, which is just above the minimum drag speed of the aircraft which is equal to the maximum glide ratio speed of $64kts$. Unfortunately, no comments are made about the altitude at which the cruise is performed. Therefore, an estimation has to be made about the cruise altitude. It is known however that general aviation aircraft do not cruise at high altitudes, therefore it is chosen to perform the cruise at an altitude of $750m$, which is approximately $2500ft$ above sea level.

From the operating handbook of this aircraft [35] it is found that the descent of the aircraft is performed at a rate of descent of $460ft/min$ at the maximum glide ratio speed. This speed and rate of descent are then kept constant during the whole descent. For the reference mission the propeller is assumed to not be able to regenerate energy, since this will change the behaviour of the descent flight. The climb is performed at the minimum power required speed (i.e. maximum C_L^3/C_D^2), such that the most power as possible is available for the climb of the aircraft. Using the estimated drag polar, it is found that this is speed is equal to approximately $50kts$ at sea level.

Finally, it is known that not the complete battery capacity can be used, since this would reduce the lifetime of the battery and some reserves are needed for diversion or loitering. For the used battery within the *Pipistrel Alpha Electro* it is assumed that the effective capacity of the battery is 80% of the total battery capacity. Meaning that the minimum state of charge of the battery at the end of the mission is equal to 20%.

A schematic overview of the reference mission profile is given in figure 4.3. The climb phase is indicated with the number 1, the cruise phase with 2 and the descent with 3. The total distance covered during the three flight phases is equal to the range of the mission, $75NM$.

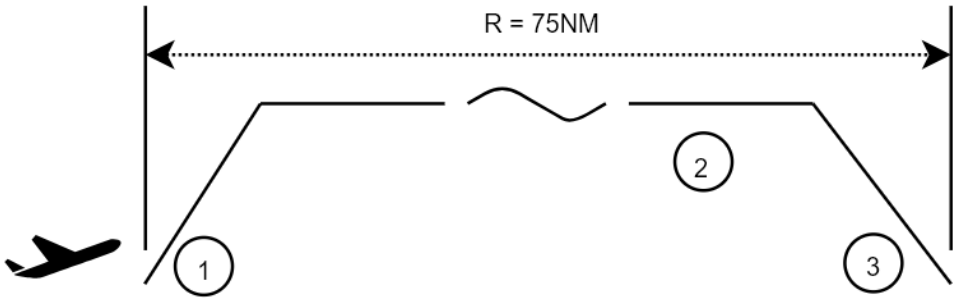

Figure 4.3: Schematic overview of the reference mission for which the aircraft will be sized.

4.1.3. Reference Propeller

Besides the drag polar and the reference mission profile, also the geometry or performance of the propeller of the *Pipistrel Alpha Electro* is not given by the manufacturer. Therefore, an estimation of the propeller geometry has to be made. From this geometry the propeller performance can be calculated using the propeller performance model.

[2] https://www.pipistrel-aircraft.com/aircraft/electric-flight/alpha-electro/

From the pictures of the propeller some details can be determined however [17]. First of all, it can be seen that a three-bladed propeller is used. The diameter of the propeller is measured to be $1.8m$, where the hub of the propeller has a diameter of $0.2m$. The airfoil cannot be determined from the given figure. Therefore, a traditional propeller airfoil has been chosen to be used for the complete propeller blades, the *Clark-Y* airfoil.

The geometry of the propeller is made using the optimisation method as described in section 3.2. Therefore, the propeller geometry is optimised such that the time-weighted average of the efficiency in climb, cruise and descent is maximised. This results in a propeller that is aimed to minimise the energy consumed during the mission and therefore reducing the battery weight. The reference aircraft does have a ground adjustable pitch propeller. However, in-flight this pitch is fixed. The pitch is optimised such that the energy used during the mission is minimised. So, the propeller that is optimised does only have a variable RPM setting.

Finally, the performance of the other parts of the drive-train is not calculated. However, their efficiencies are taken into account. It is assumed that the battery to shaft power efficiency is 95%. So, only 5% energy is lost from the energy stored in the batteries, to the energy delivered on the propeller shaft [15].

4.1.4. Mission Performance

Using the aircraft input parameters, the drag polar estimation, the reference mission and propeller geometry the aircraft can be sized. Below the results of the converged sizing of the aircraft are given, which are aimed to represent the *Pipistrel Alpha Electro* as much as possible.

The first step of the sizing tool is the creation of the wing- and power-loading diagrams, as described in section 3.1. For each component a wing- and power-loading diagram is created, resulting in a diagram for all the elements in the drive-train: the battery, electric machine, shaft and total aircraft. These four diagrams are shown below in figure 4.4.

The four constraints and the feasible design space are depicted for the four components of the drive-train, where clearly can be seen that the rate of climb constraint determines the power loading of the aircraft for all the components. Since the power of the electric machine and the weight of the *Pipistrel Alpha Electro* is known, the electric machine power loading can be calculated for this aircraft and shown in the respective graphs. From here it can be seen that the wing loading for the simulated aircraft is sized to be equal to that of the Pipistrel aircraft. However, the power loading is slightly lower, resulting in a larger electric machine per take off weight for the simulated aircraft. This increase in power loading of the calculated aircraft can be the result of a slightly lower calculated propeller efficiency at the maximum rate of climb manoeuvre than the reference aircraft.

The mission that is flown is summarised in figure 4.5. Here it can be seen that the total flight time is about 1 hour and 5 minutes. In this time the total distance of $138.9km$ is flown. Also it can be observed that the aircraft mass does not change throughout the whole mission. This makes sense, since no fuel is burned and therefore the aircraft does not become lighter during the mission. Finally, the highest battery power is needed during the climb phase of the mission,

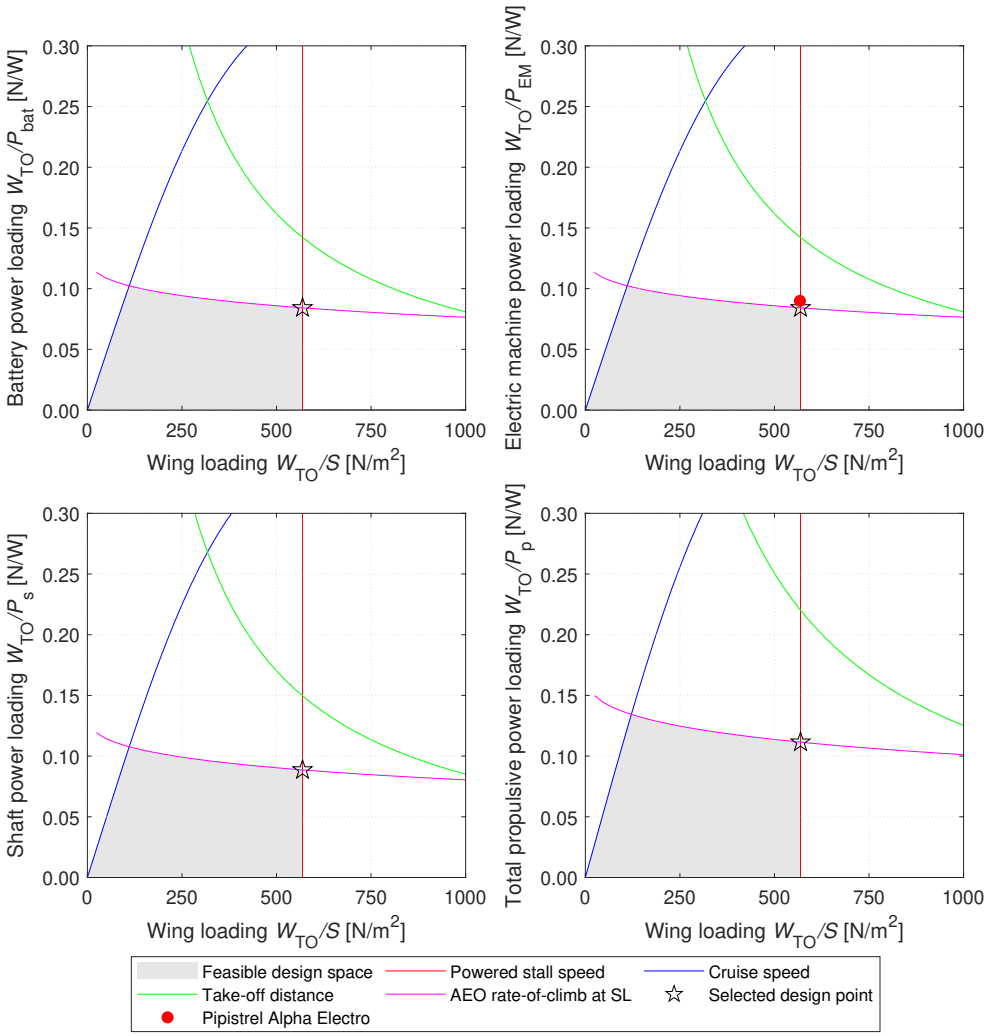

Figure 4.4: Power- and Wing loading diagram of the modeled Pipistrel Alpha Electro.

as can be seen from the high slope of the battery remaining energy figure. However, although during the cruise the battery power required is lower than during the climb, due to the longer duration of this phase the total energy consumed in the cruise phase is higher. During the descent, no power is required and therefore no battery energy is used. The gravitational force during the given descent strategy is already large enough to keep the aircraft above the minimum drag speed ($1.5m/s$ higher than the minimum drag speed) without the need for extra added flight power by the propeller.

The propeller that is used during the simulated mission is optimised using the described optimisation algorithm for the mission such that the time-weighted propeller efficiency is maximised during the mission, aimed to minimise the mission energy. The resulting propeller geometry and performance is given in figure 4.6. Here also the presence of the propeller hub is visible. The hub has a radius of $0.1m$ and therefore the propeller chord and twist is only defined at a relative radial location of $r/R > 0.11$. The propeller optimisation algorithm uses a time-weighted

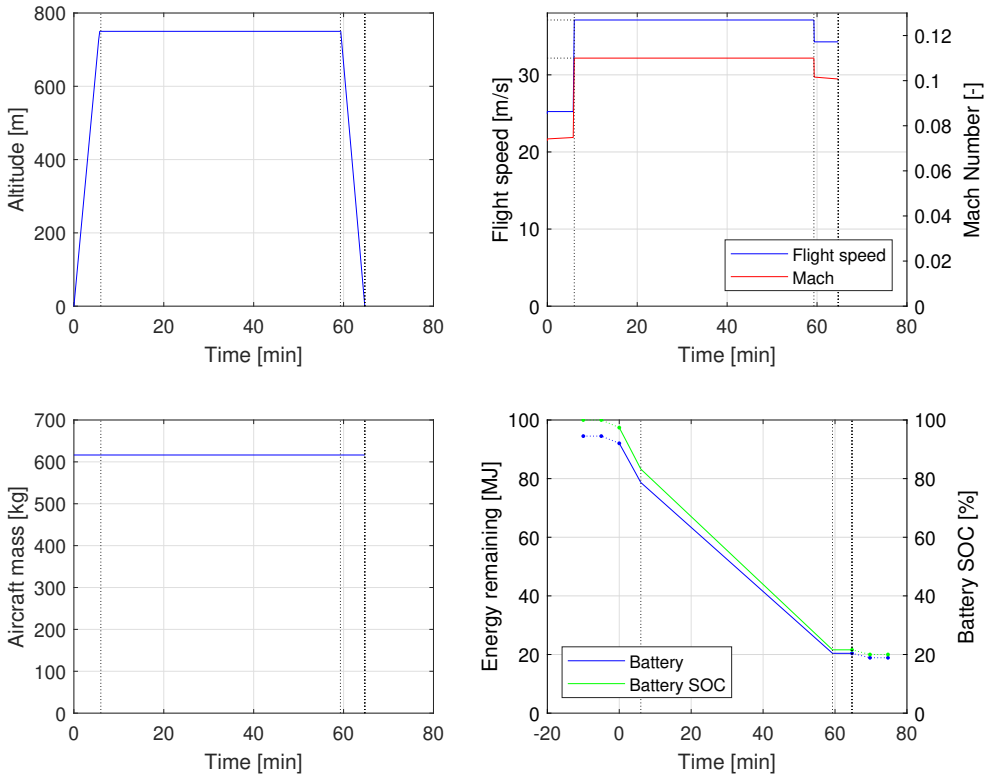

Figure 4.5: Calculated mission profile of the modeled Pipistrel Alpha Electro.

objective function to optimise the propeller for the three flight phases: climb, cruise and descent. Since the cruise phase makes up for most of the mission, this flight phase is therefore also driving in the design of the propeller geometry. The result is a propeller blade with a low solidity of 5.8%, and high efficiency in the cruise phase. The same design philosophy, to create a cruise optimised propeller, is used for the conventional (real-life) *Pipistrel Alpha*, the aircraft version with the fuel engine [17]. For the electrified version of the aircraft the propeller design was initially not adjusted. Therefore, the calculated propeller design is found to properly resemble the propeller geometry of the reference aircraft.

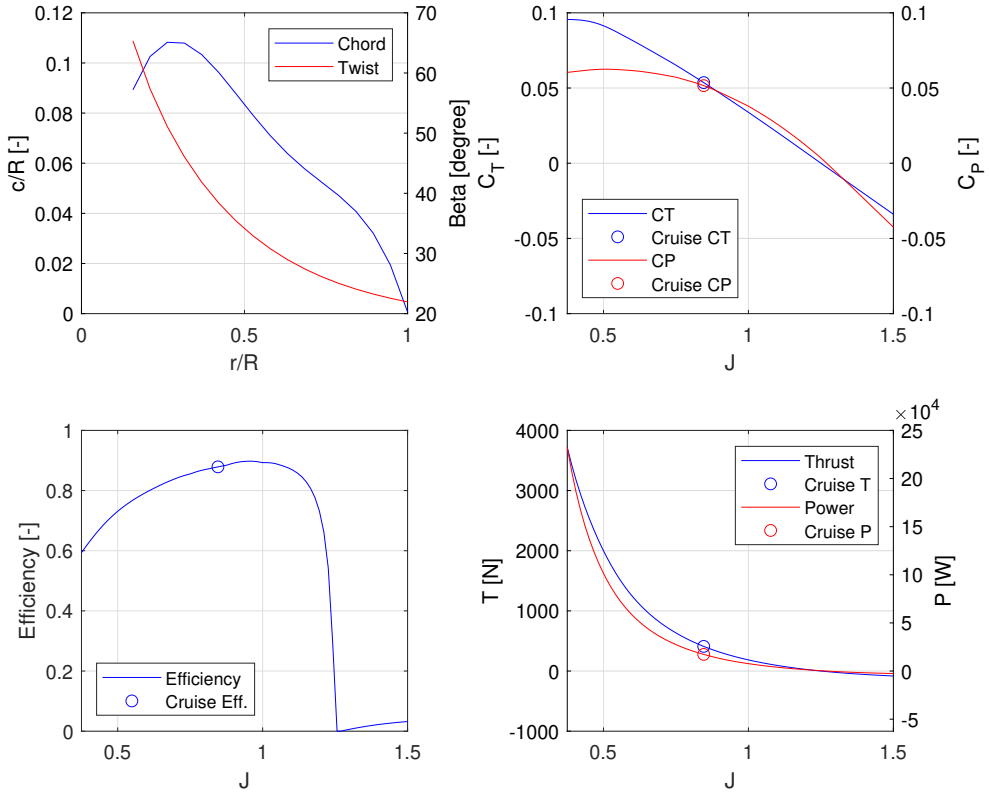

Figure 4.6: Calculated propeller geometry and cruise performance of this propeller for the modeled Pipistrel Alpha Electro.

From the propeller geometry and performance map, the performance of the drive-train during the mission is be determined, as shown in figure 4.7. For the thrust required from the mission, the advance ratio of the propeller is selected such that this thrust is produced at the given flight speed. The lowest advance ratio, and thus the highest RPM, is observed during the climb of the aircraft. This does make sense, since during this flight phase also the most thrust has to be produced. To produce the high thrust, also a high torque to the propeller has to be delivered. During the cruise phase, the thrust force required is lower, while a higher advance ratio of the propeller is observed, and a lower RPM. Therefore, the torque delivered to the propeller is also lower. During the un-powered descent, the RPM is lowered even further to make sure the propeller does not produce any thrust anymore. For this un-powered descent is assumed that no torque is required to not produce any propeller windmilling drag, resulting in that the descent energy is underestimated compared to a real propeller that is producing no thrust, but does

also not produce any windmilling drag. Since the propeller has a fixed pitch, the pitch does not change during different phases of the mission.

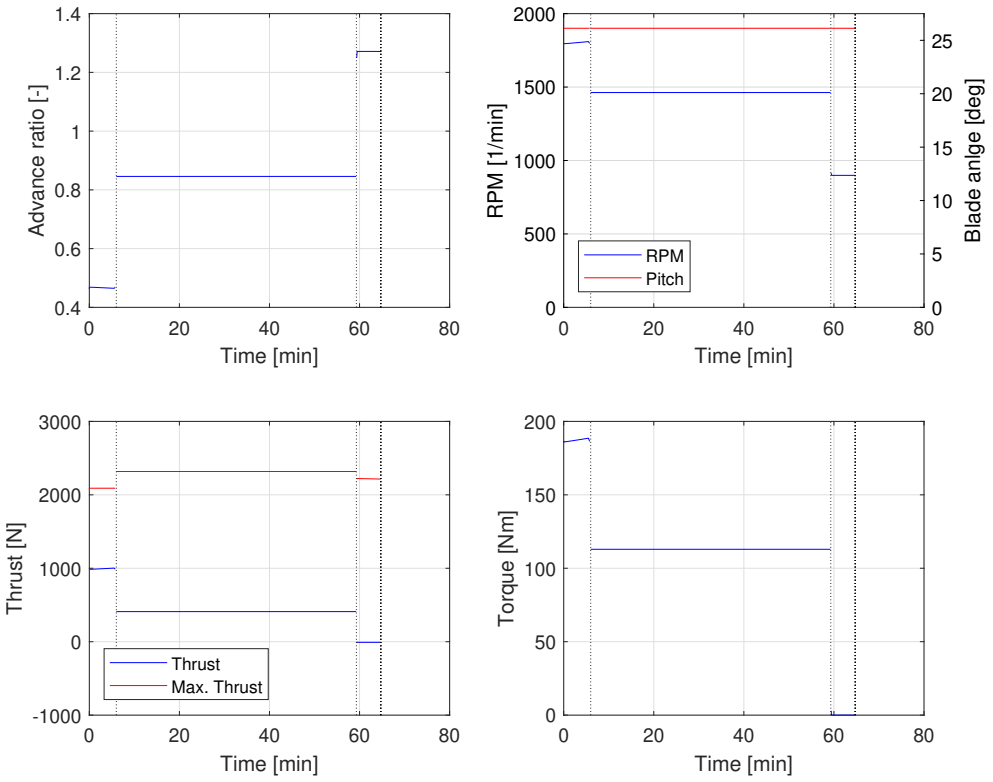

Figure 4.7: Drive-train performance of the modeled Pipistrel Alpha Electro for the complete mission.

The propeller geometry and performance, combined with the mission profile results in the power the power-train has to deliver and at which efficiency this power is converted from the energy stored in the batteries, to the final propulsive power delivered. From figure 4.8 it clearly can be seen that at each component of the drive-train power is lost due to losses between the energy conversions, resulting in that the battery has to deliver more energy than required for the flight energy.

Since the propeller is time-weighted optimised for the three flight phases, and the cruise phase makes up of the most time of the flight, the propeller is mainly optimised for the cruise phase. This can also be seen in the efficiency of the propeller. During the climb, the efficiency is lower than for the cruise phase. The efficiency during the descent is equal to 0, since the thrust is equal to 0 during the descent. Therefore, the power is also equal to zero during the descent and this very low efficiency is not reflected in the energy requirement.

The flight power is split up into three terms: the power to overcome the drag, power to accelerate the aircraft and power to climb or descent. During the climb phase, most power is needed to climb the aircraft, while in cruise, which is done at a constant altitude, this power is equal to zero and only power is needed to overcome the drag created by the aircraft. During the descent, the climb power becomes negative, meaning this power can be used for energy regeneration. Only

during the transition between the flight phases the aircraft is accelerated or decelerated. Only during these transitions flight power for acceleration is needed or available.

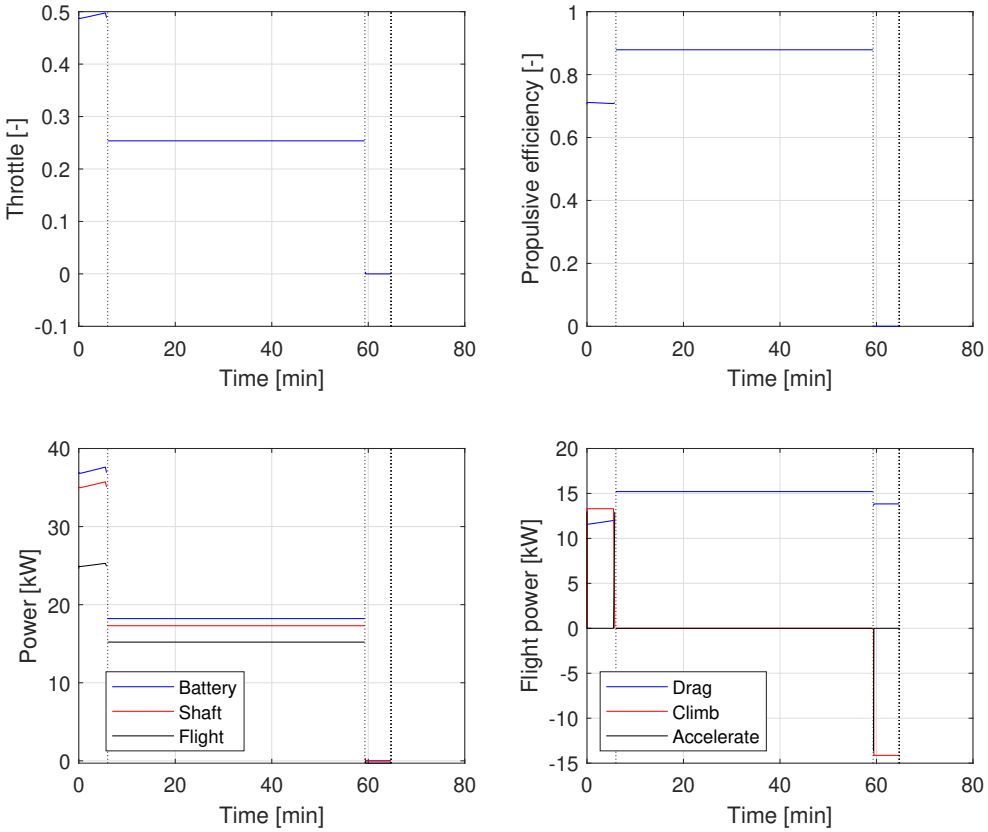

Figure 4.8: Energy conversions of the drive-train of the modeled Pipistrel Alpha Electro

To perform the whole mission as described, a total of $19.9kWh$ is required. When also the energy for take off and landing, and the minimum state of charge of the battery is taken into account, this means that the battery needs a total capacity of $26.3kWh$, resulting in a battery mass of $131kg$, which is 21.3% of the total aircraft weight. From the statistical methods to determine the operational empty mass (OEM) of the aircraft, it is found that 45.3% of the total aircraft mass is allocated to the OEM of the aircraft, as shown in figure 4.9.

The sized aircraft is modelled such that it is expected that the results are representing the *Pipistrel Alpha Electro*. Therefore, the results are compared with this aircraft, as given in the first three columns of table 4.3. Both the absolute difference and percentage difference of the calculated parameters compared with the reference values are given. The results show that the initially simulated aircraft consistently shows higher mass and energy required to perform the mission, compared to the reference aircraft by about 10 to 20 percentage points.

Especially the battery mass and energy are almost a quarter higher than the reference value. This means that the simulated aircraft is calculated to require more energy than the actual aircraft needs to perform the given mission. Multiple reasons can be given for this overestimation of the required power for the mission.

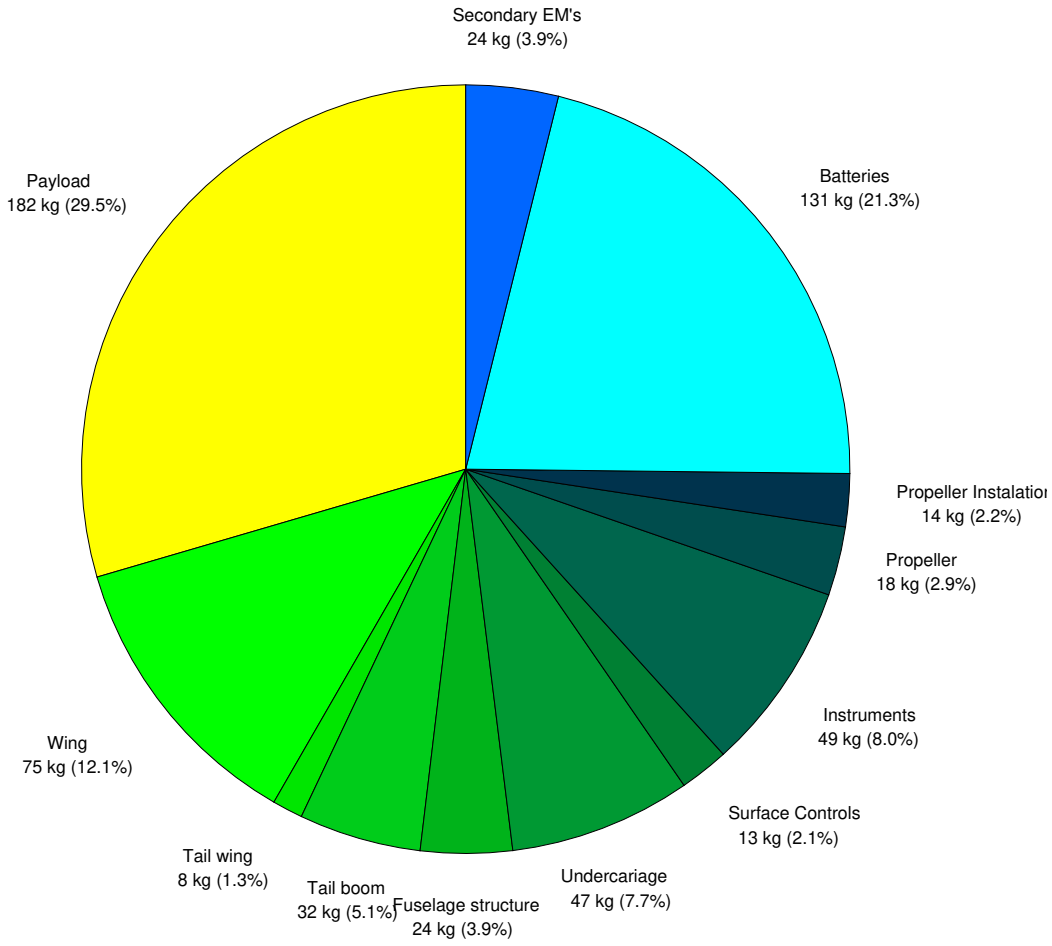

MTOM = 616.3kg, OEM = 279.1kg, S_w = 10.6 m^2, P_{EM} = 71.8 kW, E_{bat} = 26.3 kWh
(Battery sized by energy requirements)

Figure 4.9: Weight breakdown of the complete aircraft mass of the modeled Pipistrel Alpha Electro

First of all, the drag polar of the aircraft, which determines the drag during the whole simulated mission, had to be estimated from statistical methods. These methods are dating from before 1982, while this aircraft has been introduced in 2015. Therefore, due to new production- and analysis methods, the drag of the aircraft might be lower than can be expected from the statistical analysis. Unfortunately, this cannot be checked since no actual flight data of the aircraft is present.

Furthermore, the propeller performance data of the aircraft is also not available. Even the geometry of the propeller has to be estimated. This results in that the propulsive performance of the propeller during the several mission phases is estimated. Although, the propeller geometry is optimised during the sizing of the aircraft to maximise the time-weighted propeller efficiency, it might still be possible that the performance per flight phase is lower than the actual aircraft.

Finally, also the design mission of the *Pipistrel* aircraft is not exactly known. It is known that the aircraft is designed as a trainer aircraft, which has high climb performance. Although the cruise range of the aircraft is given, it is not known what the cruise altitude or the optimal climb angle or speed is. Therefore, these parameters are also estimated during the aircraft sizing mission.

Table 4.3: Comparison of the sizing parameters of the reference aircraft, the initial sized aircraft using the sizing tool and the aircraft with a scaled specific energy density of the battery.

Param.	**Reference**	**Initial**	**% diff.**	**Scaled**	**% diff.**
$W/S\ [N/m^2]$	567.4	568.9	0.3%	568.9	0.3%
$W/P\ [N/W]$	0.0899	0.0842	-6.3%	0.0853	-5.0%
$TOM\ [kg]$	550	616.4	12.1%	563.4	2.4%
$OEM\ [kg]$	242	279.1	15.3%	260.5	7.6%
$M_{bat}\ [kg]$	106	131.3	23.8%	99.2	-6.4%
$M_{EM}\ [kg]$	20	23.9	19.7%	21.6	8.0%
$S_w\ [m^2]$	9.51	10.6	11.8%	9.7	2.2%
$E_{bat}\ [kWh]$	21	26.3	25.0%	23.8	13.4%
$P_{EM}\ [kW]$	60	71.8	19.7%	64.8	8.0%
$R\ [km]$	138.9	138.9	0.0%	138.9	0.0%

It is known that the aircraft sizing tool overestimates the energy required for the *Pipistrel Alpha Electro* during the sizing of the aircraft. Therefore, also the battery mass and the whole aircraft mass is overestimated. To see how the sizing tool performs when the battery mass is more accurately given, the specific energy and power is increased by 20%. In this way, the increased energy requirement of the aircraft is compensated, and a more accurate battery mass is expected. From this new, scaled, battery mass the weight of the other aircraft are then compared with the actual aircraft to see if there is an agreement. The scaled results are also shown in table 4.3.

From the results it can be seen that the battery energy is still overestimated, however the difference has become smaller. The battery mass is now slightly underestimated, resulting in a lighter aircraft. This reduction in aircraft mass has also reduced the energy requirement for the

aircraft, resulting in the lower overestimation of the battery energy.

The total aircraft mass and the operational empty mass are now estimated within 10% of the reference aircraft, which is within the expected accuracy of a Class-I weight estimation. Therefore, it is found that the sizing tool, when corrected for the overestimated energy usage, calculates the weight distribution as can be expected from a conceptual design method. Also, for the remaining of the research it is found that the energy overestimation should not impose any problems, since different simulations will be compared to each other to find the performance increase when the regenerative mode is used. This overestimation of the required energy will be present for all simulations and does not influence the analysis. However, when comparing the simulations to the real world, care has to be taken since the energy required to perform the mission is overestimated.

4.2. Propeller Performance Model

The propeller performance model that is created using a BEM model is validated using a wind-tunnel experiment performed at the TU Delft [12]. In this experiment the thrust and power coefficient of a known propeller geometry were measured in the *Low Speed Low Turbulence* wind tunnel of the TU Delft. These measurements were taken at predetermined operating points, such that the Reynolds number at 70% of the blade radius will be approximately 200.000 for each measurement.

The same propeller geometry, with the same airfoil, is modelled in the propeller performance model. This geometry is then analysed at the same operating points as described in the experiment report [12]. The operating points that are used are shown in figure 4.10.

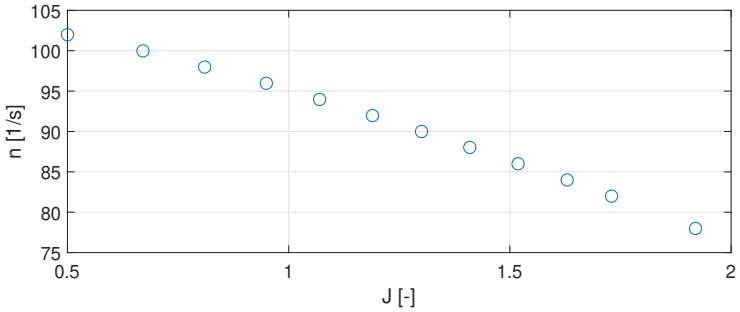

Figure 4.10: Operating points of the propeller during the wind tunnel experiment.

To simulate the thrust and power coefficient, first the lift- and drag curves of the airfoils are determined at a Reynolds number range of 60.000 to 300.000. These curves are then used to determine the correct lift- and drag coefficient at a specific angle of attack and Reynolds number. Some of these polars are given in figure 4.11. The polars for the root, middle and tip airfoil are given for both the lowest and highest expected Reynolds number during the experiment.

In the wind tunnel test, the data is also compared with $XROTOR$ simulation. Similar simulations are also performed with the propeller performance model. However, in this model also Snel's

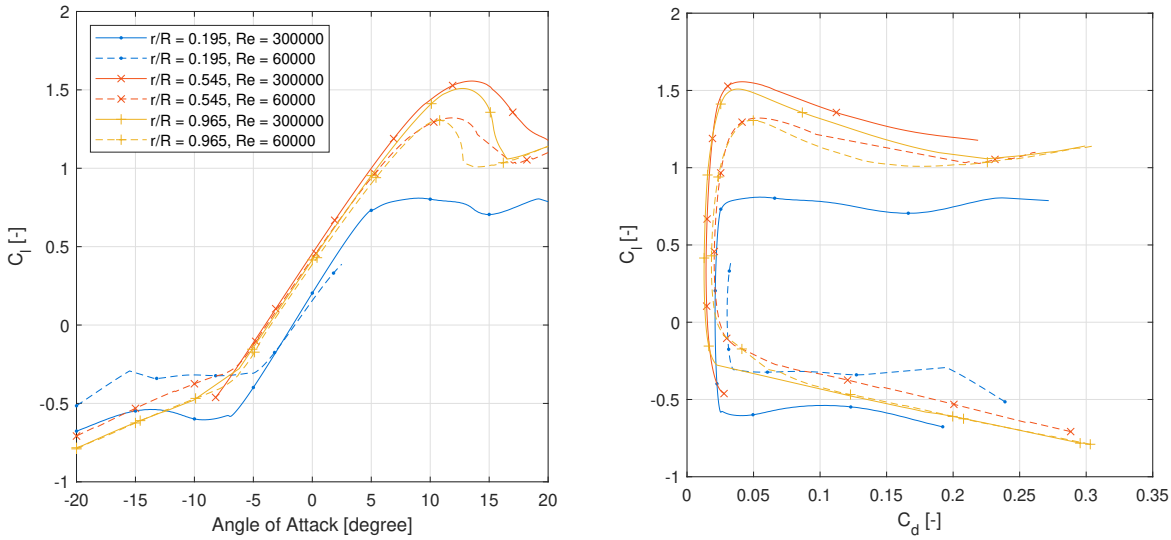

(a) (b)

Figure 4.11: Calculated airfoil polars of the propeller as calculated using $XROTOR$.

correction factor is applied in the determination of the lift- and drag coefficient. To make sure the correct propeller model is simulated, the simulation is both performed with and without the Snel's correction factor.

From the measurement data from the wind tunnel experiment [12] and the simulations, the thrust and power coefficient can be calculated using equations (4.13) and (4.14). This results in the graphs as presented in figures 4.12a and 4.12b

$$T_c = \frac{T}{qA_{disk}} \qquad (4.13) \qquad P_c = \frac{P}{qA_{disk}V} \qquad (4.14)$$

From the graphs, it can be seen that both the thrust and power coefficient follow a similar trend compared to the experimental data. However, for advance ratios higher than 1, where the propeller enters the regenerative mode, it can be seen that the simulation underpredicts the produced (negative) thrust and power. The error for each operating point between the simulations and the experimental data is shown in figures 4.13a and 4.13b.

Also here, the underprediction of the thrust and power coefficient in the simulations for high advance ratios can be observed. This is similar to the results as observed in [12]. Most likely this difference is caused by the difference in the two-dimensional stall at a negative angle of attack of the airfoil as calculated by $RFOIL$, and the actual negative stall angle of attack during the experiment. As can be seen, the Snel's correction method reduces the error up to 20 percentage points when this correction is applied.

The stall for negative angles of attack is not correctly estimated by $RFOIL$ for positive cambered airfoils, as is the case for this propeller geometry. Therefore, for highly negative angles of attack, lower than $-10°$, the lift and drag coefficient are not correctly modelled anymore. These angles of attack occur however at some locations on the blade at advance ratios higher than 1.

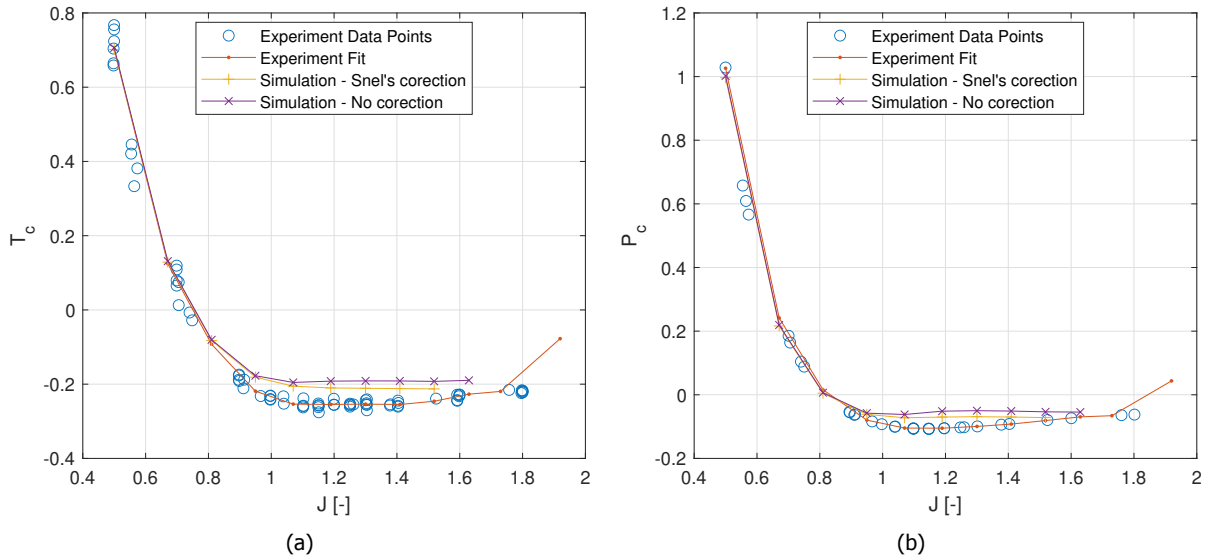

Figure 4.12: Comparison of the thrust (a) and power (b) coefficient between simulation and experiment.

So, the difference between the simulated data and experimental data is most likely caused by an incorrect prediction of the lift and drag coefficient at negative angles of attack. This prediction can be improved by applying Snel's correction method, but better lift and polar curves are required for better predictions. Unfortunately, these improved lift and drag curves can currently not be created for these airfoils, so this cannot be checked. However, when the airfoil polars can be predicted accurately, also the performance model can both predict the propulsive and regenerative performance of the propeller within the required accuracy.

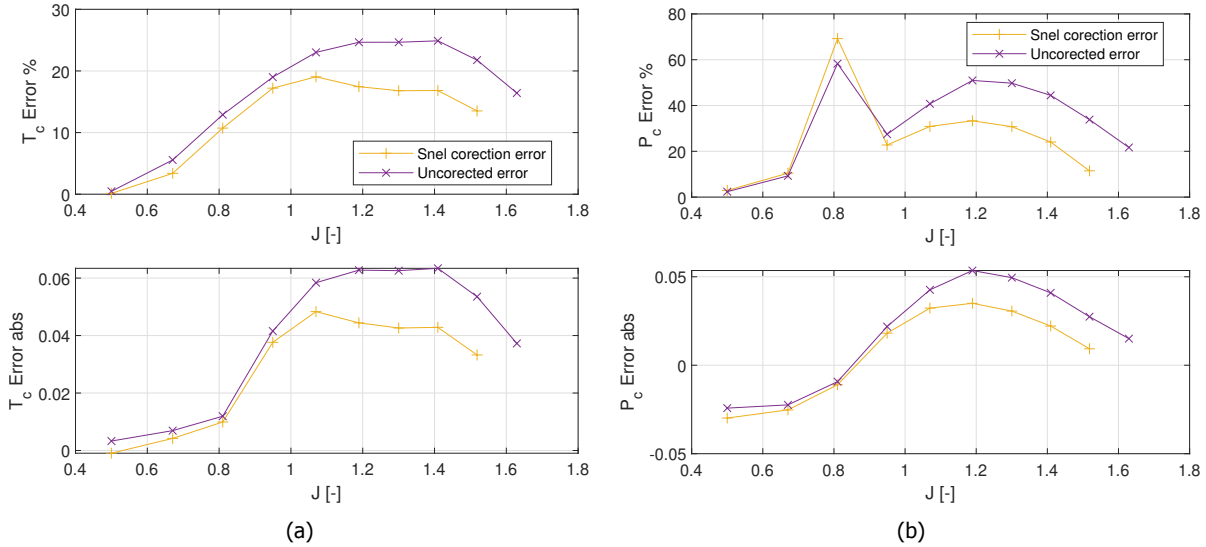

Figure 4.13: Error between the thrust (a) and power (b) coefficient between simulation and experiment.

4.3. Regenerative Flight Model

The regenerative flight model combines the propeller performance model and the descent phase of the mission analysis. The propeller performance model is able to calculate the efficiency for a given (negative) thrust setting, and therefore how much shaft power is available, while the mission analysis is used to calculate the required negative thrust.

To find if the regenerative model gives a realistic estimation of the regenerated energy, the regenerated energy from the analysis is compared to the energy regenerated during the flight test as performed by Erzen et al. [17]. During these flight test multiple propellers are fitted on the *Pipistrel Alpha Electro* to find the optimal propeller for in-flight energy regeneration, as earlier shown in figure 1.1.

Since the *Pipistrel Alpha Electro* is also used for the validation of the sizing model, the same aircraft design will be used to perform the validation of the regenerative flight model. However, this time the descent profile will be changed, such that is it matching with the performed experiment. It is expected that for a properly working regenerative flight model, the simulated regenerated energy is equal to the actual found energy that can be regenerated. In contrary to what happens within the sizing model, where an aircraft and propeller are simultaneously sized, during the experiment the same aircraft is being used with different propellers designs. Three propeller designs are used during the experiment: the original propeller, which was designed for the fuel burning version of the *Pipistrel Alpha*, a cruise propeller that is designed for the electrified version, the *Pipistrel Alpha Electro*, and a propeller that is designed for the regenerative phase of the mission. The regenerative performance results of the experiment using the propeller that is designed for the electrified version, but not designed for the regenerative mode, of the *Pipistrel Alpha* is used for the validation. This is done, since the simulated aircraft that is used for the validation, is also not optimised for the regenerative flight phase.

The experiment was performed by performing a constant power climb, at $45kW$, to an altitude of $1000ft$ at a speed of $76kts$ in $85s$, which results in a climb angle of $5.26°$. Directly after the target altitude is reached, the throttle is set to idle to start the descent. This descent is performed at a constant speed of $80kts$. The descent is performed in $74s$, resulting in an average rate of descent of $811ft/min$. This mission is also modelled for the aircraft, as sized during the validation of the sizing model. The results of the experiment and simulation are shown in table 4.4.

Table 4.4: Comparison of the 'climb and descent mission' for the experiment with the Pipistrel Alpha Electro and the simulated aircraft.

	Climb Time [s]	**Energy Used [kWh]**	**Recuperation Power [kW]**	**Descent Time [s]**	**Recuperated Energy [kWh]**	**Net. Energy [kWh]**
Experiment	85	1.06	-1.7	74	-0.03	1.03
Simulation	85	1.05	-2.2	74	-0.046	1.00

The climb part of this 'climb and descent mission' is modelled such that the time to climb is equal to that of the experimental mission. This results in a $44kW$ powered climb, which turns out to

be $1kW$ lower than is seen in the experiment. Therefore, the energy is also lower. This could be the result of the different propeller geometries as calculated for the simulation and as used in the experiment, where the simulated propeller has a higher climb efficiency than is seen in the experiment.

The descent phase is modelled such that the descent time is exactly equal to that of the experiment, resulting in that these two times are the same for both the simulation and the experiment. The energy that is regenerated is different for both missions, where the simulated mission has a higher regeneration energy of $0.016kWh$ than is observed in the experiment. Again, this could be a result of the difference in propeller geometry, where the simulated propeller has better regenerative performance. However, the simulated aircraft is also slightly heavier than the actual aircraft. This results in that for the same descent trajectory, the heavier aircraft has to generate more negative thrust, and therefore is also able to regenerate more power. Also, it assumed that the same efficiency of 95% for the drive-train can be used for the regenerative mode, however for charging the batteries this efficiency can be lower.

The total net energy difference is 2.9% lower for the simulated aircraft than for the actual aircraft, since this is again within the range of which the sizing model and regenerative model is expected to work, the models are accepted to work as expected.

5

Baseline Mission Definition

The aircraft sizing tool in combination with the propeller performance tool as described in chapter 3 is able to size an aircraft and propeller based on its input parameters, the top level aircraft requirements ($TLARs$). To answer the research question, not every $TLAR$ is investigated, but three topics are chosen to determine the effect of the regenerative mode on the aircraft performance, weight and propeller geometry. The first topic of interest is the influence of the descent strategy on the descent performance, propeller geometry and total aircraft design. The analysis of the descent strategy is given in chapter 6. Also, the propeller input parameters are inspected, where the interest is on the camber of the propeller airfoil and its effect on the regenerative performance of the aircraft. This analysis is given in chapter 7. Thirdly, in chapter 8, the analysis for the aircraft design mission profile is presented, where mainly the difference in total range is examined. However, first the definition of the baseline mission is given below.

The three analysis cases are every time based on variations made on the same baseline missions. These baseline missions are based on the same aircraft mission inputs that were used during the validation of the sizing model, as given in section 4.1. However, for the baseline mission the aircraft is allowed to regenerate energy during the descent phase. During the validation it was found that for no thrust, the minimum drag speed is already exceeded (with $1.5 m/s$) for the given descent strategy. Therefore, by allowing regeneration, the aircraft is able to fly at the exact given descent strategy, with the predetermined flight speed and rate of descent. Since the descent of the validation mission is an unpowered descent, this does not make any large changes to the design however. The inputs for the baseline mission are given in table 5.1.

Table 5.1: Mission inputs for the calculated baseline missions.

Parameter	**Value**	**Unit**
Mission Range	75	NM
Cruise Altitude	750	m
Cruise Speed	75	kts
Climb Angle	5	$^\circ$
Climb Speed	25.2 (Min. Power)	m/s
Descent RoD	460	ft/min
Descent Speed	32.7 (Min. Drag)	m/s

For the propeller blade design, also the same inputs are used as for the validation mission. This means, a propeller blade with a radius of $0.9m$ is designed, where a total of 3 blades are used on the propeller. The airfoil on the blades is assumed to be constant, where the *Clark-Y* airfoil is used.

From the validation, it is known that these baseline mission profile and propeller design inputs result in an overestimation of the mission energy required. Therefore, the designed aircraft of the baseline mission is also based on the same over-prediction of the energy requirement, since for these missions the specific energy of the battery is not scaled. This should however not impose any problems for the comparison between the sized aircraft, since the analysis results are only compared with each other.

The validation of the sizing model was only performed for a fixed pitch (vR) propeller design. However, an aircraft for the same mission profile is also sized and its performance is calculated for a variable pitch ($vRvP$) propeller. These two aircraft designs are considered the two baseline missions which will be used for the different analysis cases. The two baseline missions are calculated and summarized below, where the simulation results of the fixed pitch propeller aircraft are compared to the results of the variable pitch propeller aircraft.

First, the mission profile for both sized aircraft is given in figure 5.1. Since the same baseline mission is used as the validation mission, this mission is exactly equal to the baseline mission. Furthermore, since the mission does not change for the two sized aircraft, both missions are also the same.

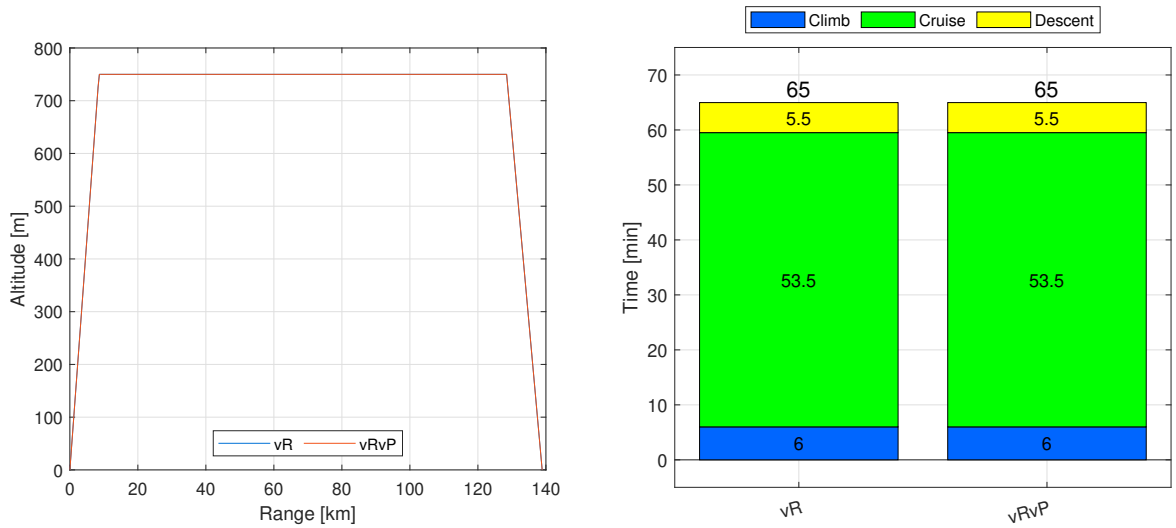

Figure 5.1: Mission profile (a) and time distribution (b) of the two baseline simulations for the fixed pitch propeller (vR) and variable pitch propeller ($vRvP$).

The aircraft mass distribution and energy consumption per flight phase is given in figure 5.2. Here it can be seen that the variable pitch propeller has a slightly reduced energy consumption ($1MJ$, which is a reduction of 1.3%) for the baseline mission, compared to the fixed pitch propeller. The variable pitch propeller does increase the propeller efficiency both during the cruise and climb

phase, resulting in a lower overall energy requirement. This reduced energy requirement results in a lower battery mass to store this energy, and therefore also resulting in a slightly lower total aircraft mass.

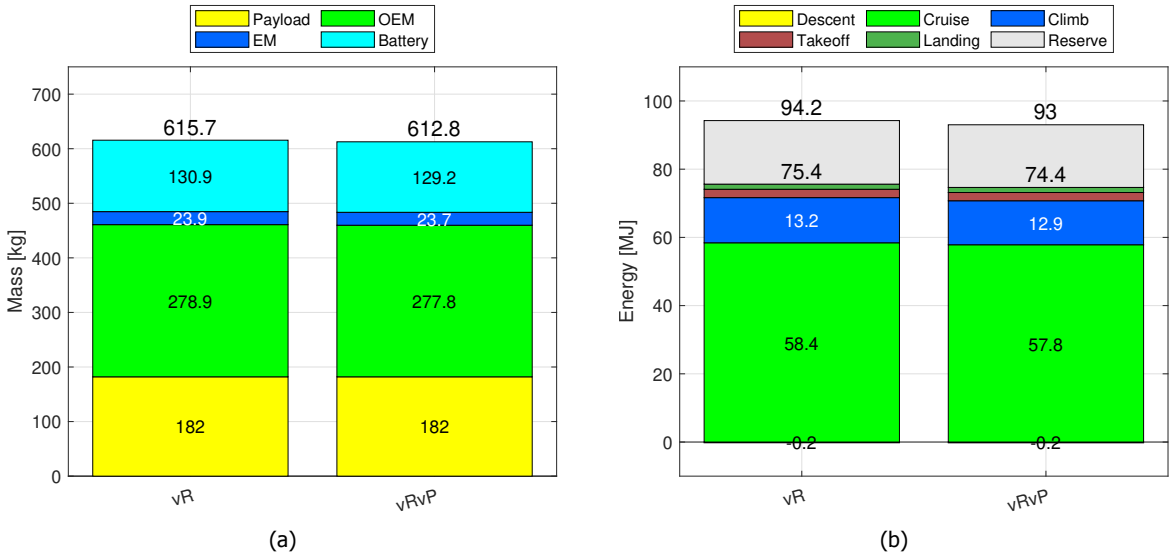

Figure 5.2: Mass (a) and energy (b) per flight phase breakdown of the two baseline simulations for the fixed pitch propeller (vR) and variable pitch propeller ($vRvP$).

The two propeller blade geometries for the baseline missions are shown in figure 5.3. The fixed pitch propeller has an increased chord length, resulting in a higher solidity, as shown in table 5.2. The variable pitch propeller is able to be more efficient, while still producing the required thrust, with a lower solidity of the propeller since it can change the pitch setting of the propeller blades to optimise the performance of the blades.

Table 5.2: Propeller solidity of the two baseline simulations for the fixed pitch propeller (vR) and variable pitch propeller ($vRvP$).

	vR	**vRvP**
Solidity	0.054	0.043

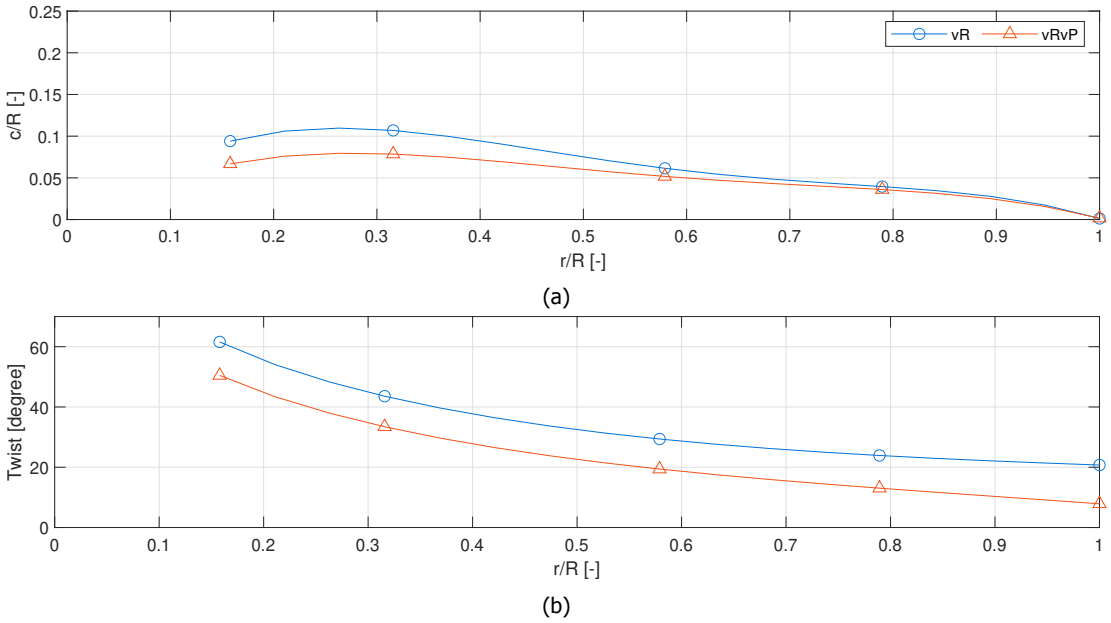

Figure 5.3: Propeller blade chord (a) and twist (b) distribution of the two baseline simulations for the fixed pitch propeller (vR) and variable pitch propeller ($vRvP$).

6

Descent Strategy Analysis

From the experiment used during the validation of the regenerative flight model it is already found that the descent profile has a large influence on how much energy can be regenerated by the aircraft [17]. To find the importance of the descent strategy on the regenerated energy and the total aircraft design, modifications to the baseline mission are made. First in section 6.1 an overview of the simulation cases that will be analysed is given, after which in section 6.2 the results of these simulations are given. Due to the large number of data points per simulation not all the details are given in this chapter, but only the results that are interesting for the respective analysis. When one is interested to see the details of each simulation, appendix A can be consulted. Finally, the results are discussed in section 6.3.

6.1. Simulation Case Studies

The descent phase analysis is always performed at a constant speed and descent rate for the whole descent phase, resulting in that the descent angle is also constant. In figure 6.1 the three parameters that define the descent strategy are shown. To find the influence of the descent strategy, these three parameters can be changed to make changes to this descent strategy.

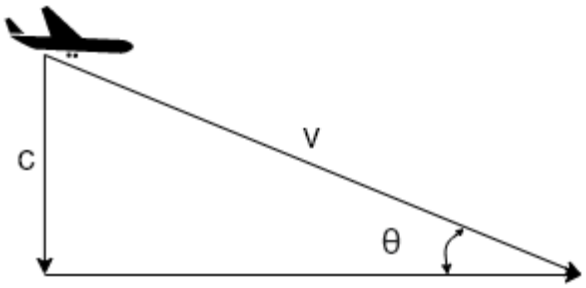

Figure 6.1: Velocity vectors in the descent phase of the aircraft.

The different simulation cases are defined in such a way that each time two parameters of the descent strategy are step-wise altered and investigated, while keeping the last variable constant. Also all the other parameters of the baseline mission are kept constant. For these changed parameters the complete convergence of the sizing loop is performed, resulting in that the found aircraft mass, mission, energy requirement, propeller geometry, etc. are sized for the specific

mission inputs. Furthermore, the analysis will be performed for the same type of propeller as the validation mission, the variable RPM, fixed pitch propeller, but also a propeller design of a variable RPM, variable pitch propeller is analysed. This will show how the variable pitch affects the propeller geometry, and therefore the whole aircraft.

The descent strategy is fixed for each sized aircraft. Therefore, the (negative) thrust that needs to be produced by the propeller is also calculated from the descent strategy. If a propeller geometry is not able to produce the required (negative) thrust, the propeller geometry is updated by the propeller optimisation algorithm such that the (negative) thrust can be achieved. Therefore, the propeller will be sized such that the given mission profile (and thus also the descent phase) can be performed, as explained in section 3.2.4.

6.1.1. Fixed Flight Speed, Variable Rate of Descent and Descent Angle

For the descent analysis with a fixed flight speed, the rate of descent is varied to see the effect on the aircraft sizing.

For the rate of descent, a total of six different rates are analysed to find the effect of the rate of descent on the descent performance, while the airspeed is kept constant at the minimum drag speed of the aircraft, which is $32.7 m/s$. The descent rate is both increased and decreased compared to the baseline value. For better comparison, the values are given in fractions of the baseline value. As shown from the velocity vectors in the descent phase, this means that the descent angle is also changing for the different rate of descent values. An increased rate of descent will thus lead to a higher descent angle, while a reduced rate of descent corresponds to a lower descent angle.

Table 6.1: Simulation inputs for the fixed flight speed analysis, where the rate of descent is varied and the baseline mission underlined.

Simulation	**1**	**2**	**3**	**4**	**5**	**6**
Baseline fraction	0.5	0.75	1	1.25	1.5	2
RoD $[ft/min]$	230	345	460	545	690	920
Descent Angle [°]	2.0	3.1	4.1	5.1	6.2	8.2

6.1.2. Fixed Rate of Descent, Variable Flight Speed and Descent Angle

For the fixed rate of descent analysis, the same type of analysis is done as with the fixed flight speed analysis. However, this time the flight speed is varied, while the rate of descent (RoD) is kept constant. The variations in flight speed are based on different optimal flight speeds. This results in the following values, as shown in table 6.2: the minimum (airframe) power required speed, the speed of 1.2 times the stall speed, the speed for minimum drag and finally a descent speed which is equal to the cruise speed. The RoD is kept constant at the baseline value of $460 ft/min$, while the descent angle follows from the flight speed and RoD.

Table 6.2: Simulation inputs for the fixed rate of descent analysis, where the flight speed is varied and the baseline mission underlined.

Simulation	**1**	**2**	**<u>3</u>**	**4**
Descent Speed	v_{minP}	1.2 v_{stall}	v_{minD}	v_{cr}
v $[m/s]$	25.2	27.8	32.7	37.1
Descent Angle [°]	5.2	4.8	4.1	3.6

6.1.3. Fixed Descent Angle, Variable Rate of Descent and Flight Speed

The final descent strategy analysis is performed such that the aircraft descent is performed at a fixed descent angle of $4.1°$ for the different simulations, while varying the flight speed again. In this case, the RoD follows from the two other parameters for the different simulations. The set flight speed is chosen to be a fraction of the minimum drag flight speed, as shown in table 6.3. The flight speed is both reduced compared to the minimum drag speed, with the descent flight speed down to 80% of the minimum drag speed, and increased compared to the minimum drag speed. The highest descent speed that is used for this simulation is 120% the minimum drag speed.

Table 6.3: Simulation inputs for the fixed descent angle analysis, where the flight speed is varied and the baseline mission underlined.

Simulation	**1**	**2**	**<u>3</u>**	**4**	**5**
Baseline fraction	0.8	0.9	1	1.1	1.2
v $[m/s]$	26.1	29.4	32.7 (v_{minD})	35.9	39.2
RoD $[ft/min]$	368	414	460	506	552

6.2. Simulation Results

The descent strategy analysis consists of two parts, the variable RPM, with a fixed pitch propeller and the case where the propeller is variable RPM and variable pitch. First, the analysis for the variable RPM, fixed pitch propeller will be given. This is also the same type of propeller as calculated for the validation mission. Afterwards, an analysis will be performed to see how a variable RPM, variable pitch propeller changes the analysis.

6.2.1. Variable RPM, Fixed Pitch

For the variable RPM, fixed pitch propeller a total of three different analyses are performed, the first analysis is the descent analysis for fixed flight speed, while varying the rate of descent. Secondly, the analysis will be performed for a fixed rate of descent, with a varying airspeed and finally the descent angle will be fixed and the descent airspeed will be varied.

1. Fixed Flight Speed

For the fixed pitch propeller, a total of five simulations are performed, where the rate of descent is changed while keeping the airspeed during the descent equal. The highest rate of descent of $920 ft/min$, with a rate of descent of two times the baseline value, did not converge to a consistent aircraft and propeller design. For this rate of descent, no propeller geometry could be found that is able to produce the required negative thrust during the descent, resulting in that this simulation is not added in the results.

The results of the five simulations for the mission profiles are given in figure 6.2a. Since the range of the mission is fixed to the reference value of $75 NM$, and a higher rate of descent means that the descent is covered in a shorter distance, the cruise distance needs to increase when the rate of descent is increased. This is also seen in the time per flight phase, in figure 6.2b. The higher the rate of descent, the longer the cruise time, where the difference between the lowest rate of descent and the highest rate of descent cruise time is equal to $9.3 min$, which is almost 15% of the baseline total mission time. The total flight time does however decrease with the increasing rate of descent, since the cruise is performed at a higher airspeed than the descent airspeed.

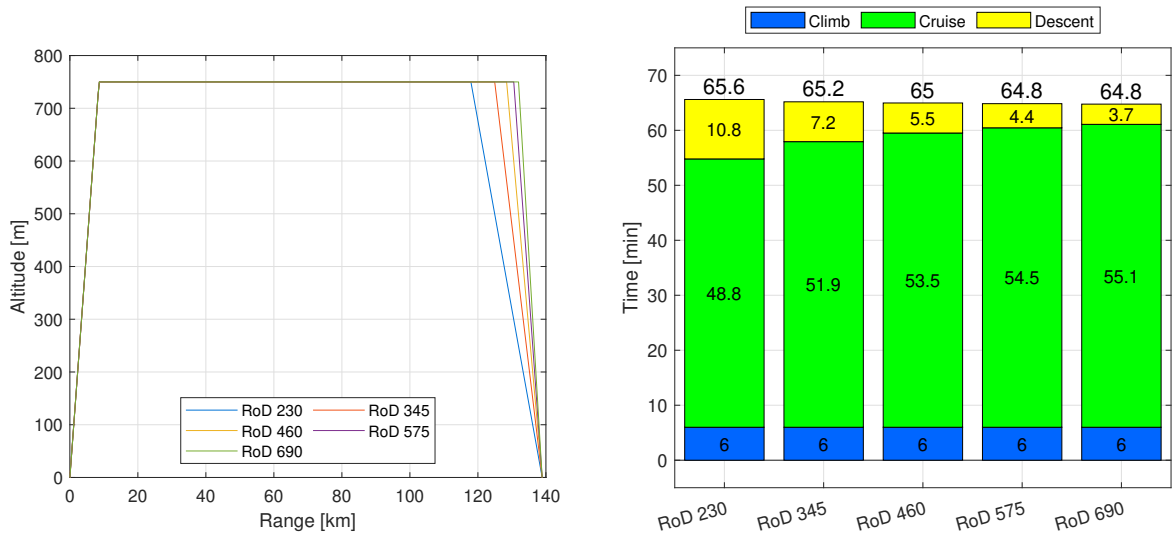

Figure 6.2: Mission profile (a) and time distribution (b) of the five simulations for the descent analysis with a fixed descent airspeed, but varying rate of descent.

The results of the descent performance of the missions are shown in figure 6.3. Since the shown descent strategies are performed at the same airspeed, the descent angle has to change with varying rate of descent. A higher rate of descent, at constant given airspeed, requires the aircraft to descent at a higher descent angle.

During the descent phase, the regeneration of energy is possible and therefore of the most interest to see if, and how much energy, can be regenerated by the aircraft. When the descent energy shows a value lower than 0 this is indicating that, instead of consuming energy during the descent, the aircraft is able to regenerate energy. It can be seen that the aircraft starts

regenerating energy at a descent angle of approximately $4°$, corresponding to a rate of descent of $460ft/min$, which is equal to the baseline value. Higher rates of descent, while keeping the descent speed equal, result in more regenerated energy, up to $1.3MJ$ for the highest descent angle and rate of descent combination. For lower descent angles, the aircraft has to deliver power to keep the aircraft at the prescribed airspeed, meaning that energy is used during the descent.

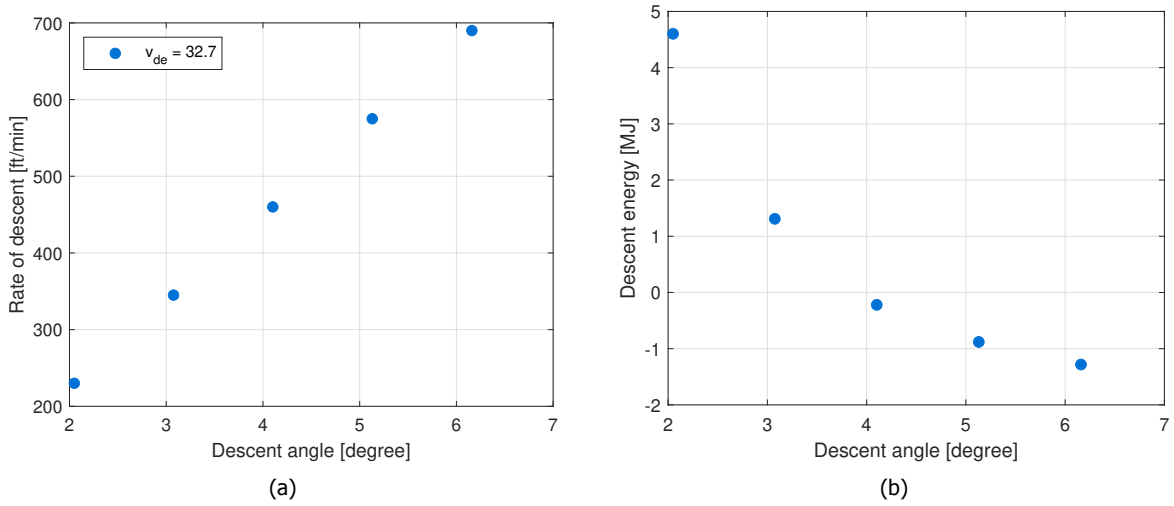

Figure 6.3: The descent strategy (a) and resulting (regenerated) descent energy (b) of the aircraft during the descent phase of the five simulations for the descent analysis with a fixed descent airspeed, but varying rate of descent with a fixed pitch propeller.

For each different analysis, the propeller and aircraft are sized to a consistent design. Hence, also the propeller geometry and aircraft weight breakdown change with the different given rates of descent. The mass breakdown and energy breakdown per flight phase are given in figure 6.4. Although the higher rate of descent strategy results in higher regenerated energy during the descent, this figure shows that the total energy consumption and aircraft mass also increase with higher rate of descent values, while keeping the descent speed constant. The highest rate of descent requires 9% more energy to complete the mission than the baseline mission, which results in a 3.5% increase in the aircraft mass. This might seem counter-intuitive, since one would expect that regenerating energy would result in a lower total energy consumption.

In table 6.4 a detailed breakdown of the energy usage per flight phase is given, while also showing the percentage of mission energy per flight phase. This breakdown shows that the heavier aircraft (with the highest rate of descent) does need more energy during the take off and climb phase of the mission, but the main difference in total energy usage is found in the cruise phase. Two reasons for this increase in cruise energy can be found. First, a high rate of descent means that the aircraft descents at a higher descent angle, thus covering less range during the descent. To reach the same range of $75NM$, the cruise distance has to be increased, meaning that more energy is used during the cruise phase, but also more distance is covered during this phase.

Secondly, due to the higher rate of descent, the propeller has to deliver more negative thrust to

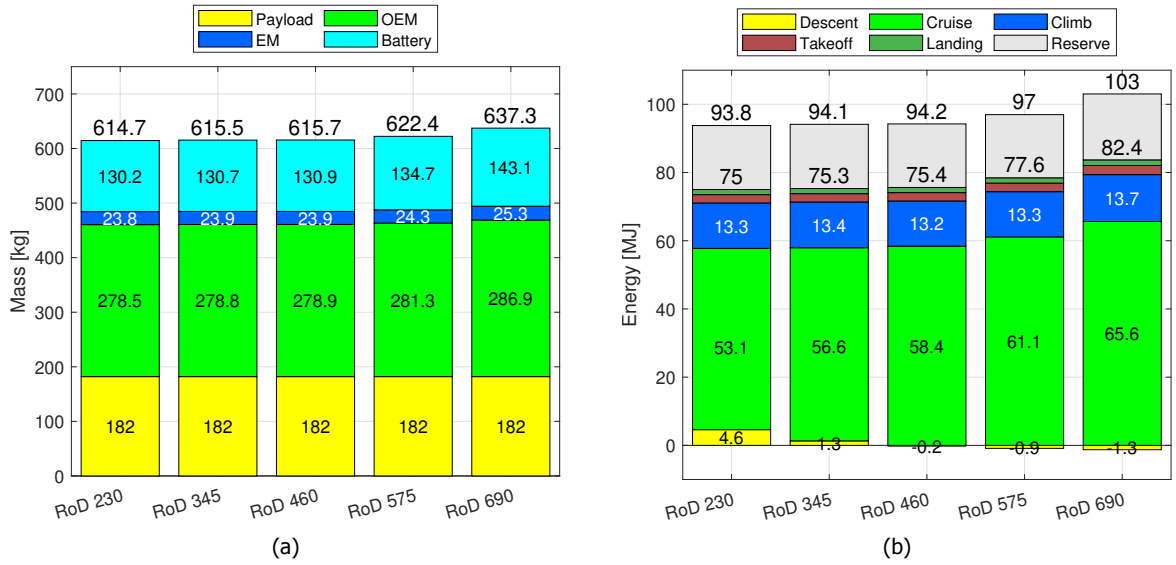

Figure 6.4: Mass (a) and energy (b) per flight phase breakdown of the five simulations for the descent analysis with a fixed descent airspeed, but varying rate of descent with a fixed pitch propeller.

Table 6.4: Energy usage per flight phase, including take off and landing, in MJ with in between parentheses the percentage of total mission energy given.

	RoD 230	**RoD 345**	**RoD 460**	**RoD 575**	**RoD 690**
Take off	2.4 (3.3%)	2.4 (3.3%)	2.5 (3.3%)	2.5 (3.3%)	2.7 (3.3%)
Climb	13.3 (17.8%)	13.4 (17.8%)	13.2 (17.6%)	13.3 (17.1%)	13.7 (16.7%)
Cruise	53.1 (70.8%)	56.6 (75.2%)	58.4 (77.5%)	61.1 (78.8%)	65.6 (79.6%)
Descent	4.6 (6.1%)	1.3 (1.7%)	-0.2 (-0.3%)	-0.9 (-1.1%)	-1.3 (-1.5%)
Landing	1.5 (2.0%)	1.5 (2.0%)	1.5 (2.0%)	1.6 (2.0%)	1.6 (2.0%)

make sure the aircraft does not speed up while descending at these high rates of descent. For a fixed pitch propeller, this means that the solidity of the propeller has to increase, making the propeller less efficient during the cruise phase. The propeller geometry for each mission is given in figure 6.5, while the calculated solidity from these geometries is given in table 6.5. Here it can be seen that for the three missions with the lowest rate of descent, the calculated propeller chord and twist do not differ from each other. However, for the higher rate of descent, the propeller chord is increasing, while the overall twist angle is reduced. Since the propeller is designed in such a way that the given descent strategy is flown, and thus the propeller has to deliver the negative drag during the descent, the propeller geometry has to adapt to this negative thrust during the descent. Since for the high rate of descent strategies more negative is required, the propeller solidity needs to increase for these descent strategies. When the propeller solidity has to increase to be able to deliver the required negative thrust during the descent, the propeller will be referred to as a 'negative thrust constraint' propeller design.

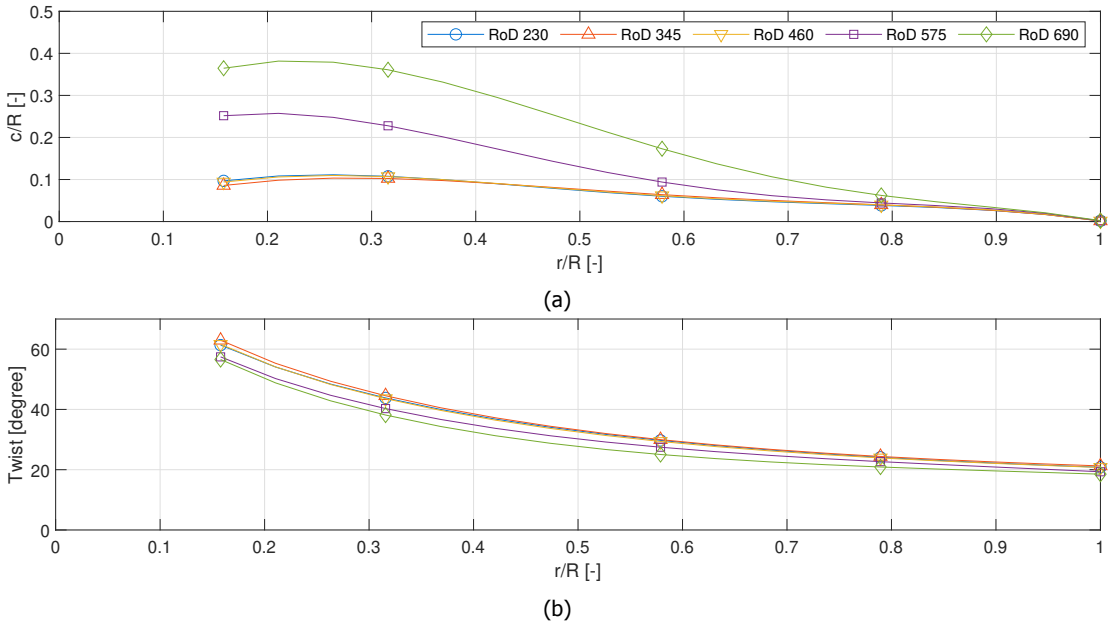

Figure 6.5: Propeller blade chord (a) and twist (b) distribution of the five simulations for the descent analysis with a fixed descent airspeed, but varying rate of descent with a fixed pitch propeller.

Table 6.5: Propeller solidity of the five simulations for the descent analysis with a fixed descent airspeed, but varying rate of descent with a fixed pitch propeller.

	RoD 230	**RoD 345**	**RoD 460**	**RoD 575**	**RoD 690**
Solidity	0.054	0.054	0.054	0.102	0.163

The efficiency of the propeller and the produced thrust during each flight phase is shown in figure 6.6. It can be seen that the increased solidity of the propeller (due to the increase in rate of descent) results in a decrease in the cruise efficiency. The highest cruise efficiency is found for the lowest rate of descent (which corresponds to the lowest descent angle), where the efficiency is equal to 87.9%, but decreases to 83.3% for the highest rate of descent.

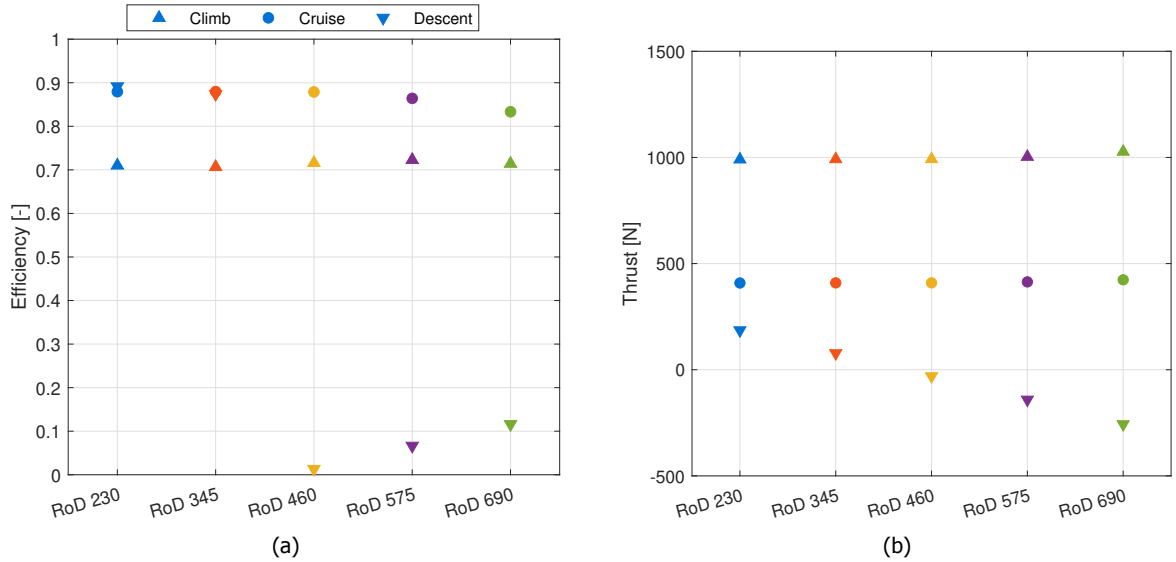

Figure 6.6: Propeller efficiency (a) and thrust (b) per flight phase of the five simulations for the descent analysis with a fixed descent airspeed, but varying rate of descent with a fixed pitch propeller.

The descent efficiency on the other hand shows two phenomena: for the descent strategies with positive thrust, the descent efficiency of the propeller is close to the efficiency of the propeller during the cruise phase. However, for the regenerative case, when the thrust has become negative the efficiency is calculated differently, as explained in chapter 3. Therefore, the efficiency is decreasing for an increase in rate of descent in the propulsive case, but the efficiency is increasing with increasing negative thrust. For the climb phase, the increase in solidity first has a positive effect on the efficiency of the propeller. However, when the solidity increases even more, and more thrust is needed for the climb phase due to the heavier aircraft, the climb propeller efficiency also decreases for an increase in the rate of descent.

2. Fixed Rate of Descent

Instead of keeping the airspeed constant, while making changes to the rate of descent the opposite is also possible: keeping the rate of descent constant for different airspeeds. Four different airspeeds are considered: the speed for minimum (airframe) power required, the speed which is 1.2 times the stall speed, the speed of minimum (airframe) drag and a descent airspeed equal to the cruise speed.

The descent phase is again summarised, with the results shown in figure 6.7. The rate of descent is kept constant, while the airspeed is changed. Although the mass flow of air through the propeller is increased when flying faster and thus more kinetic energy can be extracted from the air, less energy is regenerated when flying faster, while keeping the rate of descent constant. Two reasons can be identified that causes this contradiction. First, for the same rate of descent, the descent angle reduces when flying faster. This reduced descent angle results in a lower gravitational force along the body axis of the aircraft, resulting in lower negative thrust that is needed (or even positive thrust to keep the descent airspeed constant), which results therefore

in less energy that can be extracted from the air during the descent. Furthermore, the higher airspeed results in a higher drag force on the airframe of the aircraft, resulting again in that less negative thrust has to be produced by the propeller, to keep the aircraft on the correct (constant) airspeed, resulting in lower regenerative energy.

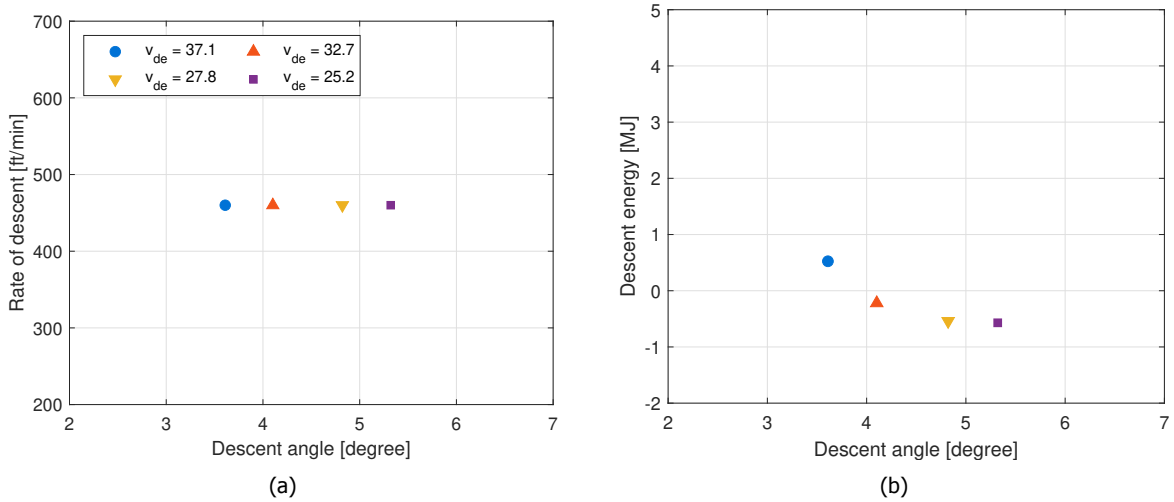

Figure 6.7: The descent strategy (a) and resulting (regenerated) descent energy (b) of the aircraft during the descent phase of the four simulations for the descent analysis with a fixed rate of descent, but varying descent airspeed with a fixed pitch propeller.

Similar to the previous analysis, the two descent strategies which regenerate the most energy (i.e. the slower descent airspeed strategies, corresponding to the higher descent angles compared to the baseline mission), also results in the highest overall energy usage, as shown in figure 6.8. This result is most likely due to the same reasons as for the fixed flight speed descent analysis: longer cruise distance (up to 1.9% increase) compared to the baseline mission and a lower propeller efficiency (up to 4.3% decrease) during the cruise phase when reducing the descent airspeed.

However, this time also speeding up compared to the baseline descent speed results in a higher total mission energy usage, which is an initially unexpected result since the cruise length is reduced for this descent strategy, resulting in less energy consumption during the cruise phase. However, it can be seen that although the cruise energy is reduced, the climb energy increases for the descent strategy with the highest descent airspeed, indicating that the propeller might not be optimal for the climb phase.

In figure 6.9 the efficiency of the propeller and the thrust per flight phase are given for the four simulations. The aircraft which is designed for the high descent flight speed is not able to regenerate energy during the descent. Due to the increased airspeed for the used fixed rate of descent, the drag on the airframe increases, resulting in that thrust is needed to keep the aircraft at the prescribed flight speed. The propeller geometry can therefore be optimised such that the propeller efficiency during the cruise is not constrained by the negative thrust the propeller has to deliver during the descent. This results in that the cruise efficiency for this propeller is 0.1% higher than the baseline cruise efficiency. However, at the same time, the climb efficiency of

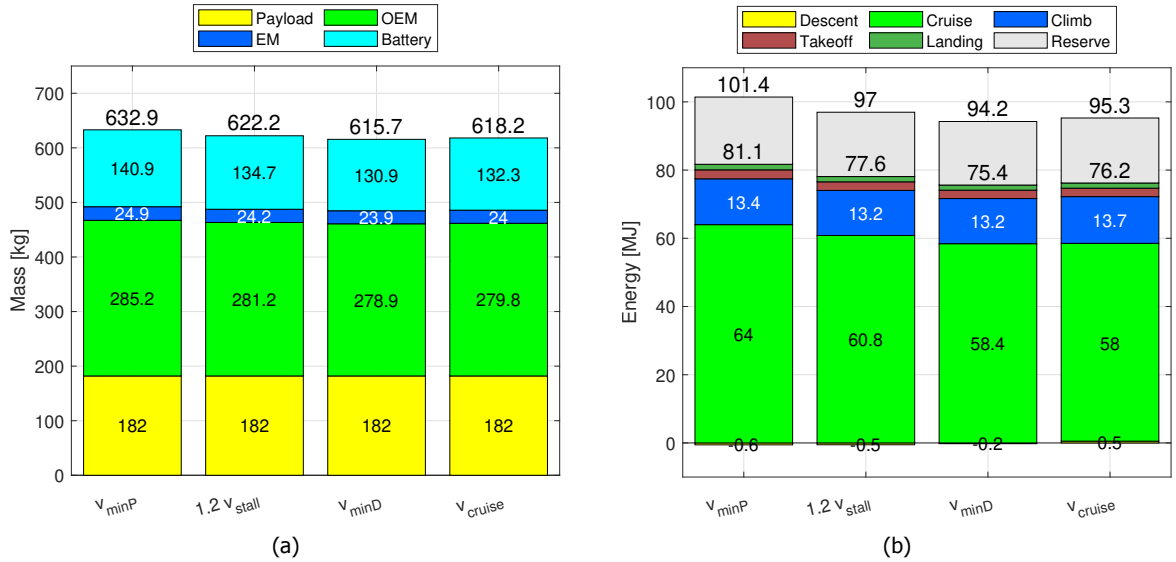

Figure 6.8: Mass (a) and energy (b) per flight phase breakdown of the four simulations for the descent analysis with a fixed rate of descent, but varying descent airspeed with a fixed pitch propeller.

this propeller is reduced by 2.9%. For the slowest descent speed strategy, an opposite effect is seen: the cruise efficiency is reduced by 4.3%, while the climb efficiency is increased up to 1.2% compared to the baseline mission.

As shown in figure 6.10, the propeller designed for the descent at cruise speed, which is the highest considered descent airspeed, has the lowest chord at the root of the propeller blade, while near the tip the chord is increased. The solidity is quantified in table 6.6. This results in a higher cruise efficiency, but the climb efficiency is reduced, resulting in a higher climb energy requirement. Since the long cruise time, compared to the lower climb time, the overall optimisation objective function is optimised in this way, as discussed in section 3.2. However, since the objective function only takes the propeller efficiency into account, and not the power setting or energy used during each flight phase, this optimisation of the objective function results in a higher overall energy usage for the aircraft. This is the effect of the optimiser objective function working differently than expected, where it was expected that an optimised time-weighted efficiency would also result in a minimisation of the overall energy usage, and therefore resulting in a higher total energy requirement for the descent strategy with the highest descent speed.

For the slowest descent speed, with the highest negative thrust, it is again seen that the propeller solidity is increased compared to the baseline mission. Also for this propeller, the negative thrust that has to be produced during the descent phase is causing the propeller chord to increase.

Table 6.6: Propeller solidity of the four simulations for the descent analysis with a fixed rate of descent, but varying descent airspeed with a fixed pitch propeller.

	v_{minP}	$1.2v_{stall}$	v_{minD}	v_{cr}
Solidity	0.106	0.080	0.054	0.054

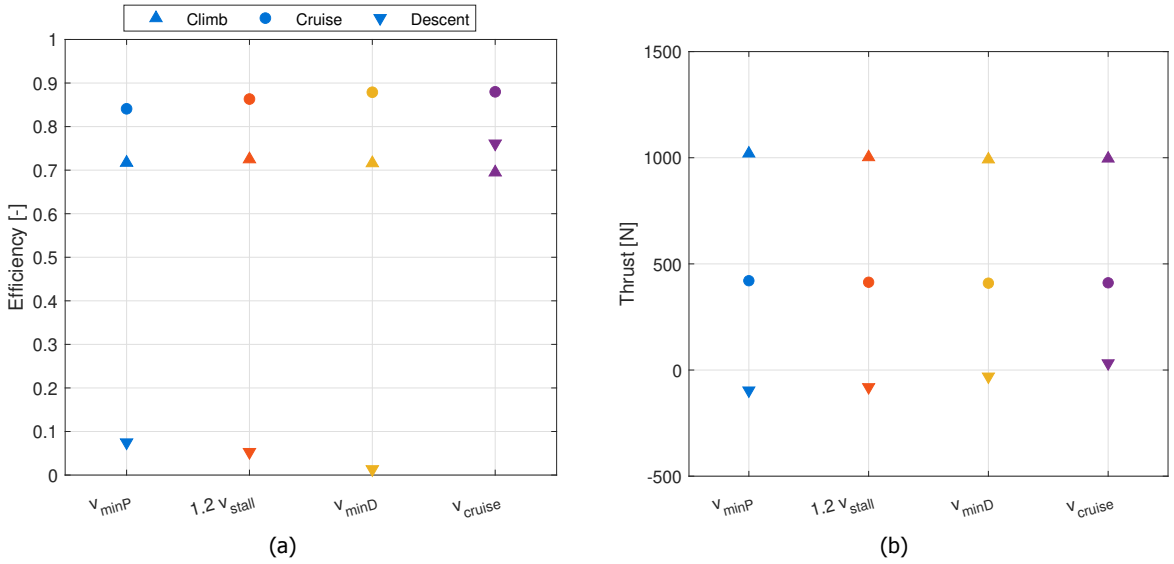

Figure 6.9: Propeller efficiency (a) and thrust (b) per flight phase of the four simulations for the descent analysis with a fixed rate of descent, but varying descent airspeed with a fixed pitch propeller.

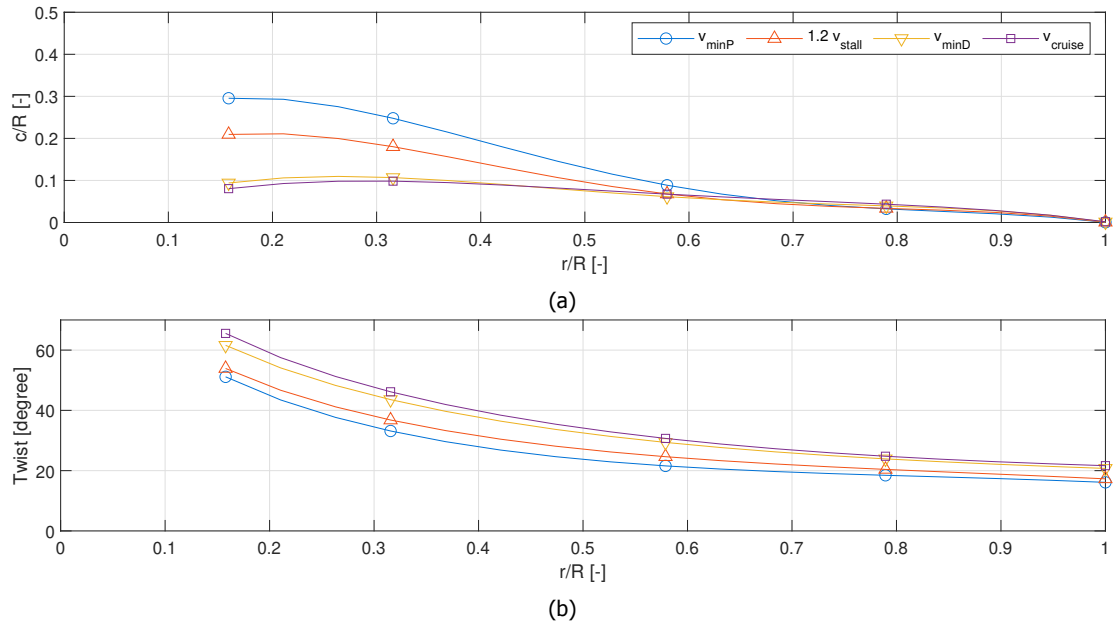

Figure 6.10: Propeller blade chord (a) and twist (b) distribution of the four simulations for the descent analysis with a fixed rate of descent, but varying descent airspeed with a fixed pitch propeller.

3. Fixed Descent Angle

The last descent analysis for the variable RPM, fixed pitch propeller is performed for descent strategies with a fixed descent angle, while varying the airspeed again. The rate of descent is thus the result of the given descent angle and airspeed. When increasing the airspeed to 1.2 times the baseline value, the descent speed would become higher than the cruise speed, which is deemed to be not feasible during nominal flight operations. Therefore, only the descent speed up to 1.1 times the baseline speed is used for the analysis.

The resulting (regenerated) descent energy is again shown in figure 6.11. For a constant descent angle, the most energy could be regenerated when flying at the minimum drag speed. Both flying faster and slower results in less energy regenerated during the descent phase, or even energy usage during the descent, since at the minimum drag speed the negative thrust that is required to be produced by the propeller is the highest.

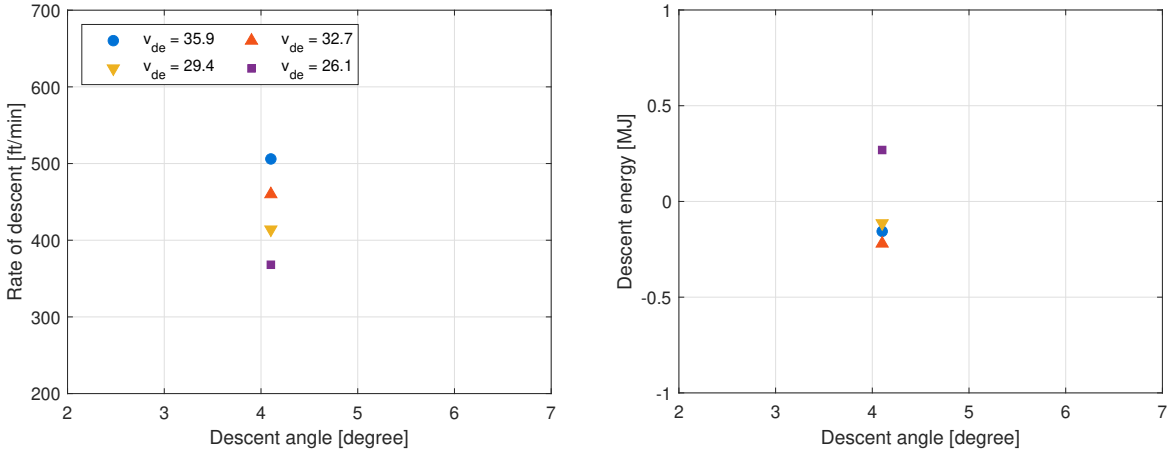

Figure 6.11: The descent strategy (a) and resulting (regenerated) descent energy (b) of the aircraft during the descent phase of the four simulations for the descent analysis with a fixed descent angle, but varying descent airspeed with a fixed pitch propeller.

Since the descent angle is kept constant, the cruise distance is also equal for all four simulations. Therefore, the difference in cruise energy used is smaller than for the previous analyses, as can be seen in figure 6.12, with the difference between the highest and the lowest cruise energy only $0.2MJ$. However, similar to the case for constant rate of descent the airspeed where the minimum total energy is used is the minimum drag speed. But also, the total energy usage differences are smaller than for the previous two analysis cases, with only $1.1MJ$ difference between the highest and lowest total mission energy.

When flying slower than the minimum drag speed, less airflow passes through the propeller. Thus, less power is available to regenerate, resulting in less regenerated energy. However, when flying faster than the minimum airframe drag speed, more airflow passes through the propeller, but also the drag on the airframe is increasing, and less negative thrust can be produced by the propeller resulting in lower regenerative propeller performance. This results in less energy that can be regenerated. So, for a given descent flight angle it is found that the best airspeed to

minimize the total aircraft mission energy is the minimum airframe drag speed. This does make sense, since at that speed the least energy is lost, resulting in that the propeller has to produce the highest negative thrust, and results thus in the highest flight efficiency. The effect of the regeneration mode at these descent strategies is very small, since the regenerated energy for all cases is less than $0.2MJ$.

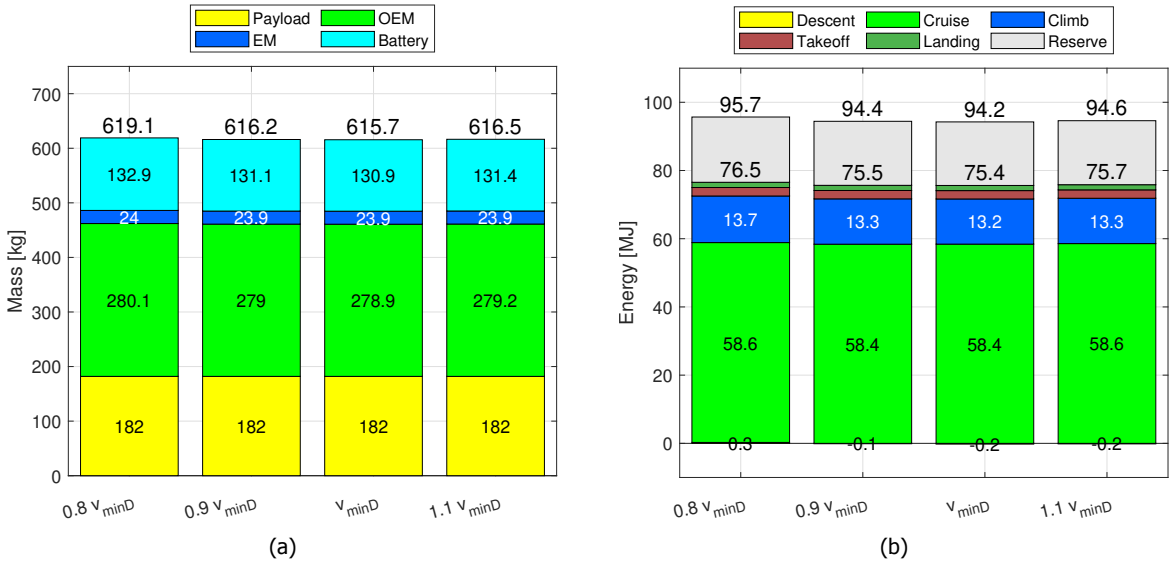

Figure 6.12: Mass (a) and energy (b) per flight phase breakdown of the four simulations for the descent analysis with a fixed descent angle, but varying descent airspeed with a fixed pitch propeller.

Also, the effect on the propeller geometry is smaller than for the other cases, as can be seen in figure 6.13. Since the differences in the descent strategy are not as large as for the previous two cases, the propeller for all cases is optimised such that the cruise efficiency is maximised, since this results in the highest weighted overall propeller efficiency.

Only the propeller solidity for the lowest descent speed has decreased, as shown in table 6.7. During this descent strategy, no energy was regenerated meaning that the propeller solidity is not constrained by the negative thrust it has to deliver during the descent. This results in a higher cruise and descent performance, but compromising the climb performance, and therefore a higher overall mission energy requirement. The same flaw as seen in the previous analysis case in the optimisation objective function is the cause of this increase in mission energy.

Table 6.7: Propeller solidity of the four simulations for the descent analysis with a fixed descent angle, but varying descent airspeed with a fixed pitch propeller.

	$0.8v_{minD}$	$0.9v_{minD}$	v_{minD}	$1.1v_{minD}$
Solidity	0.047	0.056	0.054	0.055

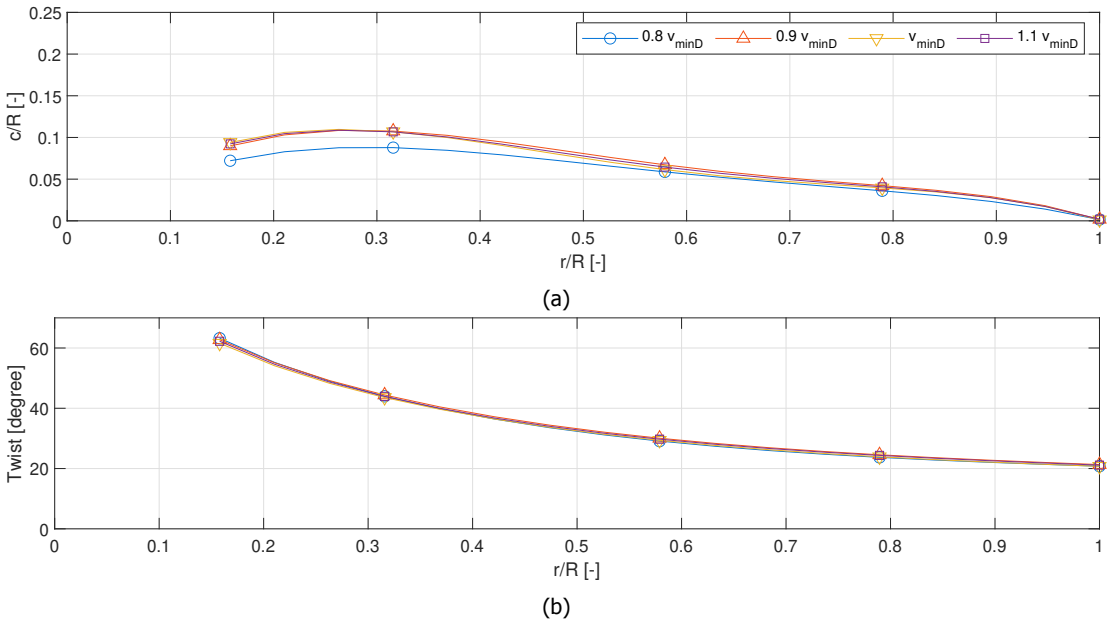

Figure 6.13: Propeller blade chord (a) and twist (b) distribution of the four simulations for the descent analysis with a fixed descent angle, but varying descent airspeed with a fixed pitch propeller.

6.2.2. Variable RPM, Variable Pitch

Up till now, all the shown results are for variable RPM, fixed pitch propellers. However, due to the large difference in operating conditions between the propulsive case and regenerative case, an in-flight variable pitch could increase the regenerative performance, without having a large impact on the cruise and climb performance, as seen as is the case for the variable RPM, fixed pitch propeller simulations.

The regenerative performance for the three cases, fixed RoD, fixed descent airspeed and fixed descent angle, are altogether shown in figure 6.14. For this propeller type, the highest rate of descent, $920 ft/min$, did converge to a consistently sized aircraft- and propeller design and therefore also this descent strategy is shown in the results.

When only the descent phase is taken into account, the performance of the variable RPM, variable pitch propeller does not show any improvements in regenerated energy compared to the fixed pitch case. The same trends in the descent energy are found for the variable pitch propeller, as for the fixed pitch propeller. This suggests that the regenerative power is determined by the amount of negative thrust that has to be produced during the descent phase. This negative thrust is a function of the descent strategy. If this is true, the regenerative power cannot drastically increase using a variable pitch propeller, while keeping the negative thrust produced and all other parameters equal. However, the other flight phases might get better performance for a variable pitch propeller.

The regenerative performance of the variable pitch propeller does not influence the propulsive performance as much as the fixed pitch propeller. To illustrate, the propeller geometries and solidities of the propellers as calculated for the fixed airspeed analysis, while varying the rate of

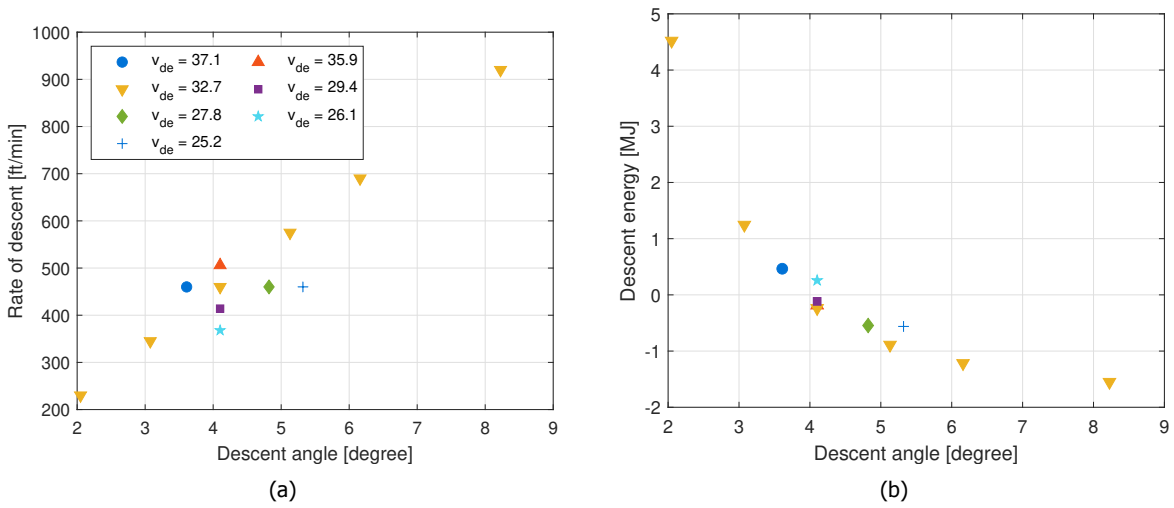

Figure 6.14: The descent strategy (a) and resulting (regenerated) descent energy (b) of the aircraft during the descent phase of the all simulations for the descent analysis with a variable pitch propeller.

descent, are shown in figure 6.15 and table 6.8 respectively. Here, it can be seen that for the maximum possible rate of descent for the fixed pitch propeller, $690ft/min$, the variable pitch propeller does only have a slight increase of 17% in solidity compared to the baseline propeller. For the highest rate of descent simulated, $920ft/min$, an increase of 67% in the solidity of the propeller is seen. However, this increase is still much lower than the increase in the propeller solidity that was necessary for the fixed pitch propeller, where a 199% increased solidity was seen for the $690ft/min$ propeller compared to the baseline propeller. This lower increase in solidity is the result of the in-flight variable pitch system. Due to the variable pitch, the twist distribution can be kept constant for all the different descent strategies. However, the in-flight pitch setting is varied, as shown in figure 6.16. For the highest rate of descent strategy, the pitch setting is reduced during the descent to make sure the required negative thrust is delivered. At the same time also the advance ratio is lowered, meaning that the RPM of the propeller is increased, to produce the negative thrust, and the rotational shaft power is increased.

For the lower rate of descent strategies, the descent phase does not seem to have an impact on the propeller geometry, since all these propeller solidities show similar behaviour. It is therefore found that for the low rate of descent strategies, where only a limited amount of negative thrust needs to be produced, the propeller geometry is not constrained by the thrust in this flight phase.

Table 6.8: Propeller solidity of the six simulations for the descent analysis with a fixed descent airspeed, but varying rate of descent with a variable pitch propeller.

	RoD 230	**RoD 345**	**RoD 460**	**RoD 575**	**RoD 690**	**RoD 920**
Solidity	0.048	0.041	0.043	0.048	0.051	0.072

The increase in propeller solidity, which is lower than the increase in solidity for the fixed pitch case, has also an effect on the cruise performance. For the high rate of descent cases, the propeller is still able to work at high efficiencies during the cruise phase, as shown in figure 6.18. Therefore, the extra energy consumed during the cruise phase is reduced for the high rate of

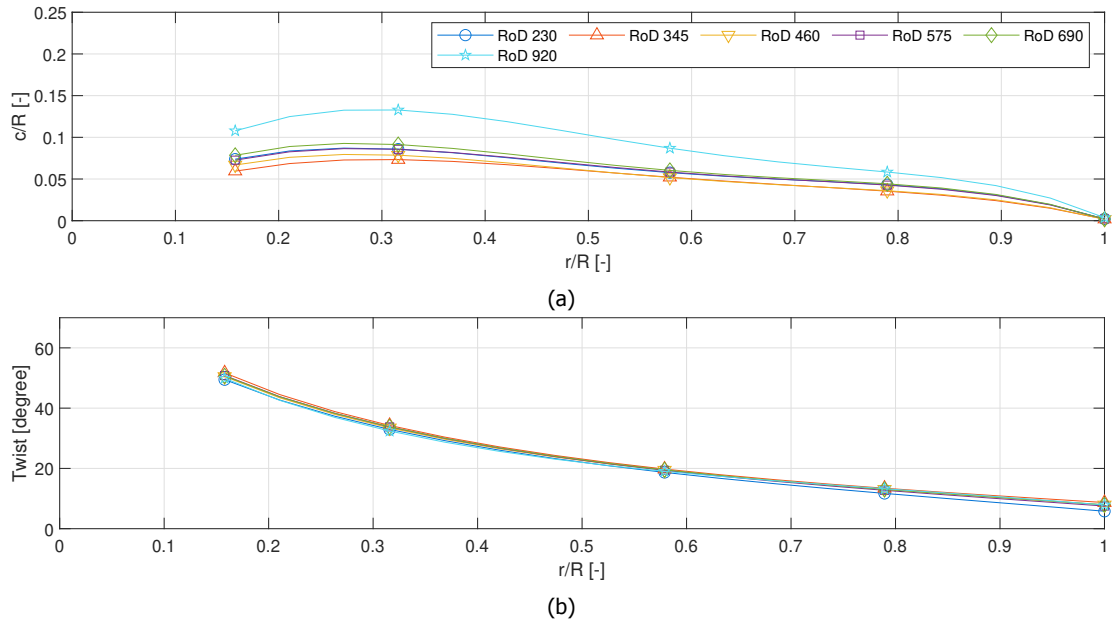

Figure 6.15: Propeller blade chord (a) and twist (b) distribution of the six simulations for the descent analysis with a fixed descent airspeed, but varying rate of descent with a variable pitch propeller.

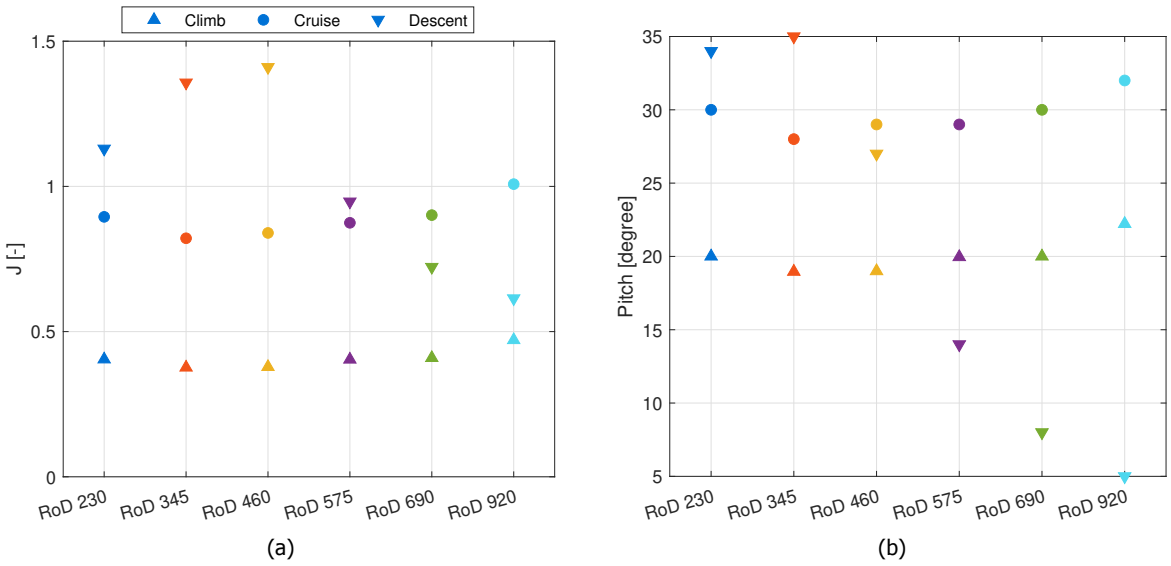

Figure 6.16: Propeller advance ratio (a) and pitch setting (b) of the six simulations for the descent analysis with a fixed descent airspeed, but varying rate of descent with a variable pitch propeller.

descent cases, compared to the fixed pitch cases, as shown in figure 6.17. Although, the cruise propeller performance has been improved for the high rate of descent cases, the cruise distance is still longer compared to the low rate of descent cases. Therefore, although the differences are lower than for the fixed pitch propeller, the high rate of descent missions still uses more energy in the cruise phase, due to the extra range flown during the cruise phase. Since the extra used energy during this longer cruise cannot be completely regenerated, the high rate of descent cases still use more energy overall than the low rate of descent cases, resulting in that the least energy is used for the mission that is not regenerating at all.

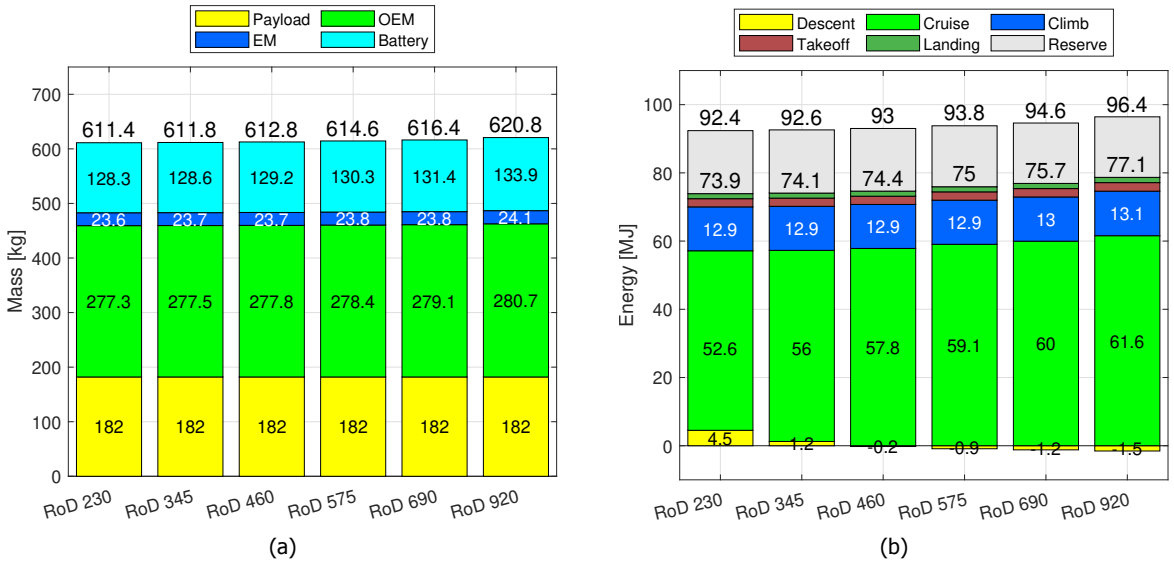

Figure 6.17: Mass (a) and energy (b) per fight phase breakdown of the six simulations for the descent analysis with a fixed descent airspeed, but varying rate of descent with a variable pitch propeller.

6.3. Discussion

The different analyses have shown the overall effects when changing the descent strategy. However, to get some more in-depth insight into how the found changes in aircraft- and propeller design can be related to the made differences in the descent strategy the results will be discussed in the following sections.

First, in section 6.3.1 the effect on the descent strategy on the aircraft- and propeller design is analysed for both the variable and fixed pitch propeller, to see how the different descent strategies affect the aircraft sizing and propeller blade geometry. Following, a more in-depth look is given into the difference between the variable- and fixed pitch propeller in section 6.3.2. During the presentation of the simulation results, it was already found that the propeller geometry optimisation did not always lead to the most energy efficient propeller design, this is touched upon in section 6.3.3.

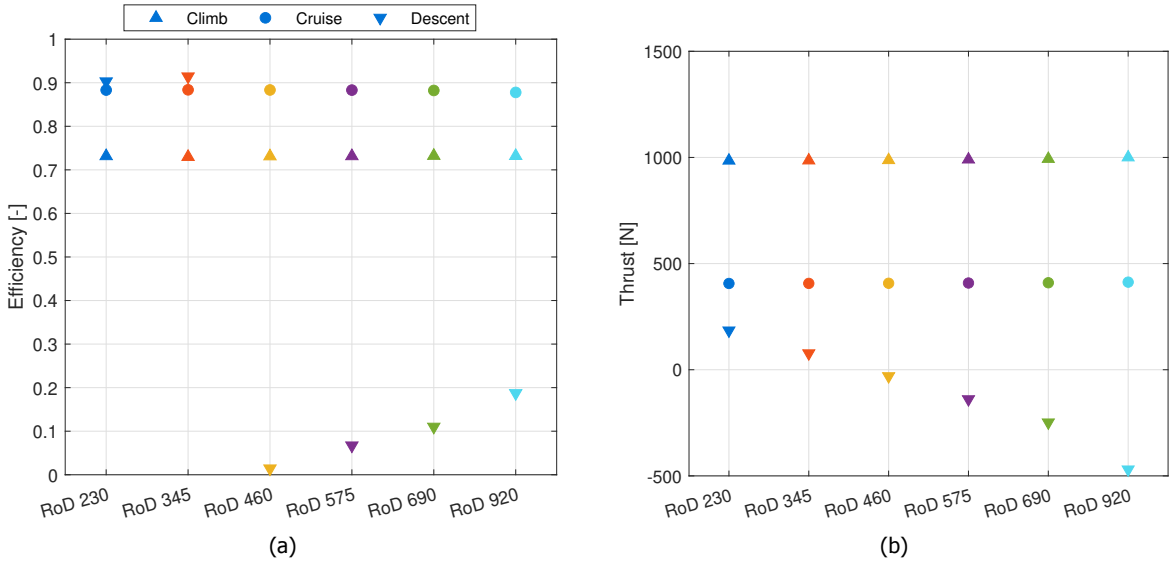

Figure 6.18: Propeller efficiency (a) and thrust (b) per flight phase of the six simulations for the descent analysis with a fixed descent airspeed, but varying rate of descent with a variable pitch propeller.

6.3.1. Optimal Descent Strategy

The results of the descent analysis have shown, that both for the variable RPM, fixed pitch propeller (vR) and the variable RPM, variable pitch propeller ($vRvP$) the total energy requirement for the total mission increases when more energy is regenerated.

At the first sight, this might be counterintuitive, since energy is regenerated, so the battery is charged during the descent flight. However, as also found, to be able to regenerate the energy a steep descent is required. Since the descent thrust is, in combination with the aircraft mass, a result of the chosen descent strategy. A higher descent angle, meaning a steeper descent, results in a reduction in descent thrust required by the propeller. The relation between the descent angle and descent thrust for all the simulations performed in the descent analysis is given in figure 6.19a. In figure 6.19b the lift-to-drag ratios for all the different simulations are plotted against the respective descent angle. The maximum L/D ratio, of approximately 15, of the aircraft corresponds to the minimum drag speed. Therefore, the descent strategies that are performed at the minimum (airframe)drag speed are performed at this high L/D ratio. The descent speeds that are performed at different airspeeds than the minimum drag speed have a lower L/D ratio. However, the effect of this lower descent L/D on the (negative) thrust required during the descent is smaller than the effect of a change in the descent angle.

During a steep descent the propeller has to produce the negative thrust, with as 'byproduct' energy regeneration. However, to be able to regenerate energy, the shaft power has to become negative. In figure 6.20a the relation between the descent angle and shaft power and is shown. From this figure it is seen that a higher negative shaft power will result in more regenerated energy. Furthermore, it is seen that for a more negative shaft power a steeper descent is required. Thus, for more energy regeneration, a steeper descent is needed, as shown in figure 6.20b.

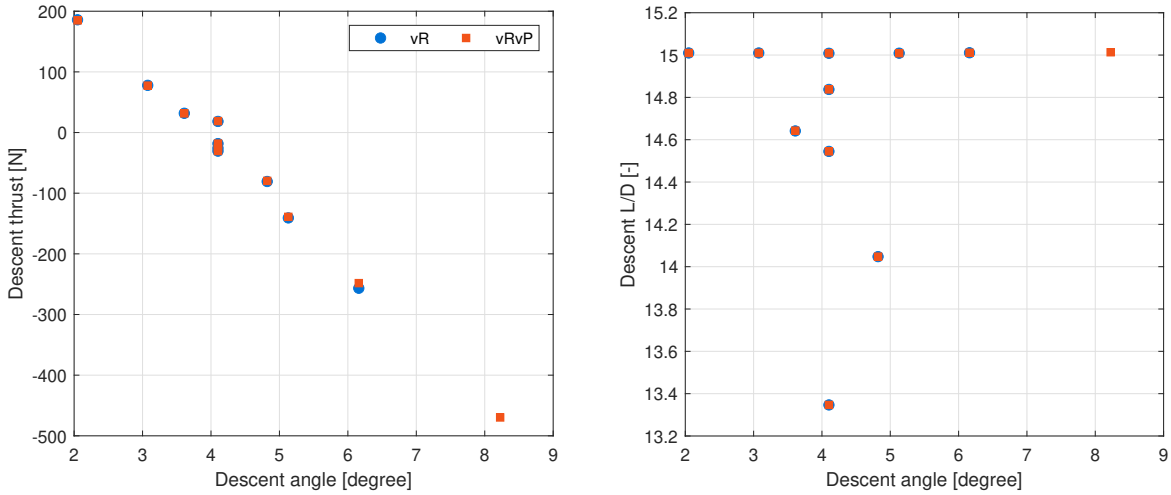

(a) (b)

Figure 6.19: Relation between the descent angle and the descent thrust (a) and between descent angle and the L/D ratio (b) plotted for all the different descent analysis simulations.

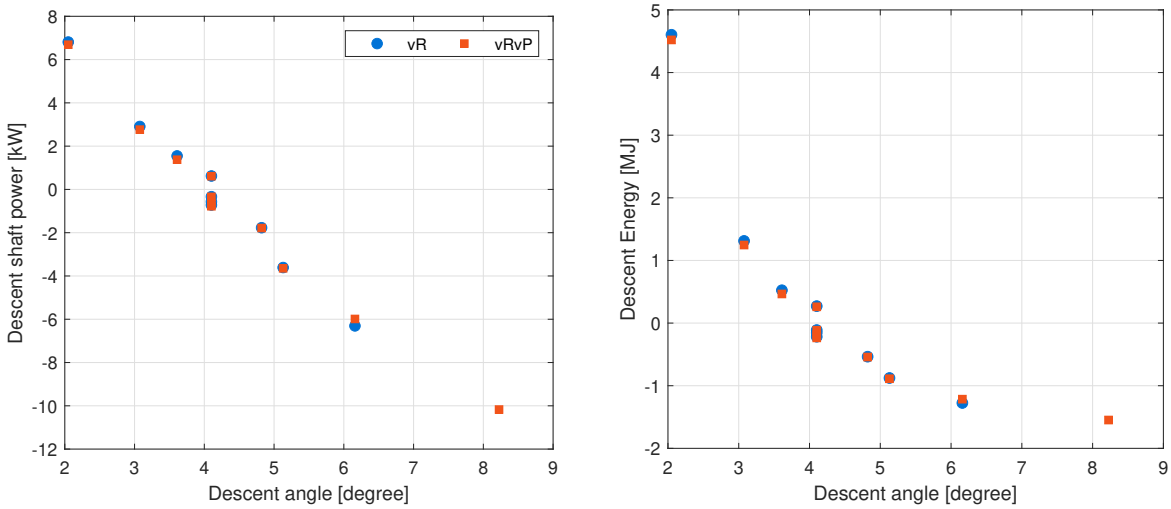

(a) (b)

Figure 6.20: Relation between the descent angle and the descent power (a) and between descent angle and the descent energy (b) plotted for all the different descent analysis simulations.

The steeper the descent, the less range is covered during the descent, but the higher the energy that is regenerated. Unfortunately, due to the steep descent, also less range is covered during the descent, meaning that to complete the same total flight distance, the duration of the cruise phase has to increase. Since energy is both lost during the cruise phase and descent phase due to the different mechanical conversion, (battery to rotational power, and rotational power to flight power) the increased cruise distance will always lead to a higher overall energy requirement for the mission. Since the overall total energy requirement determines the battery size, which plays an important role in the total aircraft mass, the total aircraft mass also increases when a steeper descent is performed. This relation is shown in figure 6.21a. Here a clear difference between the fixed pitch and variable pitch propeller is seen, but in both cases the steeper descent results in a heavier aircraft.

Thus both for the variable, as well as the fixed pitch propeller, when the total flight range is fixed, it is found that regenerating energy by increasing the descent angle of the descent will always result in an increased energy requirement, increasing the total aircraft mass needed to perform the mission. So, when the descent trajectory can be freely chosen, for a given total flight distance, in-flight energy regeneration will always lead to a higher energy consumption during the complete flight. This increased energy consumption results subsequently in a heavier aircraft.

Although the found differences in weight seem to follow the trend where a steeper descent with higher negative thrust results in heavier aircraft, the difference between the minimum and maximum found aircraft take off mass is only about $25kg$, which is approximately 5% of the baseline mission aircraft weight. From the validation of the tool, it was found that the accuracy of the tool is approximately 10%. Therefore, the found aircraft mass differences are within the accuracy of the used aircraft sizing tool. This means that when going further into the detailed design of the aircraft, the calculated aircraft masses can still differ, however it is expected that, based on the physics of the steeper descent resulting in more negative thrust and a longer cruise length, the found trends in aircraft mass for the steeper descent will still be valid.

6.3.2. Fixed Pitch versus Variable Pitch

Not only the descent energy per descent strategy, and therefore the best optimal descent strategy, was determined. Also the difference between the fixed pitch and variable pitch propellers has been investigated at the same time.

In figure 6.21a a clear difference between the fixed pitch and variable pitch propeller was already noticed. In both cases, the increased descent angle has a negative influence on the aircraft mass, meaning that the aircraft mass does increase when a steeper descent is performed. However, the increase in mass for the fixed pitch propeller is higher than for the variable pitch propeller. Also, on the propeller design side, the increase in the solidity of the fixed pitch propeller is larger than for the variable pitch propeller. This is seen in figure 6.21b, where the steepest descent requires a very high propeller solidity for the fixed pitch propeller. Reducing the descent angle, making the descent more shallow, does decrease the propeller solidity, until a point where the solidity does not decrease anymore with decreasing descent angle. At this point, the propeller solidity is not constrained anymore by the negative thrust that the propeller needs to produce

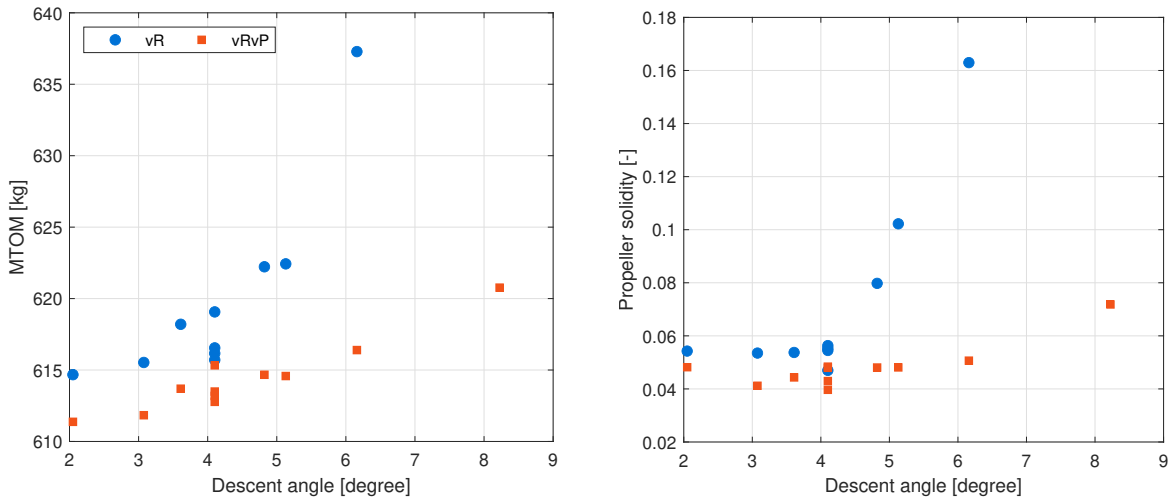

Figure 6.21: Relation between the descent angle and the $MTOM$ (a) and between descent angle and the propeller solidity (b) plotted for all the different descent analysis simulations.

during the descent phase. The point where the minimal propeller solidity is achieved, is obtained for a steeper descent angle for the variable pitch propeller, than for the fixed pitch propeller. Due to the variable pitch setting, the propeller blade chord does not have to increase to be able to generate the negative thrust. Since the high propeller solidity results in lower climb and cruise performance, the weight penalty for the variable pitch propeller is lower than the weight penalty for the fixed propeller when a steeper descent is performed, and more negative thrust is required during the descent.

This is also seen in figures 6.22a and 6.22b, the increased solidity due to the steeper descent has a negative effect on the cruise efficiency of the propeller, increasing energy usage of the cruise phase and subsequently the total aircraft mass. For the variable pitch propeller, instead of an increase in solidity, the pitch can be reduced during the descent phase, such that the propeller airfoil will be operating at negative angles of attack. During the cruise, the pitch is set to a higher setting, such that during this flight phase positive thrust is generated. This way of operating the propeller makes that the increase in cruise distance for the steep descent trajectories does not lead to the same aircraft mass increase as for the fixed pitch propeller.

It is assumed that the additional weight of the variable pitch system is neglected, such that it does not add any weight to the system. In reality, this is not valid though. A variable pitch system is a complex and heavy system, not only increasing the total weight of the aircraft, but also moving the centre of gravity of the aircraft more forward, for front mounted propellers. This change in the centre of gravity might be unwanted for control and stability reasons.

For the descent strategy where the propeller needs to produce thrust (i.e. the descent thrust is positive, which is found for descent angles larger than $-4°$) the difference between the variable pitch and fixed pitch propeller aircraft mass is only about $3kg$, which is less than 1% of the total aircraft mass. Since the weight of the variable pitch system is not taken into account, this means that the aircraft with the variable pitch would become heavier when this system is taken

into account, and consequently would also need more mission energy. Therefore, when the regenerative mode is not used during the descent, it would be more beneficial to use a fixed pitch propeller system, since this will most likely result in a lower aircraft weight. This is also what is seen on the electric aircraft that is used for the comparison during the analysis, the *Pipistrel Alpha Electro*. This aircraft is originally not designed to be able to use the regenerative mode during the descent, and features a three-bladed fixed pitch propeller.

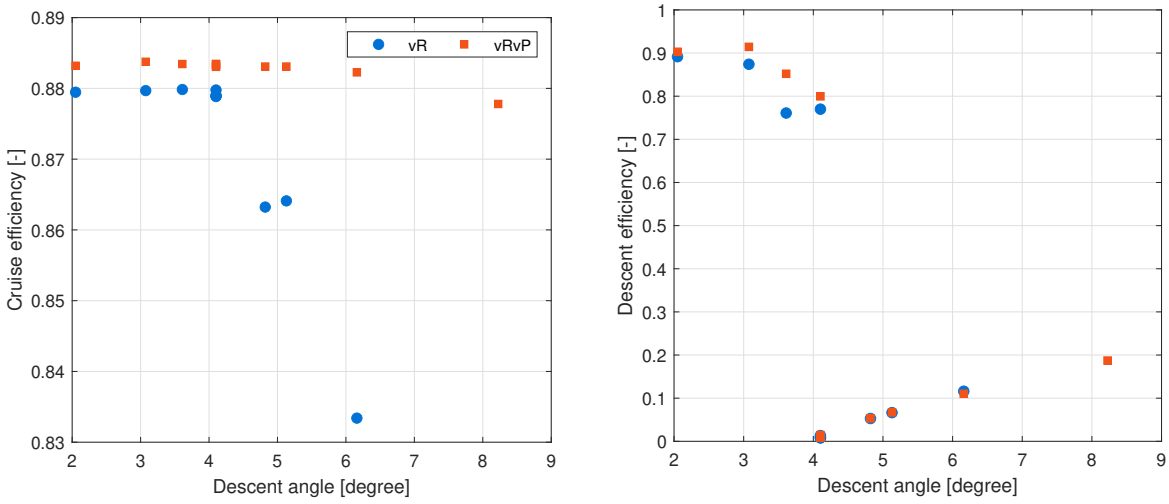

Figure 6.22: Relation between the descent angle and the cruise efficiency of the propeller (a) and between descent angle and the descent efficiency of the propeller (b) plotted for all the different descent analysis simulations.

6.3.3. Propeller Geometry Optimisation

For the used mission, with a range of $75NM$, up to 86% of the flight time is spent in the cruise phase. As shown, the length and duration of the cruise phase are dependent on the chosen descent strategy. A higher rate of descent, thus a steeper descent, results in a lower covered distance during the descent. To keep the total flown distance for the mission equal, the cruise distance has to increase. The propeller design is therefore dominated by the cruise performance of the propeller, since the optimisation objective function is a time-weighted average of the propeller efficiency of the three flight phases: the cruise, climb and descent. However, the energy distribution between these flight phases is not the same as the time distribution. During the climb, more power is delivered by the battery to the electric machine, and more thrust is generated. Therefore, during the climb phase the energy consumption per unit of time is higher than during the cruise phase.

The optimisation objective function does not take this higher power setting during the climb phase into account. Therefore, from a time-weighted point of view, it might seem that it is more energy efficient to optimise the propeller geometry such that the propeller efficiency during the cruise is maximised, while from the calculated energy usage per flight phase it turns out that this results in more energy consumption for the complete mission.

To optimise the propeller such that it does minimize the complete mission energy consumption,

the whole mission should be analysed for each function evaluation of the optimisation, where the mission energy per flight phase is calculated. The inner and outer loop of the sizing tool, as described in chapter 3 are combined in this approach, resulting in a higher number of times the propeller design routine has to be performed. This would lead to a too high computational effort in this stage of the aircraft and propeller design, and was therefore not found feasible. However, also an approach could be chosen where the objective optimisation function is not a function of the time-weighted propeller efficiency, but the mission energy usage is minimised directly using the objective function, as shown in equation (6.1). The mission energy can then be calculated using the estimated power requirement during each phase and the time of each flight phase, as shown in equations (6.2) and (6.3). For a descent with positive thrust, the efficiency of the propeller is calculated differently than for a regenerative descent as explained in section 2.1. Therefore also the calculated energy usage or regeneration is calculated differently. For a positive thrust descent the first mission energy formula is used, while for a regenerative descent the latter formula is used. However, both functions calculate the total energy usage of the three flight phases combined. The thrust requirement during the different flight phases is taken from the previous iteration. In this way, not only the time and efficiency of the propeller are taken into account, but also the power setting during the flight phase.

$$\min_{\bar{\mathbf{x}}} \quad f(\bar{\mathbf{x}}) = E_{mission}(\bar{\mathbf{x}}) \tag{6.1}$$

$$E_{mission}(\bar{\mathbf{x}}) = \frac{T_{cl} v_{cl} t_{cl}}{\eta_{cl}(\bar{\mathbf{x}})} + \frac{T_{cr} v_{cr} t_{cr}}{\eta_{cr}(\bar{\mathbf{x}})} + \frac{T_{de} v_{de} t_{de}}{\eta_{de}(\bar{\mathbf{x}})} \tag{6.2}$$

$$E_{mission}(\bar{\mathbf{x}}) = \frac{T_{cl} v_{cl} t_{cl}}{\eta_{cl}(\bar{\mathbf{x}})} + \frac{T_{cr} v_{cr} t_{cr}}{\eta_{cr}(\bar{\mathbf{x}})} + \eta_{de}(\bar{\mathbf{x}}) P_{wind} t_{de} \tag{6.3}$$

To check if the newly defined optimisation objective function works as intended, three simulations have been re-performed using this function. This has been done for the fixed pitch propeller, since for this type of propeller it was already found that the initially used optimisation function did not always lead to the most optimal propeller geometry, in terms of minimizing total mission energy. This has been done for the baseline mission, to see how the new optimisation function changes the baseline mission. Also, the steep descent strategy has been reanalysed, as well as the descent at the same descent angle as the baseline mission, but with the reduced descent airspeed to 80% of the baseline descent speed.

The results of these new simulations, compared with the simulations using the initial optimisation objective function, are given in appendix D. The three simulations are showing the expected results of the new objective function: the propeller geometry is designed such that the climb phase plays a more important factor during the optimisation. This results that the required climb energy reduces, while the cruise energy is slightly increased. Since the reduction in climb energy is larger than the increase in cruise energy, the total mission energy is decreased using the new optimisation function (ranging from $0.1MJ$ (0.1%) decrease to a $0.7MJ$ (0.9%) decrease). The reduced climb energy is a result of the increased propeller chord for the simulations. This increase

in chord results in a higher climb efficiency, while the cruise efficiency is slightly reduced. On the descent phase no effects are found, indicating that the results found with respect to the descent performance are still valid.

7

Propeller Airfoil Camber Analysis

The propeller geometry is optimised during each iteration of the sizing tool. Therefore, the propeller geometry should already be optimal (i.e. the time-weighted efficiency is maximised) for each sized aircraft. However, the inputs for the propeller geometry optimisation function can be analysed to see how these change the results of the optimisation, and consequently result in a different sized aircraft.

The parameter that is of most interest for the regenerative mode of the aircraft is the airfoil selection of the propeller blades. The reference airfoil, the *Clark-Y* airfoil is a positive cambered airfoil, which performs at the highest lift-to-drag ratios at positive angles of attack. However, during the regenerative mode the propeller blade sections operate at negative angles of attack. Therefore, it might be of interest to reduce the camber on the propeller airfoil sections, such that the performance during this regenerative mode is increased, thus regenerating more energy during the descent. This increase in the regenerative performance might have a positive impact on the total required mission energy. However, the reduced camber could also reduce the climb and cruise performance. To find the effect of the camber, the sizing is performed for five airfoils with different airfoil camber. In section 7.1 the simulation case studies are given. The most interesting results of these case studies are given in section 7.2, with a detailed overview of all the results given in appendix B. The discussion of the results is presented in section 7.3.

7.1. Simulation Case Studies

Again, the baseline airfoil, the *Clark-Y*, is used as a starting point. For the analysis of the airfoil camber, the camber of this airfoil is altered where a *100%* camber refers to the original airfoil and a *0%* is a symmetric airfoil with the same thickness distribution and location of maximum thickness as the original airfoil. The five airfoils that are to be analysed are given in table 7.1. Furthermore, the airfoil shapes of the five airfoils are given in figure 7.1.

The mission profile for this analysis is initially equal to the baseline mission, thus performing a $75NM$ range mission. The descent is performed at a rate of descent of $460ft/min$, which is equal to the baseline mission. However, the effect of the regenerative descent is expected to be stronger for a steeper descent. Therefore, not only the baseline descent is analysed, but also a steep descent strategy. This steep descent is the steepest descent possible as found in the descent analysis, which turned out to be the $690ft/min$ descent for the fixed pitch propeller,

while for the variable pitch propeller the $920ft/min$ descent can be used. Both descents are performed at the minimum drag speed of $32.7m/s$

Table 7.1: Simulation inputs for the propeller design analysis, where the propeller airfoil camber is varied with respect to the baseline propeller airfoil camber and the baseline mission underlined.

Simulation	**1**	**2**	**3**	**4**	**5**
Baseline fraction	100%	75%	50%	25%	0%

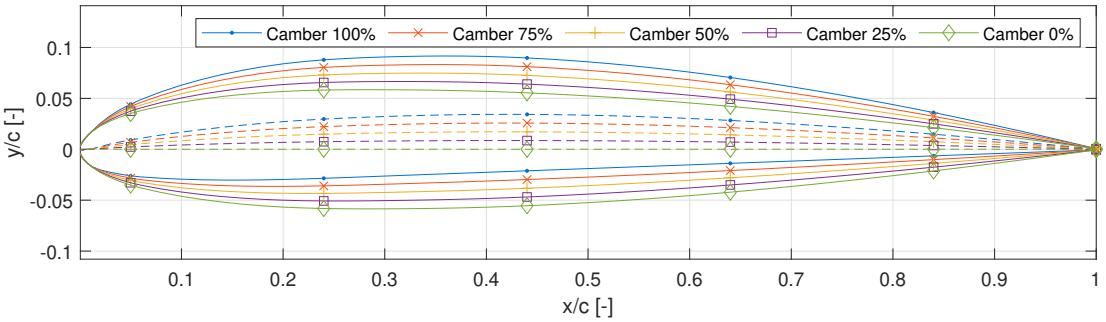

Figure 7.1: The shape of the five airfoils that are analysed, with the camber line indicated with a dashed line.

7.1.1. Airfoil Drag Polars

As found in the validation, the drag polars of the airfoils are important to understand the reliability of the calculated propeller performance. The calculated polars for three airfoils, with 100%, 50% and 0% camber are plotted in figure 7.2. For each airfoil the polar for two different Reynolds numbers are plotted: $Re = 60000$ and $Re = 300000$. These values are the expected lowest and highest calculated Reynolds number which occur on the propeller during the simulated missions.

From the figure, it can be seen that, as expected, the highest C_l is achieved for the highest camber at the highest calculated Reynolds number. Reducing the camber does reduce the maximum C_l of the airfoil, but on the other hand, the minimum lift coefficient at negative angles of attack does increase, with higher C_l/C_d values at these negative angles. The calculated stall angles are roughly at -12° and 13°, resulting in that if the local angle of attack remains between these bounds, the airfoil polars are not limiting the accuracy of the performance calculations of the propeller, as found from the propeller analysis model validation in section 4.2.

7.2. Simulation Results

From the descent analysis is it shown that the most energy can be regenerated when descending at a high rate of descent. This high rate of descent results in a high descent angle and thus more negative thrust during the descent. However, for the variable RPM, fixed pitch propeller, the solidity of the propeller has drastically increased to be able to provide the required negative thrust to make sure the prescribed descent strategy can be flown. Therefore, it is expected that by reducing the camber on the fixed pitch propeller airfoil, the negative thrust during these steep

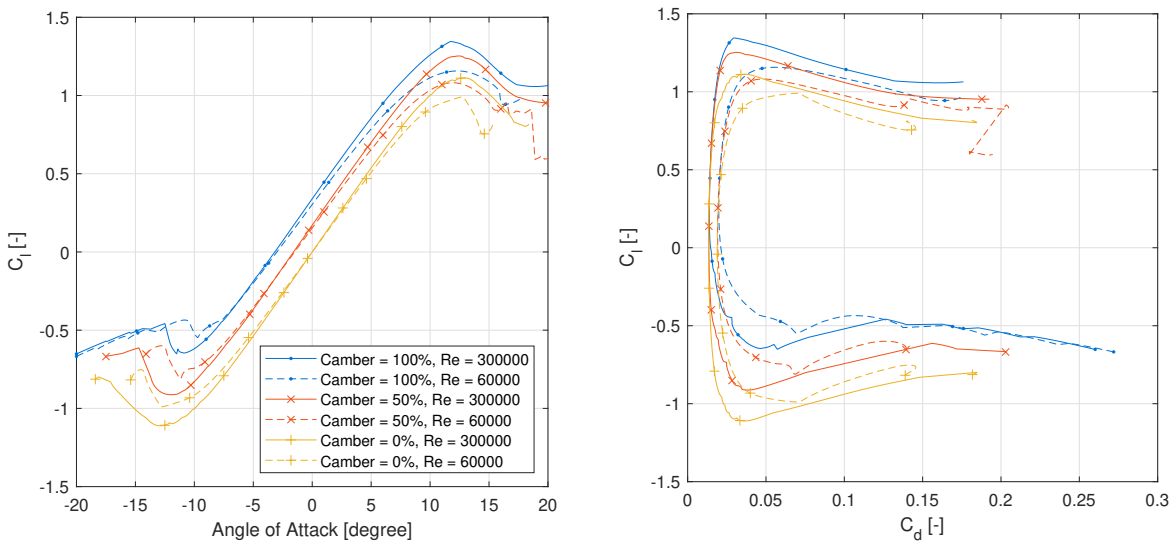

Figure 7.2: The calculated propeller airfoil polars for the minimum and maximum expected local Reynolds number for the reference airfoil (100% camber), the 50% cambered airfoil and the 0% cambered (symmetrical) airfoil.

descents can be reached with a lower solidity. Also for the variable pitch propeller the analysis will be performed, to see how the reduced airfoil camber would influence propeller geometries that are not constrained by the negative thrust.

However, first the 'shallow' descent strategy, with a rate of descent of $460ft/min$, of the baseline mission is analysed to see what the effect of the reduced propeller airfoil camber is on this descent strategy.

7.2.1. Shallow descent

The shallow descent, with a rate of descent of $460ft/min$, performed at the minimum drag airspeed, is analysed for the five different airfoil propellers. Due to the low negative thrust required for these aircraft at this rate of descent, the regenerative power is also low. This is valid for both the fixed pitch, as well as the variable pitch propeller. Moreover, this results in the same trends for both propeller variants, so for compactness only the results of the variable pitch propeller are shown, the details of the fixed pitch propeller analysis for the shallow descent can be found in appendix B.

Due to this low regenerative power, the propeller airfoil has only a very limited effect on the total regenerative energy, as can be seen in figure 7.3. The regenerative energy for the five different airfoil cambers is equal. However, as could already be seen in the airfoil polar data, the propulsive performance of the airfoils with reduced camber is lower. This results also in lower propulsive performance for the complete propeller with the airfoils with lower camber. Thus, the power required during the climb and cruise phase of these aircraft does increase. This results in a higher energy requirement for the total mission, which in turn causes a larger battery and therefore an overall heavier aircraft. The reduced propeller airfoil camber does thus not have a

positive effect on the overall aircraft performance, when the aircraft is designed for a shallow descent trajectory, where the possible regenerated energy is low, due to low negative thrust.

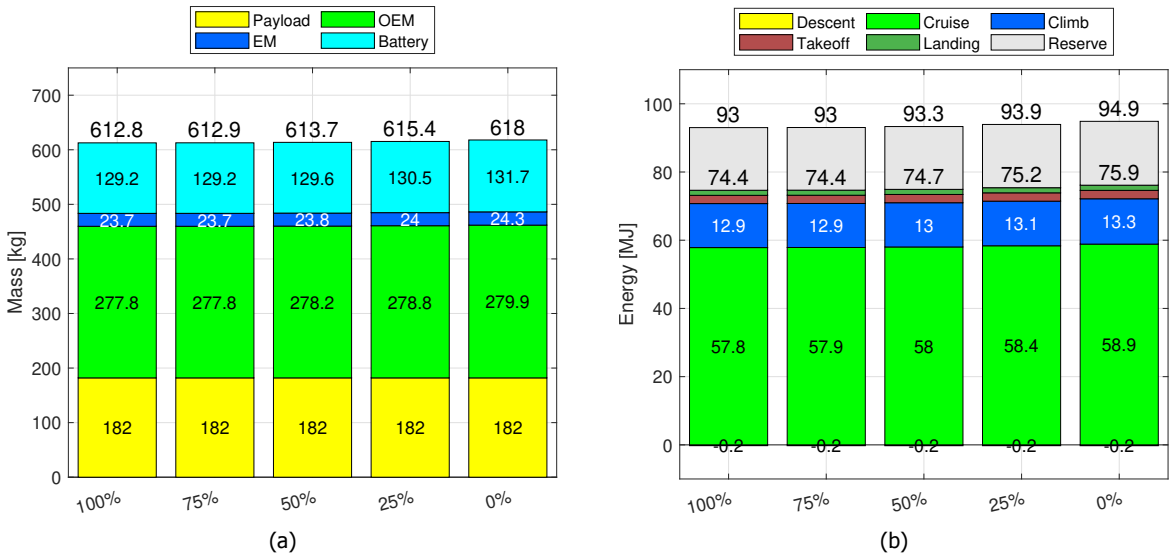

Figure 7.3: Mass (a) and energy (b) per flight phase breakdown of the five simulations with a shallow descent strategy with the propeller airfoil camber reducing from 100% (reference airfoil) to 0% (symmetrical airfoil) with a variable pitch propeller.

The propeller geometry is also only slightly affected by the reduced airfoil camber. For the lowest camber, the propeller solidity has to increase by 29% compared to the baseline airfoil to produce the same thrust. This is shown in figure 7.4 and table 7.2. Since these propeller geometries are not constrained by the negative thrust during the descent phase, no positive effect is found in reducing the propeller airfoil camber, since still the same negative thrust needs to be produced by the propeller. Thus, the differences in propeller geometries are small compared to the differences seen in the descent analysis. Hence, the differences in the propeller efficiencies are also small, with a difference in the cruise efficiency between the highest and lowest camber of only 0.7%.

Table 7.2: Propeller solidity of the five simulations with a shallow descent strategy with the propeller airfoil camber reducing from 100% (reference airfoil) to 0% (symmetrical airfoil) with a variable pitch propeller.

	100%	**75%**	**50%**	**25%**	**0%**
Solidity	0.043	0.046	0.048	0.056	0.056

7.2.2. Steep descent

Due to the limited negative thrust as produced during the 'shallow' descent trajectory, the effect of airfoil camber during the regenerative phase on the regenerated energy does not increase the overall mission performance. Therefore, also the 'steep' descent is analysed, with a rate of descent that was found to be maximal during the descent analysis. This means the rate of descent or the fixed pitch propeller is set equal to $690 ft/min$, while the variable pitch propeller rate of descent is $920 ft/min$. However, both descents are performed with the airspeed still

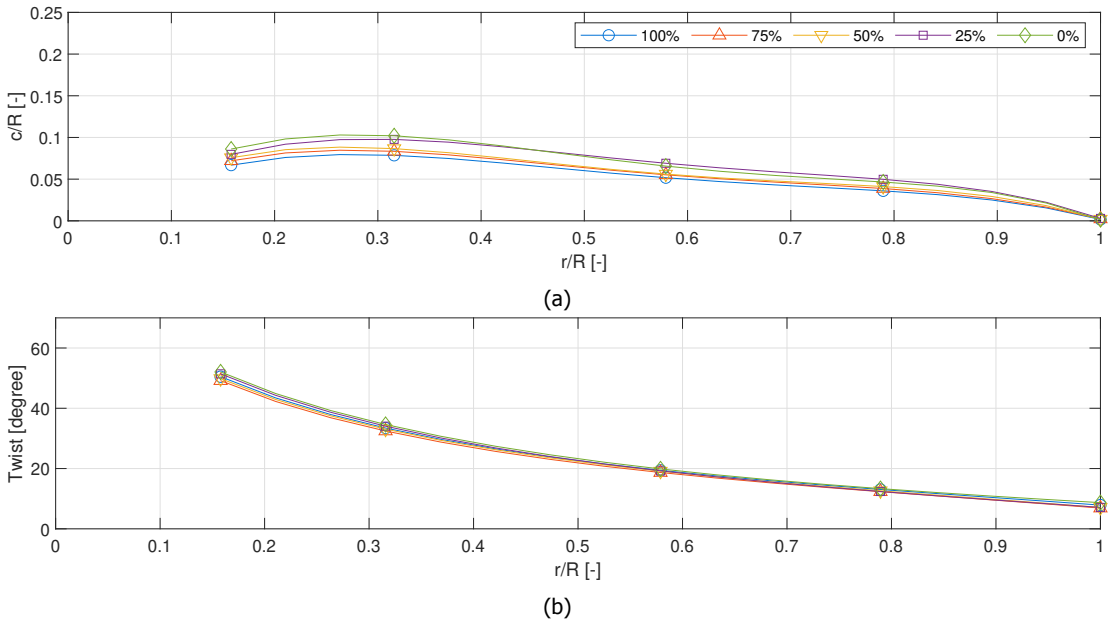

Figure 7.4: Propeller blade chord (a) and twist (b) distribution of the five simulations with a shallow descent strategy with the propeller airfoil camber reducing from 100% (reference airfoil) to 0% (symmetrical airfoil) with a variable pitch propeller.

equal to the minimum drag speed.

Fixed Pitch

The fixed pitch propeller showed an increased solidity when the descent strategy of $690 ft/min$ was used. At this rate of descent, the required negative thrust produced by the propeller could only be achieved when the propeller chord, and therefore the solidity, would be increased. The propeller geometry is therefore constrained by the descent phase of the mission.

A reduction in the propeller airfoil camber results in the same negative thrust production, while the propeller solidity is slightly, up to 17%, decreased with respect to the reference propeller airfoil, as shown in figure 7.5 and table 7.2. This reduced solidity for a reducing propeller airfoil camber is the opposite effect compared to the shallow descent strategy, where the propeller solidity did increase for reducing propeller airfoil camber.

Table 7.3: Propeller solidity of the five simulations with a steep descent strategy with the propeller airfoil camber reducing from 100% (reference airfoil) to 0% (symmetrical airfoil) with a fixed pitch propeller.

	100%	**75%**	**50%**	**25%**	**0%**
Solidity	0.163	0.149	0.142	0.137	0.134

As suggested, since the fixed pitch propeller geometry is constrained by the negative thrust during the descent, the reduction in propeller airfoil camber does indeed make it possible to reduce the propeller solidity. In figure 7.6 the effect of the reduced propeller airfoil camber, and

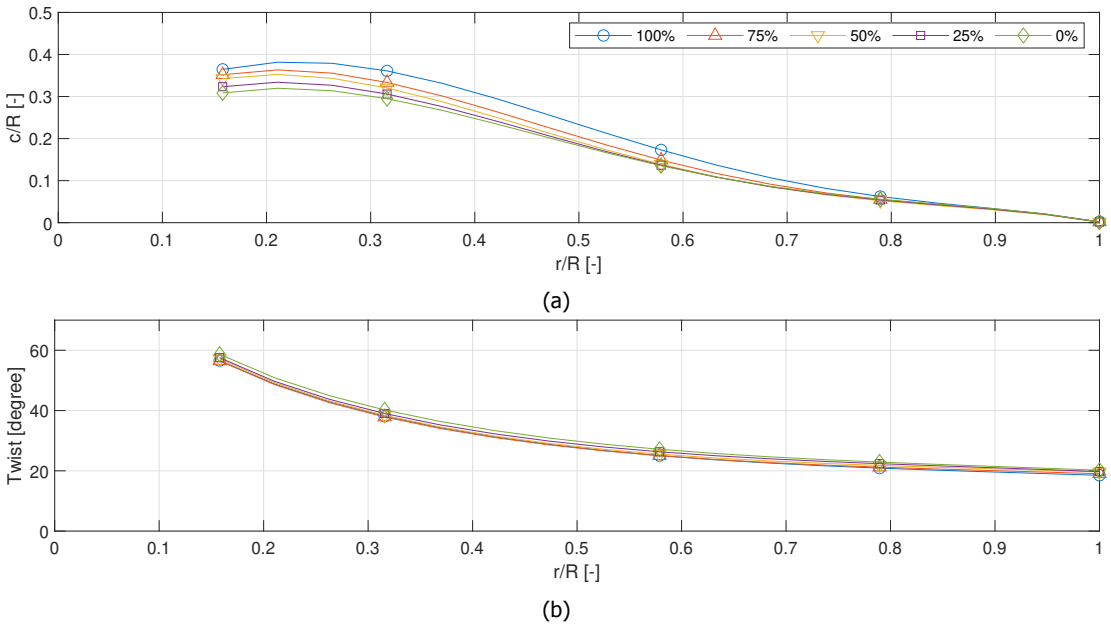

Figure 7.5: Propeller blade chord (a) and twist (b) distribution of the five simulations with a steep descent strategy with the propeller airfoil camber reducing from 100% (reference airfoil) to 0% (symmetrical airfoil) with a fixed pitch propeller.

therefore the reduced propeller solidity, is shown. Also here the opposite effect compared to the shallow descent strategy is seen. For a reduced airfoil camber, the total required mission energy reduces. The total regenerated energy for the reduced airfoil camber does however only increase with $0.1MJ$ (which is 0.1% of the baseline total mission energy). As a result, instead of an increase in aircraft weight for the reducing propeller airfoil camber, the aircraft weight does reduce, although the change in mass is only a few kilos which is less than 1% of total aircraft mass. The lowest aircraft mass, resulting from the lowest mission energy, is found for the propeller airfoil camber of 25% of the reference airfoil. Using a symmetrical airfoil, the 0% airfoil, reduces the climb and cruise performance again, resulting in a slight increase in the required mission energy, and therefore the aircraft mass.

The differences in propeller efficiencies between the different airfoil camber simulations are small. Therefore, the efficiencies of each flight phase for the five simulations are given in table 7.4. Here, it can be seen that the propeller efficiency of the 25% cambered airfoil is the highest for the climb and cruise phase. Reducing the camber even more does increase the descent efficiency, however also the climb and cruise efficiency are reducing again, resulting in an overall higher energy requirement for the mission.

To see why the propeller efficiency is increased for the reduced airfoil camber, the radial distribution of the angle of attack of the propeller blades, the local lift-to-drag ratio of the airfoil and the corresponding local lift production of the propeller blades are respectively given in figures 7.7 to 7.9.

For the reduced camber, the angle of attack needs to increase to make sure enough thrust is produced during the climb and cruise phase, as shown in figures 7.7a and 7.7b. Since the chord

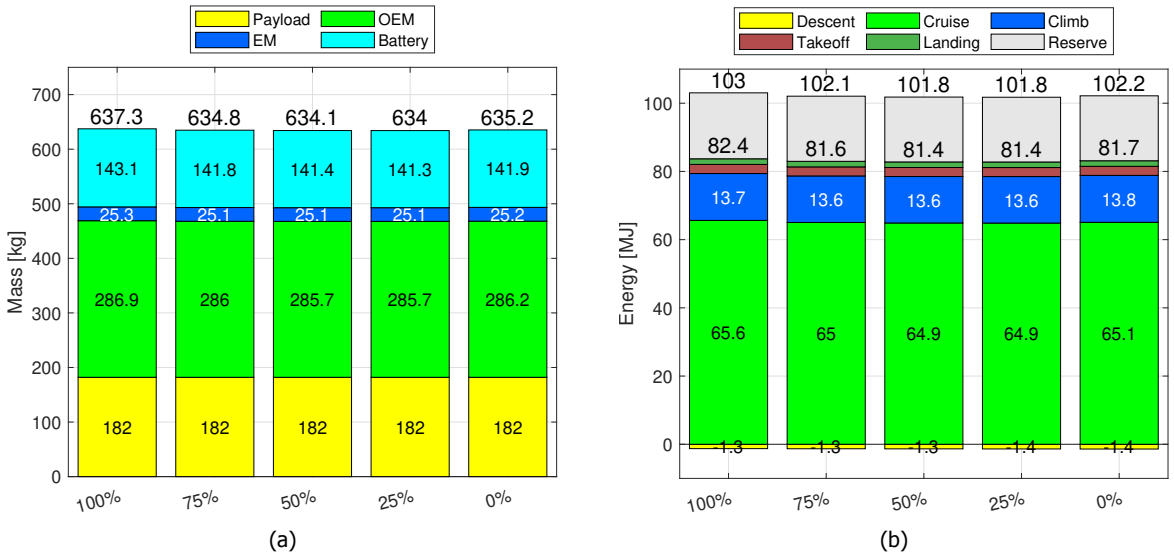

Figure 7.6: Mass (a) and energy (b) per flight phase breakdown of the five simulations with a steep descent strategy with the propeller airfoil camber reducing from 100% (reference airfoil) to 0% (symmetrical airfoil) with a fixed pitch propeller.

Table 7.4: Propeller efficiencies of the five simulations with a steep descent strategy with the propeller airfoil camber reducing from 100% (reference airfoil) to 0% (symmetrical airfoil) with a fixed pitch propeller.

	100%	**75%**	**50%**	**25%**	**0%**
η_{cl} [%]	71.41	71.66	71.67	71.63	71.09
η_{cr} [%]	83.34	83.77	83.89	83.90	83.78
η_{de} [%]	11.61	11.96	12.20	12.43	12.66

is decreased for the reduced camber, and the airfoil does produce less lift for the same angle of attack, this does make sense. However, still the same amount of lift needs to be produced. In figure 7.9, it can be seen that indeed for the climb and cruise phase the same amount of thrust is produced by each propeller blade, independent of which airfoil is used.

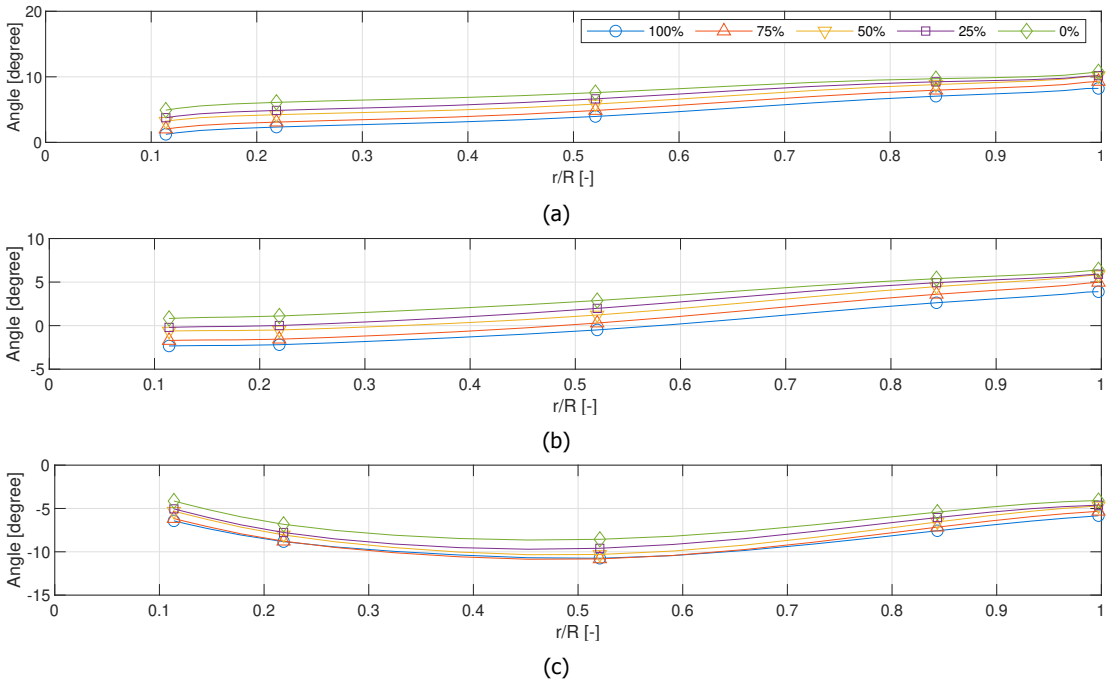

Figure 7.7: Radial distribution of the angle of attack of the propeller blade of the five simulations with a steep descent strategy with the propeller airfoil camber reducing from 100% (reference airfoil) to 0% (symmetrical airfoil) with a fixed pitch propeller. With on the top the climb phase (a), in the middle the cruise phase (b) and the bottom graph showing the descent phase (c).

For the lift-to-drag ratio of the local airfoil, the airfoil camber does not have a large influence on the climb and cruise phase, as shown in figure 7.8. The local lift-to-drag ratio is slightly reduced when reducing the camber, however, the largest effect is seen in the descent phase. For the descent phase, the most positive cambered airfoil is not able to produce the negative thrust in an efficient way, resulting in an almost two times lower lift-to-drag ratio for the most positive cambered airfoil compared to the symmetrical airfoil.

So, for the reduced camber, the local angle of attack on the propeller blade is increased during the climb and cruise phase. However, the lift-to-drag ratio is not influenced during these phases. Also, the same amount of lift is produced during these phases. During the descent however, the effect of the reduced airfoil camber is clearly seen in the lift-to-drag ratio of the local airfoil, where a lower camber can produce the negative thrust more efficiently.

Variable Pitch

The same five propeller airfoil cambers are analysed as for the fixed pitch steep descent analysis. The results for the aircraft mass and mission energy usage are given in figure 7.10. For the

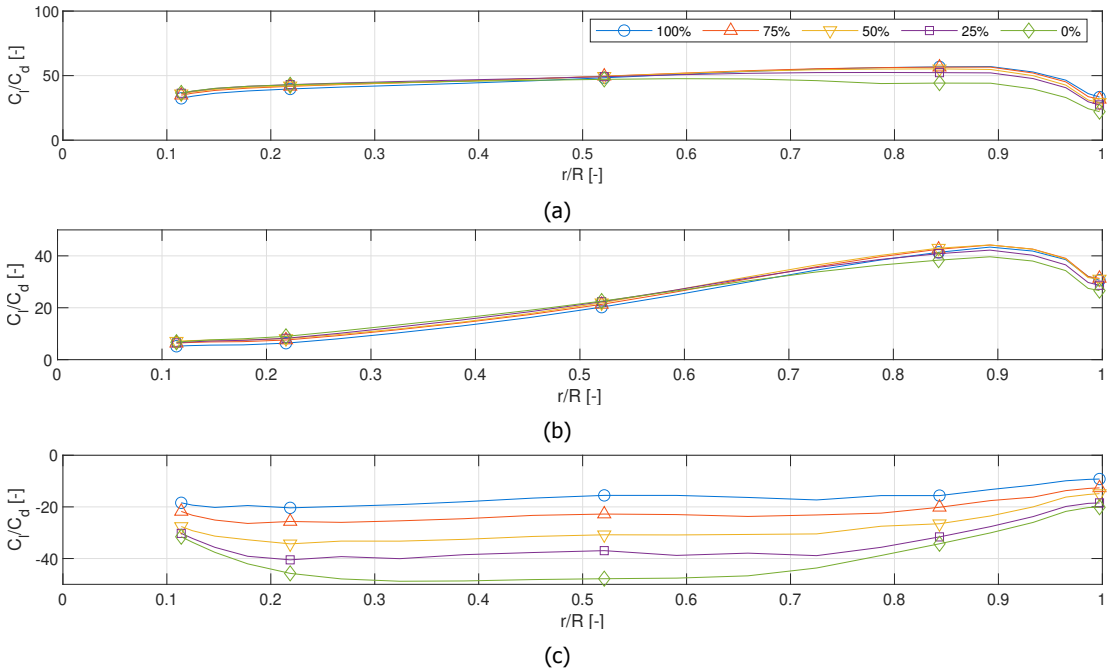

Figure 7.8: Radial distribution of the lift to drag ratio of the propeller blade of the five simulations with a steep descent strategy with the propeller airfoil camber reducing from 100% (reference airfoil) to 0% (symmetrical airfoil) with a fixed pitch propeller. With on the top the climb phase (a), in the middle the cruise phase (b) and the bottom graph showing the descent phase (c).

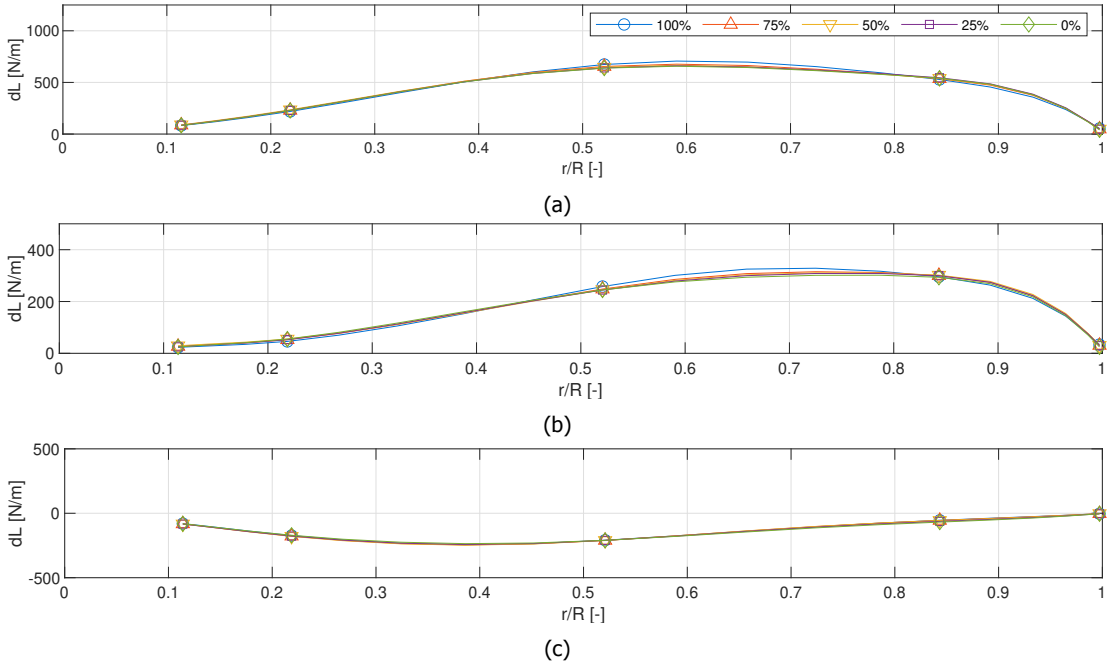

Figure 7.9: Radial distribution of the lift production of the propeller blade of the five simulations with a steep descent strategy with the propeller airfoil camber reducing from 100% (reference airfoil) to 0% (symmetrical airfoil) with a fixed pitch propeller. With on the top the climb phase (a), in the middle the cruise phase (b) and the bottom graph showing the descent phase (c).

variable pitch, steep descent, the reduction in propeller airfoil camber does have an effect on the regenerated energy during the descent phase. The symmetrical airfoil, with a camber of 0%, is able to regenerate 18% more energy than the fully cambered propeller airfoil.

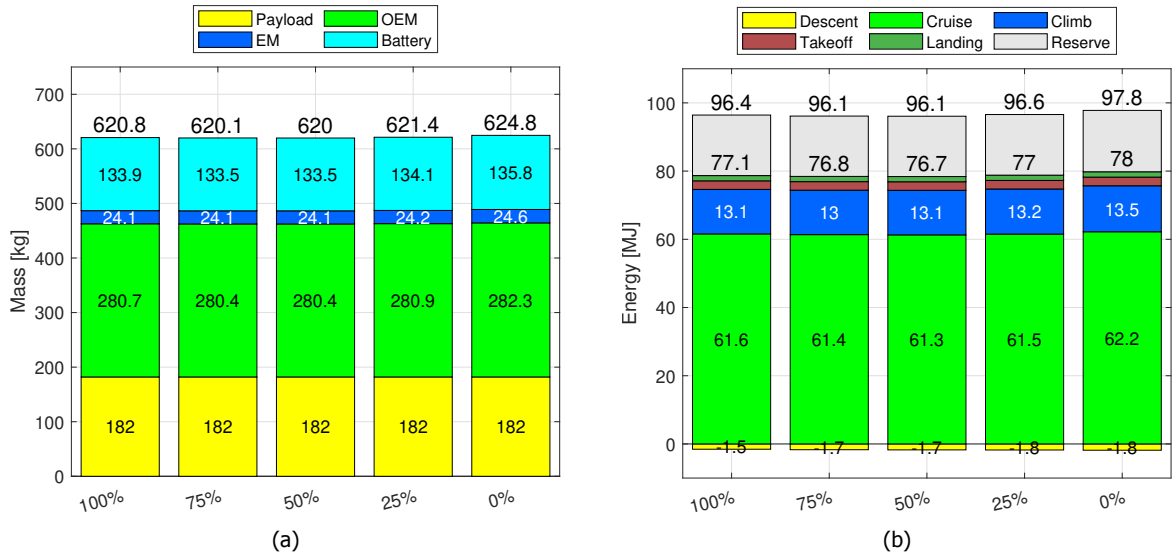

Figure 7.10: Mass (a) and energy (b) per flight phase breakdown of the five simulations with a steep descent strategy with the propeller airfoil camber reducing from 100% (reference airfoil) to 0% (symmetrical airfoil) with a variable pitch propeller.

Equally to what is seen in the fixed pitch, steep descent analysis, the total energy required for the mission initially also decrease with decreasing camber, while the regenerated energy during the mission increases. However, also the effect on the aircraft mass is small, with only a few kilo difference between the lightest and heaviest calculated aircraft. As can be seen in the energy usage per flight phase, the cruise energy is reduced for the 50% propeller airfoil camber compared to the 100% cambered airfoil, but reducing the airfoil camber even more increases the energy used during the cruise phase again. This energy increase during this flight phase is directly a result of the decreased propeller efficiency of the propeller for when reducing the propeller airfoil camber lower than 50% as can be seen in table 7.5.

From the descent analysis for the steep descent of $920 ft/min$, it was already shown that for this steep descent, the propeller solidity has to increase to make sure the negative thrust during the descent could be achieved. The propeller solidity, and therefore the propeller chord for this mission is therefore constrained by the negative thrust during the descent. When reducing the propeller airfoil camber, this negative thrust during the descent could be achieved with a propeller with a reduction of the solidity of 29%, and therefore smaller propeller chord as shown in table 7.6. This reduction in propeller chord for reducing propeller airfoil camber is shown in figure 7.11. However, here is also seen that after the 25% airfoil camber, the propeller solidity is not constrained anymore by the negative thrust during the descent phase, and when reducing the propeller airfoil camber even more, the propeller solidity starts increasing again, to make sure enough thrust can be produced during the climb and cruise phase.

Table 7.5: Propeller efficiencies of the five simulations with a steep descent strategy with the propeller airfoil camber reducing from 100% (reference airfoil) to 0% (symmetrical airfoil) with a variable pitch propeller.

	100%	**75%**	**50%**	**25%**	**0%**
η_{cl} [%]	73.20	73.24	73.01	72.39	71.32
η_{cr} [%]	87.78	87.98	88.07	87.92	87.45
η_{de} [%]	18.72	20.42	21.03	21.42	22.21

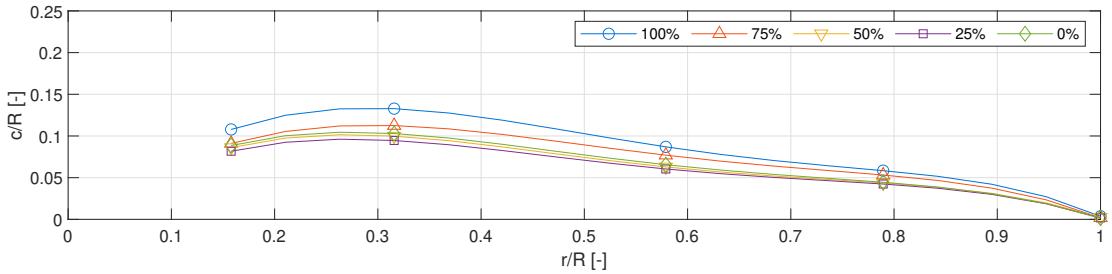

(a)

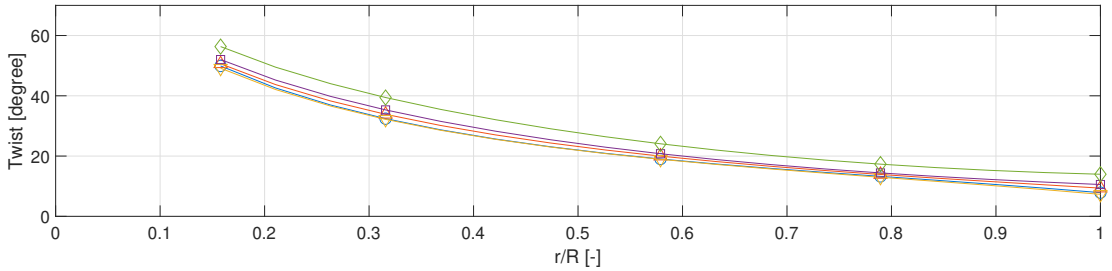

(b)

Figure 7.11: Propeller blade chord (a) and twist (b) distribution of the five simulations with a steep descent strategy with the propeller airfoil camber reducing from 100% (reference airfoil) to 0% (symmetrical airfoil) with a variable pitch propeller.

Table 7.6: Propeller solidity of the five simulations with a steep descent strategy with the propeller airfoil camber reducing from 100% (reference airfoil) to 0% (symmetrical airfoil) with a variable pitch propeller.

	100%	**75%**	**50%**	**25%**	**0%**
Solidity	0.072	0.062	0.065	0.051	0.055

7.3. Discussion

The analysis of the reduced airfoil camber of the propeller has shown two different effects. Depending on the descent strategy the aircraft mass increases or decreases when the propeller airfoil camber is reduced.

If the propeller chord is constrained by the descent negative thrust, i.e. the propeller chord has to increase to be able to deliver the negative thrust during the descent, reducing the propeller airfoil camber leads to a reduction in the propeller solidity. On the other hand, when the propeller geometry is not constrained by the descent phase the propeller solidity does increase when the propeller airfoil camber is reduced. This increase is necessary to compensate for the lower thrust during the climb and descent if the geometry would be kept constant, since the airfoils with reduced camber do produce less lift for the same local angle of attack. These two effects are show in figure 7.12.

In the same figure also the effect on the aircraft mass is seen. Here, the aircraft mass benefits (i.e. reduces) for the steep descent strategies when the propeller airfoil camber reduces. For the more shallow descent, with a rate of descent of $460ft/min$, the propeller solidity is not constrained by the descent thrust and the reduction in airfoil camber is thus not reducing the aircraft mass.

It should be noted however, that although some positive effects on the aircraft mass for the reduction of the propeller airfoil camber is found, the differences are less than 1% in weight reduction. Therefore, the added benefit of the reduced camber is within the sizing margin of 10% of the sizing tool. This means that the found weight reduction might disappear for the reduced airfoil camber when the aircraft is designed into more detail. Nevertheless, the effects of the camber analysis have shown that the reduced airfoil camber does have an effect on the performance of the propeller blades.

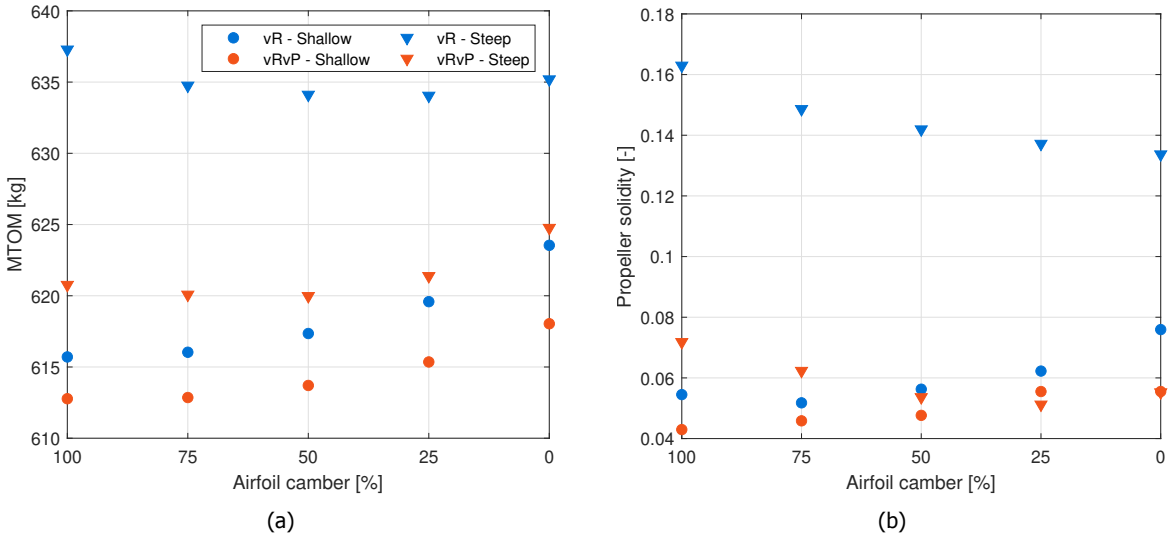

(a) (b)

Figure 7.12: Relation between the aircraft $MTOM$ and the propeller airfoil camber (a) and between the propeller solidity and propeller airfoil camber (b) plotted for all the different airfoil camber analysis simulations.

8

Design Mission Type Analysis

Finally, the aircraft mission type is of interest. The baseline mission is the longest mission the aircraft can fly, resulting in that the largest part of the mission is the cruise phase. However, the reference aircraft is made to be used as a trainer aircraft, in which the cruise phase is a smaller part of the mission and multiple climbs and descents are performed during one mission to train the pilot. This type of mission can be simulated in the sizing tool by reducing the range of aircraft, while also increasing the minimum state of charge of the battery after the mission. This results in an aircraft that is sized to perform short missions, in which the cruise phase is only a small part of the complete mission, while also being able to perform this mission multiple times in a row on one fully charged battery, just like what is expected from a trainer aircraft. In section 8.1 the different case studies for the simulations are given. The results are presented in section 8.2, with again the details of all the results given in appendix C. Finally, in section 8.3 the discussion of the results is given.

8.1. Simulation Case Studies

Besides the mission type, also two other variations around the design mission are analysed. First, the influence of the final descent on the cruise length is investigated. Afterwards, also an investigation on a steep descent is performed, where the effect of regenerative versus a non-regenerative aircraft is performed.

8.1.1. Final Descent Pattern Analysis

Not only the mission type of the aircraft is analysed to find its effects on the regenerative mode, aircraft sizing and propeller design. First, an analysis of the final part of the mission is performed. For the descent analysis, it is assumed that the steeper descents require a longer cruise distance to cover the same total range. However, the steeper descent can also lead to a reduction in cruise range, when during the final part of the mission a traffic pattern is used.

When using such a traffic pattern, as shown in figure 8.1, the aircraft flies first parallel to the runway, in the opposite direction of the landing direction, called the downwind leg. This downwind leg can still be performed at the cruise conditions and is therefore considered part of the cruise phase. After the downwind leg, a turn is made to approach the extended centre-line of

the runway which is called the base leg. In the final leg, the final descent along the extended centre-line of the runway is performed. For a steep descent, indicated with the black solid line, the distance covered during the final leg is shorter than for a shallow descent, as represented by the dashed red line. Therefore, also the downwind leg can be shorter for a steep descent approach, resulting in that the cruise phase also reduces in length. Hence, not only the descent phase is reduced in length for a steep descent, but also the cruise phase is reduced in length.

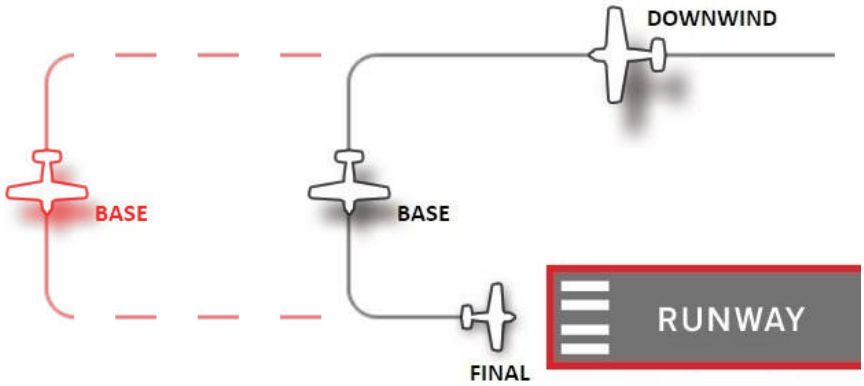

Figure 8.1: Indicative figure showing the final part of a traffic pattern, where a steeper descent (black solid line) results in a shorter cruise phase than a shallow descent (red dashed line).

This approach is different from the earlier performed descent analysis, where the total range is kept constant, while varying the descent strategy. Therefore, it is of interest to see how reducing the total range by performing a steeper descent influences the energy requirement for the total mission. In table 8.1 the different descent strategies, with the resulting total aircraft range is given which will be used as inputs for the sizing of the aircraft. All the descent strategies are again performed at the minimum drag speed.

Table 8.1: Simulation inputs for the final descent pattern analysis, where the total range and rate of descent are varied and the baseline mission underlined.

	1	**2**	**3**	**4**	**5**	**6**
Range $[km]$	149.4	142.4	138.9	136.8	135.4	133.6
RoD $[ft/min]$	230	345	460	575	690	920

8.1.2. Steep Descent Without Regeneration

Secondly, again the same long mission with a total range of $75NM$ will be analysed for the steep descent trajectories, however, this time the difference in a steep descent with and without regenerative mode is compared.

When a steep descent is performed, the airspeed of the aircraft does increase when not extra drag is created. To keep the airspeed during the descent phase at the desired level, air-brakes, such as spoilers or flaps, can be used. These air-brakes dump the excess energy into the air, while a regenerative propeller uses this excessive energy to charge the battery. This analysis

compares thus the exact same mission profile, but with and without the option for regeneration. Therefore, it will show the difference in the aircraft and propeller design when an aircraft would be able to regenerate energy compared to when this is not the case.

Since the effect of the air-brakes versus regenerative propeller case is expected to be the largest for the steepest descent, this analysis will only be performed for the steepest descent strategy. This means a rate of descent of $920ft/min$, while the airspeed is kept constant at the minimum airframe drag speed.

8.1.3. Short Mission Analysis

The last analysis is performed to find the effect of reducing the total range of the aircraft. The analysis is performed such that the aircraft is able to perform the climb and descent multiple times in a row, while using approximately the same amount of energy compared to the long range mission. In this way, the propeller geometry should be more focused on the climb and descent phase, which might change the optimal propeller geometry for these type of missions. This short design mission represents the training mission of the *Pipistrel Alpha Electro*, where multiple climb- and descent phases are possible to be performed on one fully charged battery.

For the short mission, it is chosen that the aircraft should be able to perform the climb, cruise and descent phase five times in a row, where the climb and descent strategy are equal to the long range baseline mission. This means that the cruise altitude of $750m$ is also used for the short range mission.

For the simulation of this short mission only the first pattern of the mission is simulated, the remaining four patterns (climb, cruise and descent phases) are assumed to be exactly equal to the first pattern. To be able to perform the remaining four patterns, the state of charge of the battery after the first pattern is required to be high enough such that enough energy is left to perform the final four patterns. For the range of one flight pattern of the short mission, the range cannot simply be one-fifth of the long range mission. The climb- and descent phases of the aircraft mission are less efficient than the cruise phase. Therefore, by making the mission range for one flight pattern five times smaller than the long range mission, the mission energy for one pattern is not expected to be five times reduced. The range is therefore reduced by more than a factor of five to compensate for this effect.

From the baseline mission it is found that the climb and descent phase make up of approximately 16% of the mission energy, while covering slightly less than $20km$ ground distance. Therefore, the short mission range is set to have a range of $20km$, in which the battery state of charge should be 80.6% after this mission, such that it can perform the mission multiple times, as would be the case in a training type mission.

Furthermore, to see if the effect of the mission descent is similar for a short mission, compared to the long baseline mission, two different descent approaches for the short mission are simulated. A 'shallow' descent, similar to the baseline mission on $460ft/min$ and a 'steep' descent, where the rate of descent is doubled to $920ft/min$, both performed at the minimum drag speed of the airframe. This result in a total of four mission types, summarised in table 8.2.

Table 8.2: Simulation inputs for the short range, trainer type, mission where the cruise range, minimum state of charge and descent strategy are varied and the baseline mission underlined.

Simulation	**1**	**2**	**3**	**4**
Range $[km]$	138.9	138.9	20.0	20.0
RoD $[ft/min]$	460	920	460	920
min SoC [%]	20	20	80.6	80.6

8.2. Simulation Results

The previous two analysis cases were both performed for a, for full-electric aircraft, relative long mission of $75NM$, while keeping this total range equal for all the simulations. However, the *Pipistrel Alpha Electro* is not intended to use as a cruiser aircraft. Therefore, three types of analysis are performed to see how this long, constant, range affects the design of the aircraft and propeller, and how reducing the range influences the regeneration mode and aircraft- and propeller design.

8.2.1. Final Descent Pattern Analysis

For the case where the final descent is flown using a traffic pattern, the different descent approaches are analysed, but now also the total range is compensated for the change in cruise and descent distance. This results in a longer flight distance for the shallow descent, while the steepest descent strategy also results in the lowest total range covered. The flight profile of these missions is given in figure 8.2, showing the reduced total range of the steep descent mission, while the shallow descent has an increased total range, compared to the baseline mission. The effect of this longer range can also be seen in the energy requirement for these descent strategies, as shown in figure 8.3. The longest mission also requires the most energy, where the steeper the descent becomes, the energy requirement also reduces, due to the shorter total distance flown. However, due to the difference in the total distance flown the comparison of the total energy requirement is not the fairest comparison.

In table 8.3 a comparison is made based on the payload-range energy efficiency ($PREE$) of the different missions, using equation (8.1). A higher $PREE$ means that the payload can be flown over the total mission distance with less energy than a mission with a lower $PREE$. In this table, it can be seen that the $PREE$ is the highest for the mission with a rate of descent of $690ft/min$. This means that not only the energy is reduced for the steeper descent missions, but also the efficiency is increased. This shows that when the steeper descent, during which the regenerative mode is active, is used for the descent, and this also reduces the cruise distance the total energy requirement of the mission can be reduced, also resulting in a lighter aircraft design.

$$PREE = \frac{W_{Payload} R}{E_{mission}} \tag{8.1}$$

Looking at the propeller geometry, in figure 8.4 the same trends can be seen as for the descent analysis, with a constant total range. Similar, the solidity does also show the same trend as

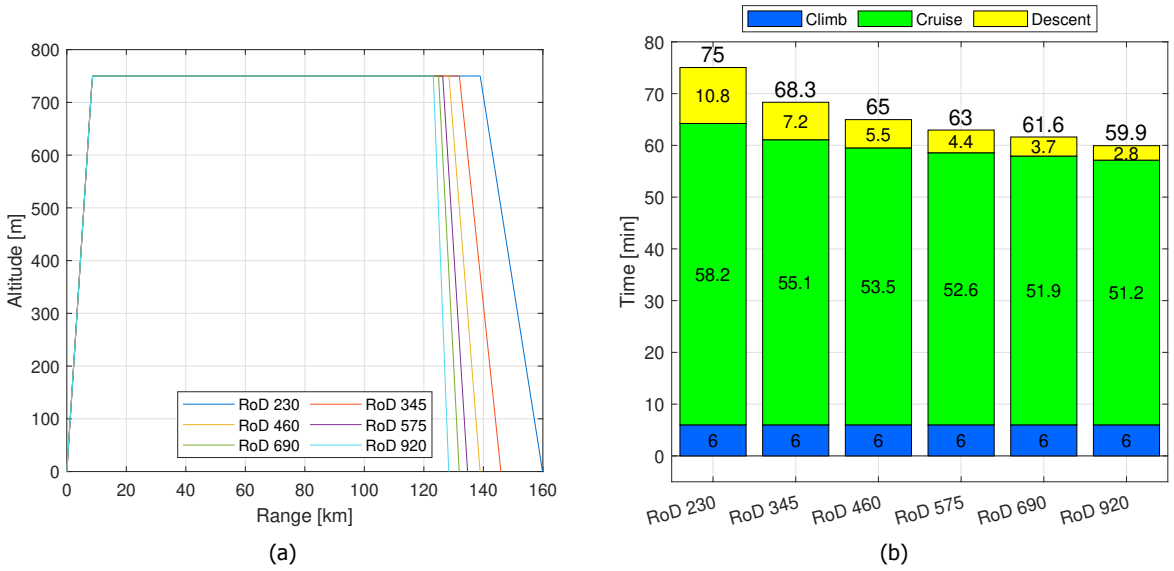

Figure 8.2: Mission profile (a) and time distribution (b) of the six simulations with varying rate of descent, while also the total range is reduced with increasing rate of descent, with a variable pitch propeller.

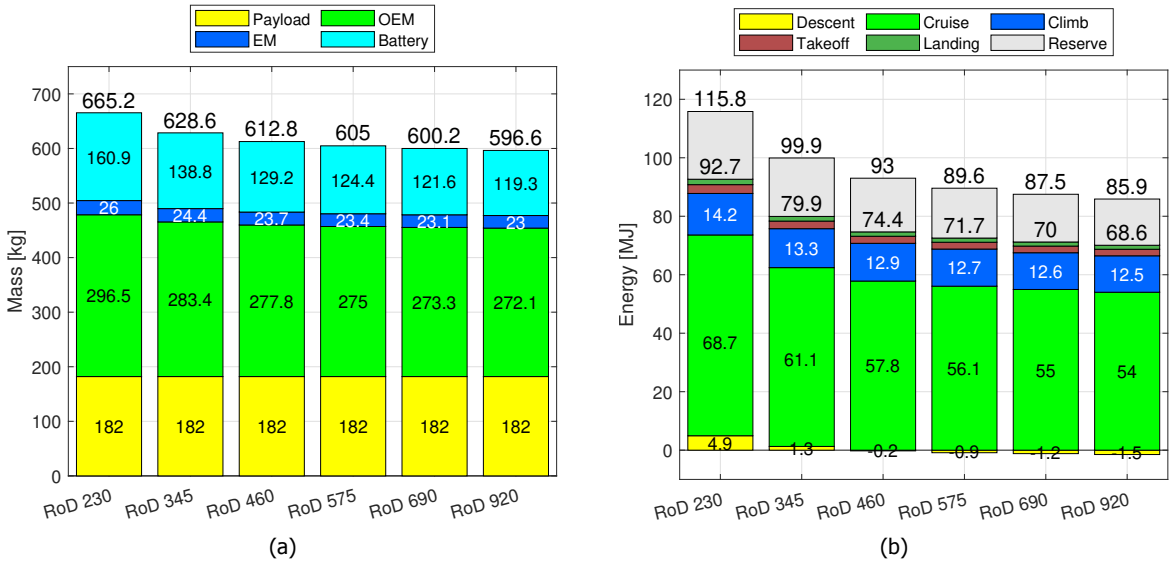

Figure 8.3: Mass (a) and energy (b) per flight phase breakdown of the six simulations with varying rate of descent, while also the total range is reduced with increasing rate of descent, with a variable pitch propeller.

Table 8.3: Payload-Range energy efficiency of the six simulations with varying rate of descent, while also the total range is reduced with increasing rate of descent, with a variable pitch propeller.

	RoD 230	**RoD 345**	**RoD 460**	**RoD 575**	**RoD 690**	**RoD 920**
PREE [–]	3.252	3.439	3.517	3.541	3.550	3.527

shown in table 8.4. The highest rate of descent requires a higher solidity, to be able to generate enough negative during the descent phase. This increased solidity negatively impacts the cruise performance, resulting in the lower found $PREE$ for this descent approach. All the other propeller geometries are more optimised with respect to the cruise phase, since the longest time of the mission is performed in this phase.

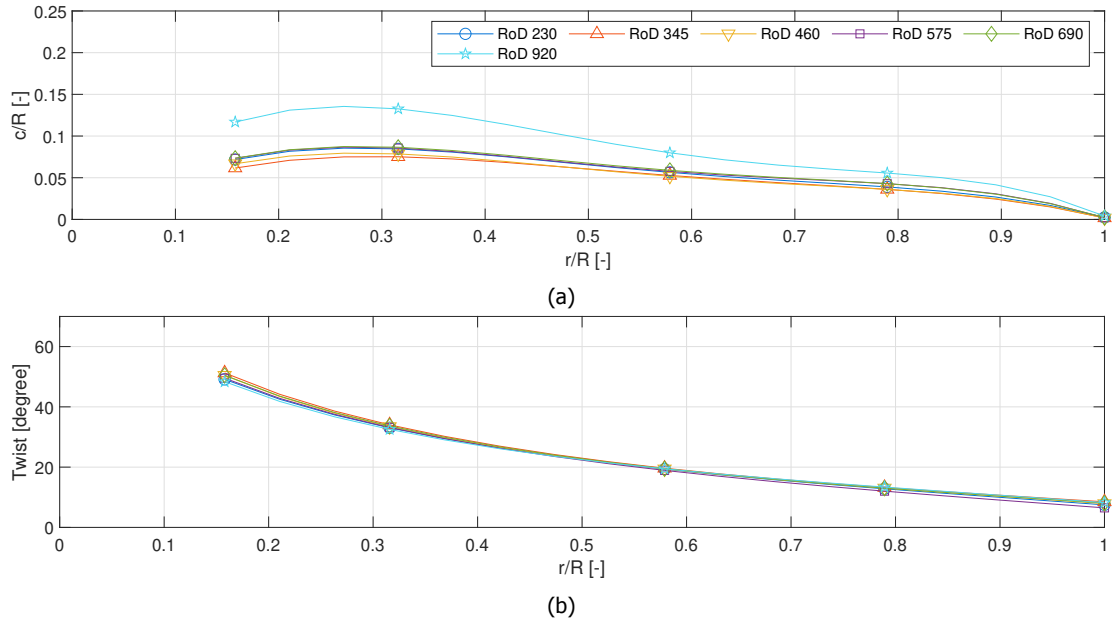

Figure 8.4: Propeller blade chord (a) and twist (b) distribution of the six simulations with varying rate of descent, while also the total range is reduced with increasing rate of descent, with a variable pitch propeller.

Table 8.4: Propeller solidity of the six simulations with varying rate of descent, while also the total range is reduced with increasing rate of descent, with a variable pitch propeller.

	RoD 230	**RoD 345**	**RoD 460**	**RoD 575**	**RoD 690**	**RoD 920**
Solidity	0.046	0.042	0.043	0.048	0.049	0.070

8.2.2. Steep Descent without Regeneration

The analysis for the case where the steep descent is performed with and without a regenerative propeller is performed for the variable pitch propeller. The steep descent is chosen because for missions when a steep descent is required the potential regenerated energy is the highest. Therefore the baseline mission, but with a rate of descent of $920 ft/min$ is used for the comparison. The mass and energy distribution of the two missions are shown in figure 8.5. Clearly, in the mission where the air-brakes are used instead of the regenerative propeller, no energy is used or regenerated during the descent, since the additional drag that is needed to fly at the prescribed airspeed and rate of descent is generated by the air-brakes, which do not regenerate the excess energy. This causes that the total mission energy increases, with as a result that the battery mass also increases. The increased battery mass results then in a higher total aircraft mass, resulting in that the energy used during the climb- and cruise phase is also increasing.

So although only $1.5MJ$ is regenerated by the regenerative propeller, the total mission energy is reduced by $2.3MJ$. The regenerative energy does not only affect the descent performance in this case, but also has a positive on the other phases, due to the reduced battery size.

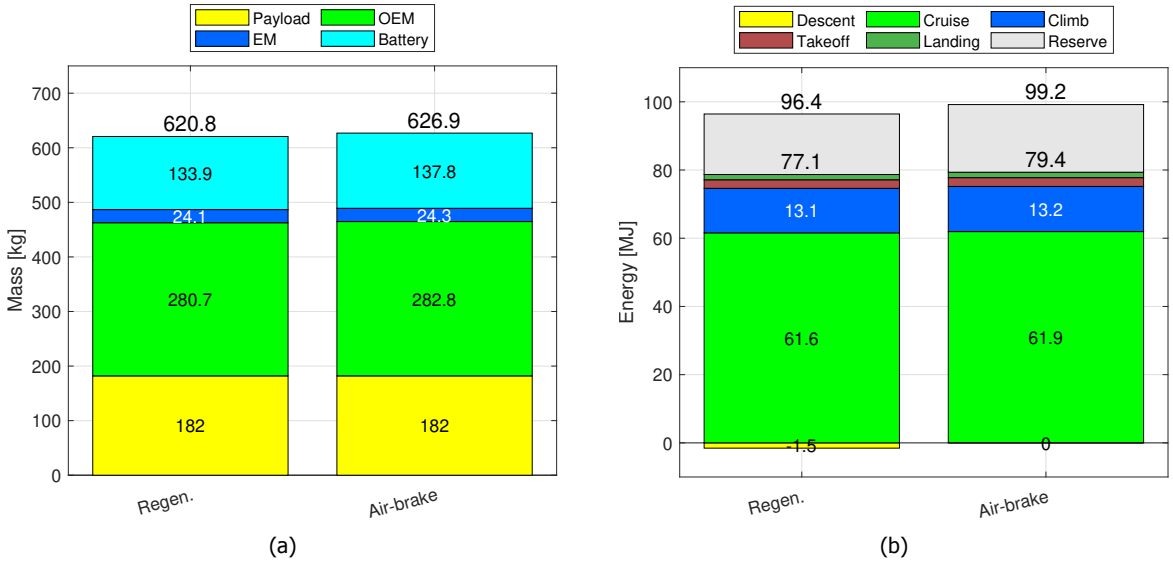

Figure 8.5: Mass (a) and energy (b) per flight phase breakdown of the two simulations with and without regeneration, with a variable pitch propeller.

For the case of the air-braked mission, compared to the regenerative mission, the propeller does not need to provide the negative thrust during the descent phase. Thus, the propeller does not need to be sized for this flight phase. The propeller geometry can be more optimised towards the climb and cruise phase, resulting in a lower solidity and higher efficiency during the climb and cruise, as shown in figure 8.6 and table 8.5. Although the propeller is more efficient during these phases, the energy that is not regenerated during the descent phase is higher, resulting in a higher total mission energy requirement. Therefore, it is found that regeneration during the descent phase, when a steep descent is performed, would be an effective way to minimize the energy penalty associated with these steep descents. Such steep descents could be beneficial to reduce noise exposure around airports.

Table 8.5: Propeller solidity of the two simulations with and without regeneration, with a variable pitch propeller.

	Regenerative	**Air-brakes**
Solidity	0.072	0.049

8.2.3. Short Mission Analysis

Finally, the short mission (SM) analysis is performed, where the short, trainer-type, mission is compared to the long range mission (LM). The short mission consists of a $20km$ range mission, which has to be performed five times to simulate the trainer-type mission.

Only the first climb, cruise and descent phase is modelled for the short mission, where the

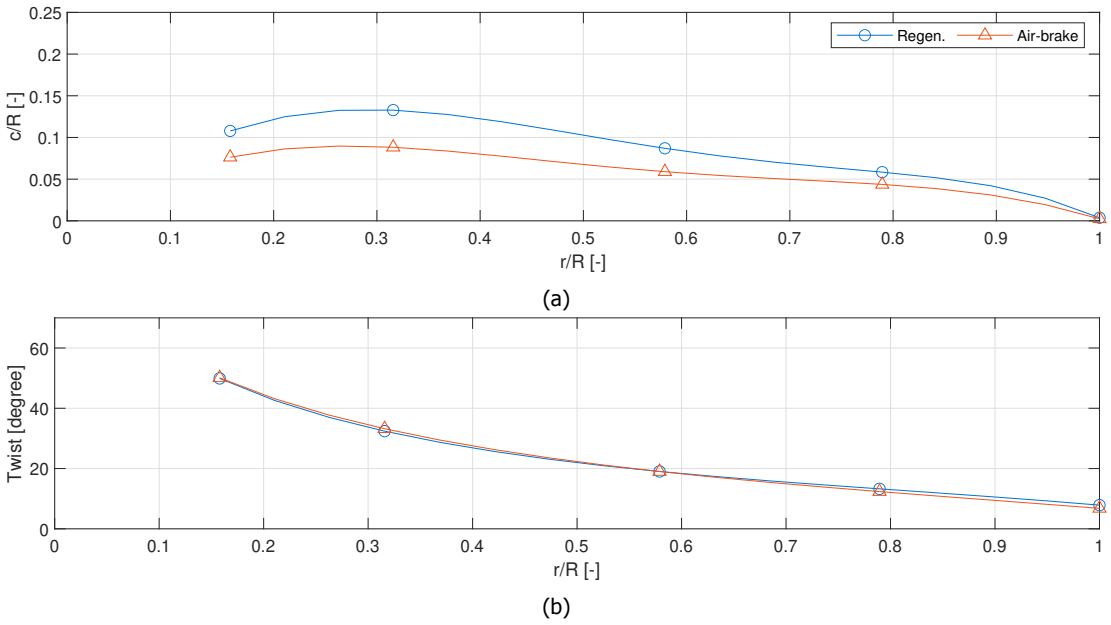

Figure 8.6: Propeller blade chord (a) and twist (b) distribution of the two simulations with and without regeneration, with a variable pitch propeller.

showed reserve energy can be used to perform multiple times the climb, cruise and descent phases. For one full pattern, with the take off, climb, cruise, descent and landing, the battery should have 80.6% battery charge remaining. In this way, the four remaining patterns can be flown, such that at the end of these patterns the minimum required state of charge of 20% is approximately reached.

In figure 8.7 the mission profile of the long range mission is shown, as well as the short range mission for both the shallow and steep descent. From this figure, the repetition in the mission profile of the short mission is shown, indicating the trainer type mission. Also, from the time distribution it can be seen that for the short mission, the time spend in the cruise phase is shorter than for the long range mission. The mass and energy distribution of these aircraft are given in figure 8.8. For the energy usage, both the single pattern mission is shown, as well as the short mission where the five patterns are flown adjacent to each other.

The energy distributions are shown in tables 8.6 and 8.7. For both the shallow and steep descent mission for the short mission, the energy distribution is given for the single pattern flight, but also how much energy is consumed when the five patterns are flown adjacent to each other, where the take off is only performed before the five patterns, and the landing afterwards, resulting in that these flight phases are only performed once.

Since the missions are quite different in nature, the comparison for the energy and weight distribution between the long and short missions does not provide helpful information. However, within the mission a difference is made in the descent strategy, with a shallow descent, with a rate of descent of $460 ft/min$, and a steep descent, with a rate of descent of $920 ft/min$. For both the long and short missions, it can be seen that the steep descent, although regenerating

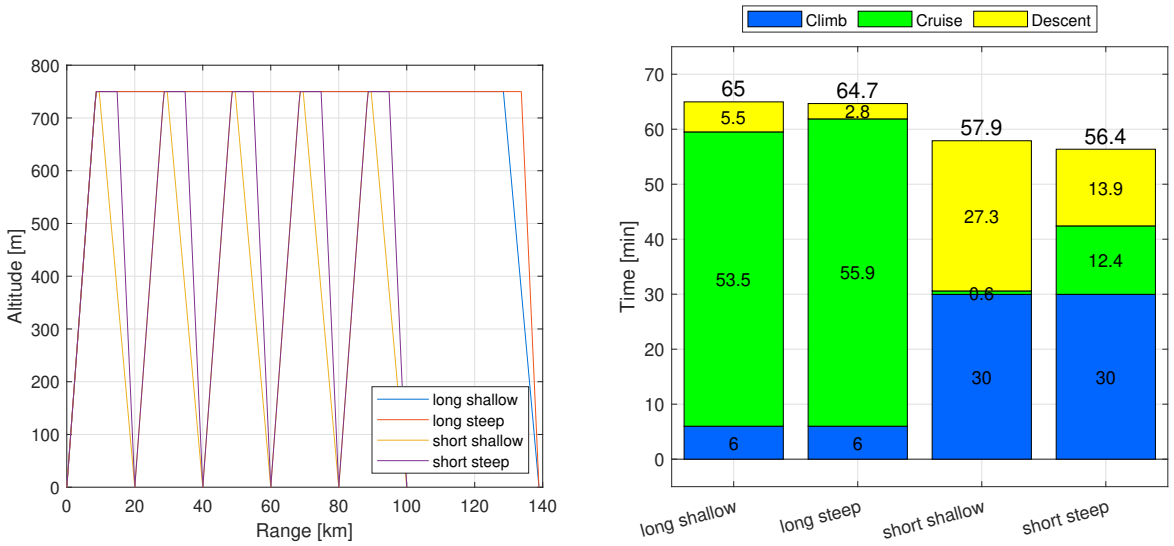

Figure 8.7: Mission profile (a) and time distribution (b) of the four simulations of the long and short mission, with steep and shallow descent strategies, with a variable pitch propeller.

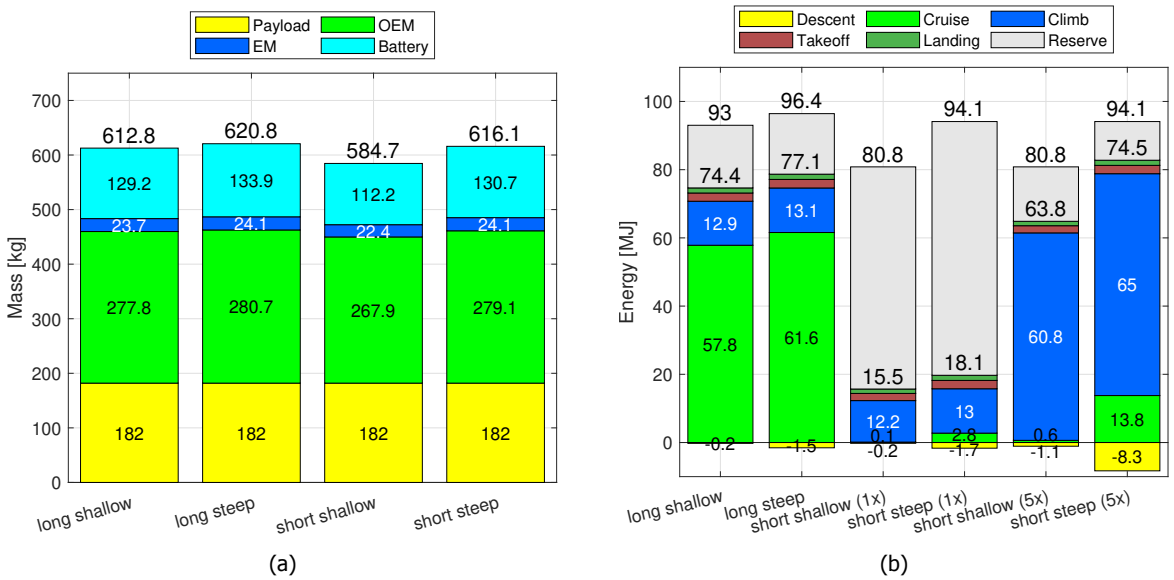

Figure 8.8: Mass (a) and energy (b) per flight phase breakdown of the four simulations of the long and short mission, with steep and shallow descent strategies, with a variable pitch propeller.

Table 8.6: Energy usage per flight phase, for the long mission (LM) and the short mission (SM) with the shallow descent strategy, including take off and landing, in MJ with in between parentheses the percentage of total mission energy given.

	Take off	Climb	Cruise	Descent	Landing	Total
SM - (1x)	2.1 (13.6%)	12.2 (78.6%)	0.1 (0.8%)	−0.2 (−1.4%)	1.3 (8.4%)	15.5
SM - (5x)	2.1 (3.3%)	61.0 (95.4%)	0.6 (1.0%)	−1.0 (−1.7%)	1.3 (2.0%)	63.8
LM	2.4 (3.3%)	12.9 (17.3%)	57.8 (77.7%)	−0.2 (−0.3%)	1.5 (2.0%)	74.4

Table 8.7: Energy usage per flight phase, for the long mission (LM) and the short mission (SM) with the steep descent strategy, including take off and landing, in MJ with in between parentheses the percentage of total mission energy given.

	Take off	Climb	Cruise	Descent	Landing	Total
SM - (1x)	2.4 (13.6%)	13.0 (72.0%)	2.8 (15.3%)	−1.7 (−9.2%)	1.3 (8.4%)	18.1
SM - (5x)	2.4 (3.3%)	65.0 (87.3%)	13.8 (18.5%)	−8.3 (−11.1%)	1.3 (2.0%)	74.5
LM	2.5 (3.3%)	13.1 (16.9%)	61.6 (79.8%)	−1.5 (−2.0%)	1.5 (2.0%)	77.4

more energy, requires more energy than the shallow descent strategy. The same reasons as for the descent analysis can be used, the steep descent requires a longer cruise range, resulting in a higher overall energy consumption.

The weight penalty for the short, steep descent, mission is much higher though, both absolute as percentage-wise, than for the long mission. The long mission requires an $8kg$ (1.3%) heavier aircraft for the steep mission, while the short mission requires a $31kg$ (5.4%) heavier aircraft. Since this mission is very short, the increase in cruise distance is relatively much larger than for the long mission, resulting in that for the steep descent the cruise phase becomes a more significant part of the flight, increasing the total energy requirement, and therefore the aircraft mass.

The short mission propeller geometry can be more optimised towards the climb and descent phases, since these phases make up a larger part of the mission, compared to the long mission. This results in that the solidities of the short missions are higher compared to the long missions, as shown in figure 8.9 and table 8.8. The shallow descent, short mission has an increased solidity of 15% compared to the long mission, while for the steep mission the solidity increases by 63%.

Table 8.8: Propeller solidity of the four simulations of the long and short mission, with steep and shallow descent strategies, with a variable pitch propeller.

	Long Shallow	Long Steep	Short Shallow	Short Steep
Solidity [%]	0.043	0.072	0.049	0.117

This increased solidity for the short mission also has a small influence on the propulsive performance of the propeller in the different flight phases, as shown in table 8.9. For the long mission, the propeller is more optimised towards the cruise, since this has the highest weight-factor during the optimisation. For the short missions, the climb and descent phases have a

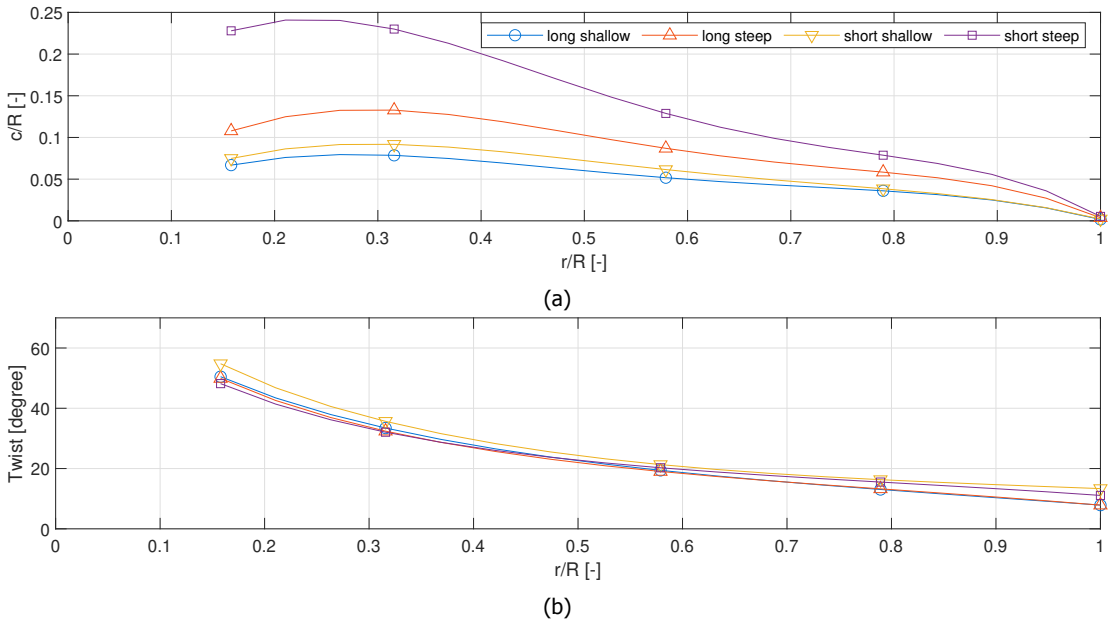

Figure 8.9: Propeller blade chord (a) and twist (b) distribution of the four simulations of the long and short mission, with steep and shallow descent strategies, with a variable pitch propeller.

higher weight-factor, resulting in the increased climb and descent efficiencies for these phases, compared to the long mission with the same descent strategy. For the shallow descent, the climb efficiency of the propeller has increased 1.2% for the short mission, compared to the long mission. Since only very little energy is regenerated for this mission, the descent efficiency is similar for both missions. For the steep mission, the largest increase in propeller efficiency is found in the descent phase. The descent efficiency is 7.5% higher for the short mission than for the long mission, while the cruise efficiency is almost equal for both missions.

Table 8.9: Propeller efficiencies of the four simulations of the long and short mission, with steep and shallow descent strategies, with a variable pitch propeller.

	Long Shallow	**Long Steep**	**Short Shallow**	**Short Steep**
η_{cl} [%]	73.12	73.20	74.00	72.92
η_{cr} [%]	88.34	87.78	88.46	86.73
η_{de} [%]	1.43	18.72	1.32	20.14

8.3. Discussion

The descent strategy analysis and the propeller airfoil camber analysis were both performed for the same long range cruise mission, with a total range of $75NM$. Both these analyses showed that to regenerate energy during the descent, more energy has to be spent during the complete mission, resulting in a heavier aircraft. Although lowering the propeller airfoil camber does reduce the increase in total energy usage and therefore aircraft mass, the aircraft is still heavier,

compared to the non-regenerative case.

In section 8.3.1 the effect of the reduced mission range is discussed, after which in section 8.3.2 a discussion around aircraft missions that are different from the design mission is presented.

8.3.1. Design Mission Profile

The *Pipistrel Alpha Electro* is fitted with a regenerative system, and experiments have shown that using the regenerative mode more flight patterns can be flown [17]. Thus, for a single flight pattern of the experiment, the energy requirement was reduced. For the long range mission, with a constant total range, the opposite results were found however. Therefore, also an investigation on the design mission profile was performed. The mission range has been reduced, such that the same climb and descent of the long mission could be performed five times in a row, with a total energy requirement for these five climbs and descent approximately equal to the long range mission.

From the results it is shown that the short mission does influence the propeller geometry, resulting in a propeller with higher solidity, which has a higher efficiency in the climb and descent phase, compared to the lower solidity propeller. However, also the same effect on the energy requirement can be seen for the short mission. A steeper descent, resulting in more regenerated energy does also result in a higher energy consumption for the whole mission. Again, the longer cruise phase plays an important role in this increased energy requirement.

Using the negative thrust as provided by the propeller, a steeper descent can be performed while keeping the flight speed constant. Therefore, keeping the same flight speed, a steeper descent can be performed using a regenerative propeller. This means that in a shorter flown distance, the same number of climbs and descent can be performed. From the flight pattern analysis, it was shown that indeed when the steeper descent results also in a short cruise, and therefore total mission length, the energy requirement of the aircraft is reduced, while the $PREE$ is increased. Indicating that more flight patterns can be flown when the steeper, regenerative, descent is used which also results in a reduction in the cruise distance. Unfortunately, it is not known if the increase in flight patterns during the performed experiment [17] is also a result of the reduced cruise distance. However, from the performed analysis this is the most likely explanation.

Not only does the reduced cruise distance due to a steep, regenerative descent reduce the energy consumption, as shown in the flight pattern analysis, also, the time in which these climbs and descent are performed decreases. Since the cost of a trainer mission is not only directed by the fuel (or energy) used during the mission, but also the time the instructor needs to spend on the training, this reduced mission time could reduce the total costs of regenerative flight training missions.

8.3.2. Off-design Descent Performance

Up till now, it is assumed that the aircraft mission profile can be freely chosen and flown. However, in the real world some airports may have restrictions on the approach, for instance a steep descent is required to reduce the noise exposure of the aircraft on the ground. This can lead to

that the aircraft has to fly on descent profiles steeper than the aircraft is designed for. To make sure the aircraft does not pick up too much speed during these descent strategies, air-brakes such as lift-dumpers or spoilers are used to keep the airspeed of the aircraft at the desired speed. Aircraft with the possibility to use the regenerative mode, can use the negative thrust produced during the regenerative descent to keep the airspeed under control. Instead of creating additional drag to make sure the aircraft does not accelerate during the descent, the propeller is used to generate power which is regenerated by the electric motor and then stored in the batteries. The results have shown that indeed, for missions with steep descent trajectories, it is more beneficial to use the regenerative propeller to charge the battery, than to add extra additional drag using the air-brakes.

Since the steep descent would not be needed for all missions, the aircraft can be designed for the mission which is the most energy efficient, but with the possibility to use the regenerative mode. In this way, the propeller geometry is not constrained by the high negative thrust it needs to produce during the steep descent, but it is also not able to produce this high negative thrust. For this off-design mission, the propeller can be used to provide the maximum negative thrust it is able to produce for the off-design steep descent, while the air-brakes can be used to keep the speed of the aircraft at the desired speed.

In figure 8.10 the mass distribution and energy consumption for the compared aircraft is given. First, the baseline aircraft design is given, which is the design for the mission of the fixed pitch propeller, performing the long 'cross-country' mission, with the descent strategy with a rate of descent of $460ft/min$ performed at the minimum airframe drag speed. This same aircraft design is then used to perform the steep descent mission (with a rate of descent of $690ft/min$). Two strategies are chosen two perform this steep descent. First, the air-brakes are used and no regeneration is applied. All the additional drag to stay at the required airspeed, the minimum airframe drag speed, is created by the air-brakes. Secondly, the steep descent is performed where the propeller is applying the maximum negative thrust possible, and using the air-brakes to generate the additional drag to stay at the given airspeed. These three analysis cases are based on the same aircraft design, hence also the aircraft mass distribution of the aircraft is identical and equal to $615.7kg$. Therefore, also the battery is equal in size and has a capacity of $94.2MJ$, but the required mission energy differs between the mission. Finally, also the results are shown of the aircraft which is designed for the steep descent mission.

As can be seen, the steep descent trajectory for the baseline aircraft design does increase the total energy requirement for the mission. The regenerative mode is only able to regenerate $0.4MJ$ using the propeller that was not designed for the steep descent strategy, where the propeller that is designed for this steep descent can regenerate $1.3MJ$. Also should be noted that for the off-design steep descent strategy mission the minimum state of charge of the battery during the mission reaches levels below 20% (17.8% and 18.3% respectively for the air-brake and regenerative mission), stating that is mission is undesirable, since this negatively impacts the battery life duration.

The same effects are seen for the variable pitch propeller design, as shown in figure 8.11. Also here, first the baseline, reference, mission is given for the variable pitch propeller. Also, the two off-design mission profiles of this aircraft are given, where the first off-design mission is only using the air-brakes, while the second off-design mission is both using the regeneration mode

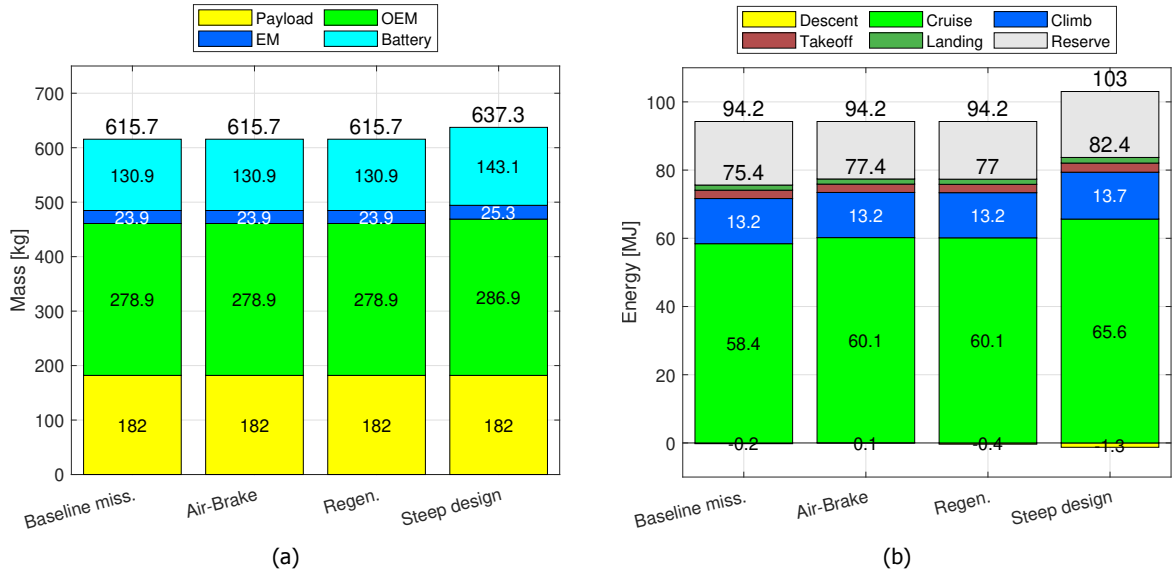

Figure 8.10: Mass (a) and energy (b) per flight phase breakdown of the sized aircraft for the fixed pitch propeller baseline mission, when flown on a steep descent strategy and the sized aircraft for the steep descent strategy.

and air-brakes during the steep descent. Finally, the design is given for the aircraft that has been designed for the steep descent.

Thus, a regenerative off-design steep descent strategy is possible to be performed by the aircraft, when also the air-brakes are used to keep the airspeed during the descent at the correct speed. However, the regeneration which can be done by the propeller is smaller compared to the propeller that is designed for the steep descent. Furthermore, the off-design steep descent strategy does for both propellers result in an increased energy consumption, resulting in that the minimum state of charge of 20% is exceeded. So, although the off-design steep descent is possible, it is undesirable to be performed since exceeding the minimum state of charge will reduce the battery life.

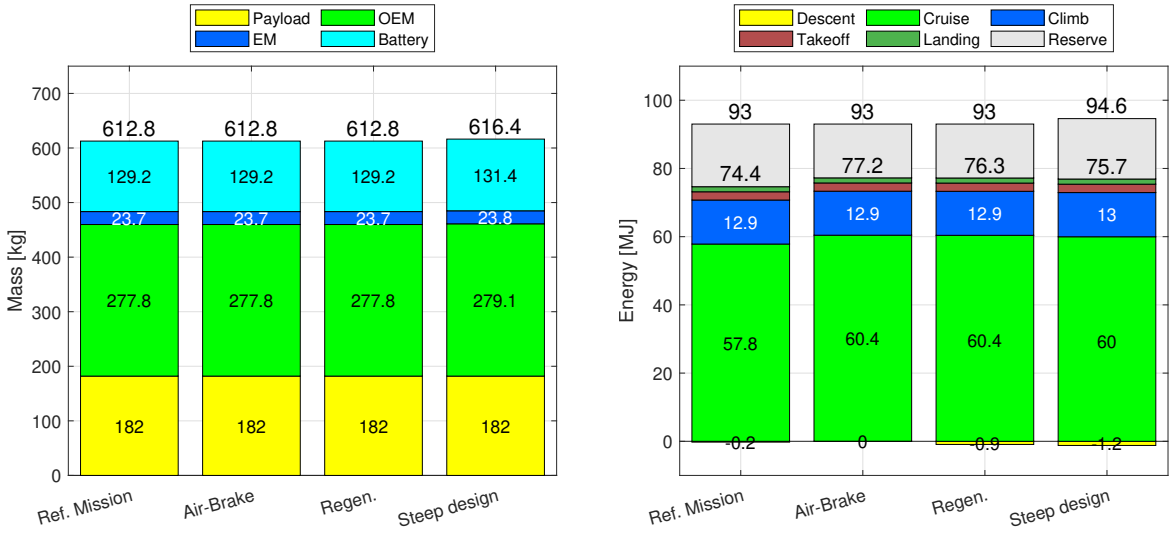

Figure 8.11: Mass (a) and energy (b) per flight phase breakdown of the sized aircraft for the variable pitch propeller baseline mission, when flown on a steep descent strategy and the sized aircraft for the steep descent strategy.

9

Conclusion

During the thesis work the effect of adding the regeneration mode on the aircraft- and propeller design, as well as the effect on the required mission energy, is investigated. This is done by creating a sizing method in which not only a full-electric aircraft can be sized, but also the propeller is simultaneously designed during the aircraft sizing. Both the aircraft sizing loop, the regenerative flight mode and the propeller analysis methods have been validated using experimental data, giving extra confidence in the working of the sizing method.

Using this design method the *Pipistrel Alpha Electro* has been simulated, from which the mission profile was used as the baseline mission for the different performed analyses. First, the descent strategy of the mission has been analysed to find out what the influence is of the chosen strategy on the regenerated energy and how the descent strategy is influencing the aircraft and propeller design, which are also influencing the other flight phases: the climb and cruise phase.

This analysis showed that for a freely chosen descent strategy, where a constant rate of descent and a constant airspeed is maintained throughout the whole descent phase, and a fixed mission range is used, regenerative descent will always lead to a higher mission energy requirement, up to 9% for a fixed pitch propeller. When the aircraft is designed around these missions, this higher energy consumption will lead to a heavier aircraft. This will always be the case, since for the steeper descent strategies, where more energy can be regenerated, the cruise phase has to become longer. This longer cruise phase will require extra cruise energy and due to the losses associated with producing thrust, more energy is lost during the cruise phase. This extra used energy cannot be regenerated during the descent, since also during the descent phase losses are present in the regeneration of energy.

Looking at the descent phase only, it is seen that the propeller geometry is highly dependent on the negative thrust it has to produce during the regenerative descent phase. Especially for the fixed pitch propeller, the solidity of the propeller has to increase, up to 199% compared to the baseline mission, to be able to produce the high negative thrust during the descent. This increased solidity does negatively influence the performance during the cruise phase, increasing the energy requirement for this phase. The variable pitch propeller can produce higher negative thrust values, without the need to increase the chord, resulting in better cruise performance for the variable pitch propeller. However, since the added weight of a variable pitch system is not taken into account, it is not known if the higher propeller efficiency offered by the variable pitch propeller indeed leads to a reduction in the aircraft mass, and therefore the energy requirement of the mission.

After the descent analysis, the influence of the propeller design on the regenerative mode and the aircraft sizing has been investigated. Since the propeller has to work both in the propulsive mode and the regenerative mode, with positive and negative angles of attack respectively, the influence of the airfoil camber has been investigated.

For both the fixed- and variable pitch propeller it is seen that although the solidity needs to increase to be able to produce the required negative thrust, the shaft power is only related to the negative thrust. The difference in propeller solidity for the different simulations has no found influence on the power generation by the propeller. This is true when the propeller airfoil is not varied between the different calculated propellers. When the propeller geometry is constrained by the negative thrust during the descent, the propeller solidity can be reduced, up to 17% for a fixed pitch propeller or 29% for a variable pitch propeller, by reducing the propeller airfoil camber. The reduced airfoil camber can produce more negative thrust for the same geometry, resulting in that for a given negative thrust the solidity can reduce.

Finally, the analysis on the mission profile has been explored, where different types of missions are analysed, including a short training type mission. This shows the influence of the different types of missions that can be performed and how this influences the aircraft and propeller design.

The strategy where the regenerative mode does reduce the total energy requirement for the mission and therefore also the aircraft mass, is when the final phase of the mission is flown using a traffic pattern. When the steeper descent strategy is used, the flown distance of the downwind leg, which is considered as part of the cruise phase, is also reduced. This results in that the steeper regenerative descent results not only in a reduction in descent distance, but also in cruise distance. For a reduction of 4% of the total mission range, an 8% reduction of the required mission energy was found. This shorter total range of the mission, in combination with the regenerated energy has a positive effect on the total mission energy, and therefore a reduction of the aircraft mass is possible.

To summarise, the regenerative mode on a full-electric aircraft does only reduce the total energy requirement when the regenerative descent does reduce the total distance flown. Furthermore, for high regenerative descent strategies, where high negative thrust is needed the propeller solidity needs to increase to be able to produce the negative thrust. This increase in solidity can be compensated with a reduction of the propeller airfoil camber. The resulting mission energy requirement determines the battery mass, which is an important factor in the total aircraft mass, due to the snowball effect.

10

Recommendations

The presented conclusion are based on different assumptions made throughout the thesis work. Therefore, to find more details about the results of the simulations, further research is needed to find the effect of these assumptions. Recommendations are given for further research to investigate the influence of these assumptions.

In the discussion of the descent strategy analysis, it was already noticed that the optimisation objective function does not take the power setting of the flight phases into account, resulting in that the high powered flight phases (i.e. the climb phase) are not weighted correctly by the used objective function. When the optimisation function is adjusted for this behaviour, also the climb phase will be taken more correctly into account for the propeller geometry design. This effect is already shortly examined in section 6.3.3, but a more thorough analysis would be needed to check if the newly suggested function does indeed work as intended.

Moreover, the descent strategy analysis only considered variations in the descent strategy with respect to the baseline mission. However, it might be that for the ideal descent strategy requires more modifications to the descent strategy than made changes. For instance, a high speed, steep descent has not been analysed in the descent strategy analysis. To get a broader overview of the optimal descent strategy more descent strategies should be analysed to see also these effects.

Furthermore, for the propeller design currently only the aerodynamic properties are used to find the optimal geometry for the given mission. The structural integrity, manufacturability and noise emissions are not taken into account for the propeller geometry optimisation. The results showed that the tip of the propellers have a small chord length which is unfavourable for the structural integrity of the propeller. Taking these factors into account would result in a propeller that can also be produced for experimental testing.

Also regarding the propeller design, it is assumed that the propeller airfoil is constant for the complete propeller blade. It is however known that the tip and root of the propeller blade experience different loads and local angles of attack in the propulsive and regenerative mode. Therefore, optimising the airfoil distribution along the blade span as well could result in both regenerative and propulsive efficiency increase.

On the aircraft design level, the control and stability of the aircraft are not taken into account during the design of the aircraft. However, for the chosen reference aircraft, the *Pipistrel Alpha Electro*, the propeller is located in front of the horizontal and vertical stabilizers. Especially during

the regenerative flight phase, energy is taken away from the wake of the propeller. Since these two stabilizers are placed within the wake of the propeller, their effectiveness can reduce resulting in a less stable or controllable aircraft. Therefore, to make sure that the regenerative mode does not negatively influence the controllability of the aircraft, this analysis should also be included in the design method.

Bibliography

[1] C. Mikkelson, J. Bober, and A. Mitchell, "Summary of Recent NASA Propeller Research," in *AGARD Fluid Dyn. Panel Meeting on Aerodyn. and Acoustics of Propellers*. Toronto, Canada: NASA Lewis Research Center; Cleveland, OH, United States, Jan. 1984, p. 42.

[2] T. M. Young and M. Hirst, "Jet engine design drivers: Past, present and future," in *Innovation in Aeronautics*. Woodhead Pubishing, 2012, pp. 56–82.

[3] T. Cooper, I. Reagan, C. Porter, and C. Precourt, "Global Fleet & MRO market forcecast commentary," 14-01-19.

[4] S. J. Gerssen-Gondelach and A. P. C. Faaij, "Performance of batteries for electric vehicles on short and longer term," *Journal of Power Sources*, vol. 212, pp. 111–129, Aug. 2012.

[5] R. Henke and R. Winkler, "Zero Emission Aviation," Nov. 2020.

[6] C. Friedrich and P. A. Robertson, "Hybrid-electric propulsion for automotive and aviation applications," *CEAS Aeronautical Journal*, vol. 6, no. 2, pp. 279–290, Jun. 2015.

[7] B. J. Brelje and J. R. R. A. Martins, "Electric, hybrid, and turboelectric fixed-wing aircraft: A review of concepts, models, and design approaches," *Progress in Aerospace Sciences*, vol. 104, pp. 1–19, Jan. 2019.

[8] W. F. Durand, B. Melvill Jones, and L. Kerber, *Aerodynamic Theory: A General Review of Progress, Under a Grant of the Guggenheim Fund for the Promotion of Aeronautics / Vol. V.* Berlin: Springer, 1935.

[9] C. Adkins and R. H. Liebeck, "Design of optimum propellers," *Journal of Propulsion and Power*, vol. 10, no. 5, pp. 676–682, 1983.

[10] R. MacNeill and D. Verstraete, "Optimal Propellers for a Small Hybrid Electric Fuel-Cell UAS," in *2018 AIAA/IEEE Electric Aircraft Technologies Symposium*. American Institute of Aeronautics and Astronautics, 2018.

[11] T. Sinnige, T. Stokkermans, N. van Arnhem, and L. L. Veldhuis, "Aerodynamic Performance of a Wingtip-Mounted Tractor Propeller Configuration in Windmilling and Energy-Harvesting Conditions," in *AIAA Aviation 2019 Forum*, ser. AIAA AVIATION Forum. American Institute of Aeronautics and Astronautics, Jun. 2019.

[12] B. van der Beek, "Modeling Propeller Performances in Energy Harvesting Conditions," p. 38, Aug. 2019.

[13] M. van Neerven, "Design of a Variable Pitch, Energy-Harvesting Propeller for In-Flight Power Recuperation on Electric Aircraft," Master Thesis, TU Delft Aerospace Engineering, Delft, 2020.

[14] E. Torenbeek, *Synthesis of Subsonic Airplane Design*. Dordrecht: Kluwer Academic Publishers Group, 1982.

[15] R. de Vries, M. Brown, and R. Vos, "Preliminary Sizing Method for Hybrid-Electric Distributed-Propulsion Aircraft," *Journal of Aircraft*, vol. 56, no. 6, pp. 2172–2188, 2019.

[16] M. Cavcar, "Bréguet Range Equation?" *Journal of Aircraft*, vol. 43, no. 5, pp. 1542–1544, Sep. 2006.

[17] D. Erzen, M. Andrejasic, and T. Kosel, "An Optimal Propeller Design for In-Flight Power Recuperation on an Electric Aircraft," in *2018 Aviation Technology, Integration, and Operations Conference*. Atlanta, Georgia: American Institute of Aeronautics and Astronautics, Jun. 2018.

[18] F. L. Faurote, *The Aircraft Year Book for 1919*. New York, USA: Manafacturers Aircraft Association, 1919.

[19] E. Torenbeek, *Advanced Aircraft Design: Conceptual Design, Analysis and Optimization of Subsonic Civil Airplanes*. New York, UNITED KINGDOM: John Wiley & Sons, Incorporated, 2013.

[20] D. P. Raymer, *Aircraft Design: A Conceptual Approach*, ser. AIAA Education Series. Washington, D.C: American Institute of Aeronautics and Astronautics, 1989.

[21] J. Roskam, *Airplane Design*, 2nd ed. Lawrence, KS, USA: DARcorporation, 1985.

[22] S. Gudmundsson, "The Anatomy of the Propeller," in *General Aviation Aircraft Design*. Elsevier, 2014, pp. 581–659.

[23] W. Z. Stepniewski and C. N. Keys, *Rotary-Wing Aerodynamics*. Courier Corporation, Jan. 1984.

[24] M. K. Rwigema, "Propeller Blade Element Momentum Theory with Vortex Wake Deflection," *27th International Congress of the Aeronautical Sciences*, Sep. 2010.

[25] Q. R. Wald, "The aerodynamics of propellers," *Progress in Aerospace Sciences*, vol. 42, no. 2, pp. 85–128, Feb. 2006.

[26] P. J. Schubel and R. J. Crossley, "Wind Turbine Blade Design," *Energies*, vol. 5, no. 9, pp. 3425–3449, Sep. 2012.

[27] J. P. Barnes, "Regenerative Electric Flight Synergy and Integration of Dual role Machines," in *53rd AIAA Aerospace Sciences Meeting*. Kissimmee, Florida: American Institute of Aeronautics and Astronautics, Jan. 2015.

[28] Lutze, *Level Flight Performance*. Virgina: The Department of Aerospace and Ocean Engineering, May 2011.

[29] R. de Vries, M. F. M. Hoogreef, and R. Vos, "Aero-Propulsive Efficiency Requirements for Turboelectric Transport Aircraft," *AIAA Scitech 2020 Forum*, 2020.

[30] D. F. Finger, R. de Vries, R. Vos, C. Braun, and C. Bil, "A Comparison of Hybrid-Electric Aircraft Sizing Methods," in *AIAA Scitech 2020 Forum*. American Institute of Aeronautics and Astronautics, 2020.

[31] R. Willemsen, "Thesis - A sensitivity study on the aerodynamic performance of a wingtip-mounted tractor propeller-wing system," 2020.

[32] H. Snel, R. Houwink, J. Bosschers, and Energieonderzoek Centrum Nederland., *Sectional prediction of lift coefficients on rotating wind turbine blades in stall*. [Petten]: [Netherlands Energy Research Foundation], 1994.

[33] M. Ceze, M. Hayashi, and E. Volpe, "A Study of the CST Parameterization Characteristics," in *27th AIAA Applied Aerodynamics Conference*. San Antonio, Texas: American Institute of Aeronautics and Astronautics, Jun. 2009.

[34] B. Kulfan, "A Universal Parametric Geometry Representation Method - "CST"," in *45th AIAA Aerospace Sciences Meeting and Exhibit*. Reno, Nevada: American Institute of Aeronautics and Astronautics, Jan. 2007.

[35] Pipistrel, "Pilot's operating handbook - alpha electro aircraft," Jul. 2017.

[36] M. Niţă and D. Scholz, "Estimating the Oswald Facor from Basic Aircraft Geometrical Parameters," in *Deutscher Luft- Und Raumfahrtkongress 2012*. Berlin, Germany: Hamburg University of Applied Sciences, Sep. 2012.

A

Appendix A: Detailed Descent Analysis Results

Below are all the results presented for the performed simulations within the descent strategy analysis, as presented in section 6.2.

A.1. vR - Fixed Flight Speed

Sizing Parameters

Table A.1: Aircraft sizing parameters of the descent analysis with fixed flight speed and fixed pitch propeller.

	RoD 230	**RoD 345**	**RoD 460**	**RoD 575**	**RoD 690**
$W/S\ [N/m^2]$	568.9	568.9	568.9	568.9	568.9
$W/P_{EM}\ [N/W]$	0.0843	0.0843	0.0844	0.0838	0.0823
$MTOM\ [kg]$	614.7	615.5	615.7	622.4	637.3
$M_{bat}\ [kg]$	130.2	130.7	130.9	134.7	143.1
$M_{EM}\ [kg]$	23.8	23.9	23.9	24.3	25.3
$M_{OEM}\ [kg]$	278.5	278.8	278.9	281.3	286.9
$M_{PL}\ [kg]$	182.0	182.0	182.0	182.0	182.0
$E_{bat}\ [MJ]$	93.77	94.13	94.25	96.97	103.04
$E_{TO}\ [MJ]$	2.44	2.45	2.45	2.52	2.68
$E_{cl}\ [MJ]$	13.33	13.41	13.24	13.26	13.74
$E_{cr}\ [MJ]$	53.15	56.63	58.42	61.12	65.64
$E_{de}\ [MJ]$	4.60	1.31	-0.22	-0.88	-1.28
$E_{L}\ [MJ]$	1.50	1.51	1.51	1.55	1.65
$E_{res}\ [MJ]$	18.75	18.83	18.85	19.39	20.61

Mission Parameters

Table A.2: Aircraft mission parameters of the descent analysis with fixed flight speed and fixed pitch propeller.

	RoD 230	**RoD 345**	**RoD 460**	**RoD 575**	**RoD 690**
t_{cl} $[s]$	359.7	359.7	359.7	359.7	359.7
t_{cr} $[s]$	2928.2	3116.7	3211.0	3267.7	3305.6
t_{de} $[s]$	648.7	434.7	327.8	263.6	220.8
v_{cl} $[m/s]$	25.2	25.2	25.2	25.2	25.2
v_{cr} $[m/s]$	37.1	37.1	37.1	37.1	37.1
v_{de} $[m/s]$	32.7	32.7	32.7	32.7	32.7
c_{cl} $[ft/min]$	433	433	433	433	433
c_{de} $[ft/min]$	-230	-345	-460	-575	-690
Θ_{cl} $[degree]$	5.0	5.0	5.0	5.0	5.0
Θ_{de} $[degree]$	-2.0	-3.1	-4.1	-5.1	-6.2
R_{cl} $[km]$	9.0	9.0	9.0	9.0	9.0
R_{cr} $[km]$	108.7	115.7	119.2	121.3	122.7
R_{de} $[km]$	21.2	14.2	10.7	8.6	7.2

Performance Parameters

Table A.3: Aircraft peformance parameters of the descent analysis with fixed flight speed and fixed pitch propeller.

	RoD 230	**RoD 345**	**RoD 460**	**RoD 575**	**RoD 690**
CL_{cl} $[-]$	1.504	1.504	1.504	1.504	1.504
CL_{cr} $[-]$	0.725	0.725	0.725	0.725	0.725
CL_{de} $[-]$	0.903	0.903	0.904	0.904	0.901
CD_{cl} $[-]$	0.116	0.116	0.116	0.116	0.116
CD_{cr} $[-]$	0.049	0.049	0.049	0.049	0.049
CD_{de} $[-]$	0.060	0.060	0.060	0.060	0.060

Propeller Parameters

Table A.4: Propeller performance parameters of the descent analysis with fixed flight speed and fixed pitch propeller.

	RoD 230	**RoD 345**	**RoD 460**	**RoD 575**	**RoD 690**
T_{cl} $[N]$	990.4	991.8	992.0	1002.9	1026.8
T_{cr} $[N]$	408.6	409.1	409.3	413.7	423.6
T_{de} $[N]$	185.9	77.8	-30.6	-140.8	-256.7
$P_{shaft_{cl}}$ $[kW]$	35.19	35.40	34.95	34.99	36.27
$P_{shaft_{cr}}$ $[kW]$	17.24	17.26	17.28	17.77	18.86
$P_{shaft_{de}}$ $[kW]$	6.81	2.91	-0.72	-3.61	-6.31
J_{cl} $[-]$	0.436	0.441	0.440	0.479	0.506
J_{cr} $[-]$	0.793	0.805	0.791	0.792	0.782
J_{de} $[-]$	0.893	1.042	1.263	1.441	1.431
$Pitch_{cl}$ $[degree]$	25.2	25.5	25.0	23.6	21.6
$Pitch_{cr}$ $[degree]$	25.2	25.5	25.0	23.6	21.6
$Pitch_{de}$ $[degree]$	25.2	25.5	25.0	23.6	21.6
η_{cl} $[-]$	71.00	70.66	71.60	72.29	71.41
η_{cr} $[-]$	87.95	87.97	87.88	86.41	83.34
η_{de} $[-]$	89.16	87.41	1.33	6.64	11.612

A.2. vR - Fixed Rate of Descent

Sizing Parameters

Table A.5: Aircraft sizing parameters of the descent analysis with fixed rate of descent and fixed pitch propeller.

	v_{minP}	$1.2v_{stall}$	v_{minD}	v_{cr}
$W/S\ [N/m^2]$	568.9	568.9	568.9	568.9
$W/P_{EM}\ [N/W]$	0.0830	0.0840	0.0844	0.0841
$MTOM\ [kg]$	632.9	622.2	615.7	618.2
$M_{bat}\ [kg]$	140.9	134.7	130.9	132.3
$M_{EM}\ [kg]$	24.9	24.2	23.9	24.0
$M_{OEM}\ [kg]$	285.2	281.2	278.9	279.8
$M_{PL}\ [kg]$	182.0	182.0	182.0	182.0
$E_{bat}\ [MJ]$	101.41	96.96	94.25	95.27
$E_{TO}\ [MJ]$	2.64	2.52	2.45	2.48
$E_{cl}\ [MJ]$	13.44	13.21	13.24	13.70
$E_{cr}\ [MJ]$	64.00	60.82	58.42	57.99
$E_{de}\ [MJ]$	-0.56	-0.54	-0.22	0.52
$E_{L}\ [MJ]$	1.62	1.55	1.51	1.52
$E_{res}\ [MJ]$	20.28	19.39	18.85	19.05

Mission Parameters

Table A.6: Aircraft mission parameters of the descent analysis with fixed rate of descent and fixed pitch propeller.

	v_{minP}	$1.2v_{stall}$	v_{minD}	v_{cr}
t_{cl} $[s]$	359.7	359.7	359.7	359.7
t_{cr} $[s]$	3274.2	3249.3	3211.0	3178.5
t_{de} $[s]$	336.2	334.2	327.8	321.0
v_{cl} $[m/s]$	25.2	25.2	25.2	25.2
v_{cr} $[m/s]$	37.1	37.1	37.1	37.1
v_{de} $[m/s]$	25.2	27.8	32.7	37.1
c_{cl} $[ft/min]$	433	433	433	433
c_{de} $[ft/min]$	-460	-460	-460	-460
Θ_{cl} $[degree]$	5.0	5.0	5.0	5.0
Θ_{de} $[degree]$	-5.3	-4.8	-4.1	-3.6
R_{cl} $[km]$	9.0	9.0	9.0	9.0
R_{cr} $[km]$	121.5	120.6	119.2	118.0
R_{de} $[km]$	8.4	9.3	10.7	11.9

Performance Parameters

Table A.7: Aircraft performance parameters of the descent analysis with fixed rate of descent and fixed pitch propeller.

	v_{minP}	$1.2v_{stall}$	v_{minD}	v_{cr}
CL_{cl} $[-]$	1.504	1.504	1.504	1.504
CL_{cr} $[-]$	0.725	0.725	0.725	0.725
CL_{de} $[-]$	1.517	1.247	0.904	0.698
CD_{cl} $[-]$	0.116	0.116	0.116	0.116
CD_{cr} $[-]$	0.049	0.049	0.049	0.049
CD_{de} $[-]$	0.118	0.089	0.060	0.048

Propeller Parameters

Table A.8: Propeller performance parameters of the descent analysis with fixed rate of descent and fixed pitch propeller.

	v_{minP}	$1.2v_{stall}$	v_{minD}	v_{cr}
T_{cl} $[N]$	1019.8	1002.5	992.0	996.1
T_{cr} $[N]$	420.7	413.6	409.3	410.9
T_{de} $[N]$	-96.3	-80.7	-30.6	31.8
$P_{shaft_{cl}}$ $[kW]$	35.88	34.88	34.95	36.16
$P_{shaft_{cr}}$ $[kW]$	18.57	17.78	17.28	17.33
$P_{shaft_{de}}$ $[kW]$	-1.87	-1.77	-0.72	1.55
J_{cl} $[-]$	0.404	0.417	0.440	0.447
J_{cr} $[-]$	0.642	0.694	0.791	0.829
J_{de} $[-]$	1.067	1.195	1.263	1.181
$Pitch_{cl}$ $[degree]$	19.0	21.3	25.0	25.9
$Pitch_{cr}$ $[degree]$	19.0	21.3	25.0	25.9
$Pitch_{de}$ $[degree]$	19.0	21.3	25.0	25.9
η_{cl} $[-]$	71.71	72.50	71.60	69.48
η_{cr} $[-]$	84.09	86.32	87.88	87.98
η_{de} $[-]$	7.48	5.28	1.33	76.10

A.3. vR - Fixed Descent Angle

Sizing Parameters

Table A.9: Aircraft sizing parameters of the descent analysis with fixed descent angle and fixed pitch propeller.

	$0.8v_{minD}$	$0.9v_{minD}$	$\underline{1.0v_{minD}}$	$1.1v_{minD}$
$W/S\ [N/m^2]$	568.9	568.9	568.9	568.9
$W/P_{EM}\ [N/W]$	0.0842	0.0843	0.0844	0.0843
$MTOM\ [kg]$	619.1	616.2	615.7	616.5
$M_{bat}\ [kg]$	132.9	131.1	130.9	131.4
$M_{EM}\ [kg]$	24.0	23.9	23.9	23.9
$M_{OEM}\ [kg]$	280.1	279.0	278.9	279.2
$M_{PL}\ [kg]$	182.0	182.0	182.0	182.0
$E_{bat}\ [MJ]$	95.68	94.42	94.25	94.60
$E_{TO}\ [MJ]$	2.49	2.46	2.45	2.46
$E_{cl}\ [MJ]$	13.66	13.29	13.24	13.29
$E_{cr}\ [MJ]$	58.59	58.39	58.42	58.57
$E_{de}\ [MJ]$	0.27	-0.11	-0.22	-0.16
$E_{L}\ [MJ]$	1.53	1.51	1.51	1.51
$E_{res}\ [MJ]$	19.14	18.88	18.85	18.92

Mission Parameters

Table A.10: Aircraft mission parameters of the descent analysis with fixed descent angle and fixed pitch propeller.

	$0.8v_{minD}$	$0.9v_{minD}$	$\underline{1.0v_{minD}}$	$1.1v_{minD}$
t_{cl} $[s]$	359.7	359.7	359.7	359.7
t_{cr} $[s]$	3206.6	3208.0	3211.0	3215.3
t_{de} $[s]$	416.0	368.0	327.8	293.6
v_{cl} $[m/s]$	25.2	25.2	25.2	25.2
v_{cr} $[m/s]$	37.1	37.1	37.1	37.1
v_{de} $[m/s]$	26.1	29.4	32.7	35.9
c_{cl} $[ft/min]$	433	433	433	433
c_{de} $[ft/min]$	-368	-414	-460	-506
Θ_{cl} $[degree]$	5.0	5.0	5.0	5.0
Θ_{de} $[degree]$	-4.1	-4.1	-4.1	-4.1
R_{cl} $[km]$	9.0	9.0	9.0	9.0
R_{cr} $[km]$	119.0	119.1	119.2	119.3
R_{de} $[km]$	10.8	10.8	10.7	10.5

Performance Parameters

Table A.11: Aircraft performance parameters of the descent analysis with fixed descent angle and fixed pitch propeller.

	$0.8v_{minD}$	$0.9v_{minD}$	$\underline{1.0v_{minD}}$	$1.1v_{minD}$
CL_{cl} $[-]$	1.504	1.504	1.504	1.504
CL_{cr} $[-]$	0.725	0.725	0.725	0.725
CL_{de} $[-]$	1.409	1.115	0.904	0.747
CD_{cl} $[-]$	0.116	0.116	0.116	0.116
CD_{cr} $[-]$	0.049	0.049	0.049	0.049
CD_{de} $[-]$	0.106	0.077	0.060	0.050

Propeller Parameters

Table A.12: Propeller performance parameters of the descent analysis with fixed descent angle and fixed pitch propeller.

	$0.8v_{minD}$	$0.9v_{minD}$	$1.0v_{minD}$	$1.1v_{minD}$
T_{cl} $[N]$	997.5	992.8	992.0	993.4
T_{cr} $[N]$	411.5	409.6	409.3	409.8
T_{de} $[N]$	18.3	-18.2	-30.6	-25.6
$P_{shaft_{cl}}$ $[kW]$	36.07	35.09	34.95	35.09
$P_{shaft_{cr}}$ $[kW]$	17.36	17.29	17.28	17.31
$P_{shaft_{de}}$ $[kW]$	0.62	-0.34	-0.72	-0.57
J_{cl} $[-]$	0.415	0.453	0.440	0.446
J_{cr} $[-]$	0.770	0.817	0.791	0.805
J_{de} $[-]$	1.096	1.272	1.263	1.253
$Pitch_{cl}$ $[degree]$	24.8	25.6	25.0	25.4
$Pitch_{cr}$ $[degree]$	24.8	25.6	25.0	25.4
$Pitch_{de}$ $[degree]$	24.8	25.6	25.0	25.4
η_{cl} $[-]$	69.76	71.38	71.60	71.41
η_{cr} $[-]$	87.98	87.90	87.88	87.89
η_{de} $[-]$	77.00	0.85	1.33	0.78

A.4. vRvP - Fixed Airspeed

Sizing Parameters

Table A.13: Aircraft sizing parameters of the descent analysis with fixed flight speed and variable pitch propeller.

	RoD 230	**RoD 345**	**RoD 460**	**RoD 575**	**RoD 690**	**RoD 920**
$W/S\ [N/m^2]$	568.9	568.9	568.9	568.9	568.9	568.9
$W/P_{EM}\ [N/W]$	0.0845	0.0846	0.0846	0.0845	0.0845	0.0842
$MTOM\ [kg]$	611.4	611.8	612.8	614.6	616.4	620.8
$M_{bat}\ [kg]$	128.3	128.6	129.2	130.3	131.4	133.9
$M_{EM}\ [kg]$	23.6	23.7	23.7	23.8	23.8	24.1
$M_{OEM}\ [kg]$	277.3	277.5	277.8	278.4	279.1	280.7
$M_{PL}\ [kg]$	182.0	182.0	182.0	182.0	182.0	182.0
$E_{bat}\ [MJ]$	92.38	92.59	93.02	93.80	94.61	96.43
$E_{TO}\ [MJ]$	2.40	2.41	2.42	2.44	2.46	2.51
$E_{cl}\ [MJ]$	12.87	12.91	12.90	12.93	12.96	13.06
$E_{cr}\ [MJ]$	52.64	56.03	57.84	59.06	59.97	61.57
$E_{de}\ [MJ]$	4.52	1.25	-0.24	-0.89	-1.22	-1.55
$E_{L}\ [MJ]$	1.48	1.48	1.49	1.50	1.51	1.54
$E_{res}\ [MJ]$	18.48	18.52	18.60	18.76	18.92	19.29

Mission Parameters

Table A.14: Aircraft mission parameters of the descent analysis with fixed flight speed and variable pitch propeller.

	RoD 230	**RoD 345**	**RoD 460**	**RoD 575**	**RoD 690**	**RoD 920**
t_{cl} $[s]$	359.7	359.7	359.7	359.7	359.7	359.7
t_{cr} $[s]$	2928.2	3116.7	3211.0	3267.7	3305.6	3353.0
t_{de} $[s]$	648.7	434.7	327.8	263.6	220.8	167.4
v_{cl} $[m/s]$	25.2	25.2	25.2	25.2	25.2	25.2
v_{cr} $[m/s]$	37.1	37.1	37.1	37.1	37.1	37.1
v_{de} $[m/s]$	32.7	32.7	32.7	32.7	32.7	32.7
c_{cl} $[ft/min]$	433	433	433	433	433	433
c_{de} $[ft/min]$	-230	-345	-460	-575	-690	-920
Θ_{cl} $[degree]$	5.0	5.0	5.0	5.0	5.0	5.0
Θ_{de} $[degree]$	-2.0	-3.1	-4.1	-5.1	-6.2	-8.2
R_{cl} $[km]$	9.0	9.0	9.0	9.0	9.0	9.0
R_{cr} $[km]$	108.7	115.7	119.2	121.3	122.7	124.4
R_{de} $[km]$	21.2	14.2	10.7	8.6	7.2	5.4

Performance Parameters

Table A.15: Aircraft performance parameters of the descent analysis with fixed flight speed and variable pitch propeller.

	RoD 230	**RoD 345**	**RoD 460**	**RoD 575**	**RoD 690**	**RoD 920**
CL_{cl} $[-]$	1.504	1.504	1.504	1.504	1.504	1.504
CL_{cr} $[-]$	0.725	0.725	0.725	0.725	0.725	0.725
CL_{de} $[-]$	0.903	0.903	0.904	0.904	0.901	0.897
CD_{cl} $[-]$	0.116	0.116	0.116	0.116	0.116	0.116
CD_{cr} $[-]$	0.049	0.049	0.049	0.049	0.049	0.049
CD_{de} $[-]$	0.060	0.060	0.060	0.060	0.060	0.060

Propeller Parameters

Table A.16: Propeller performance parameters of the descent analysis with fixed flight speed and variable pitch propeller.

	RoD 230	**RoD 345**	**RoD 460**	**RoD 575**	**RoD 690**	**RoD 920**
T_{cl} $[N]$	985.1	985.8	987.3	990.2	993.2	1000.2
T_{cr} $[N]$	406.4	406.7	407.3	408.5	409.7	412.6
T_{de} $[N]$	184.9	77.4	-30.5	-139.0	-248.3	-469.7
$P_{shaft_{cl}}$ $[kW]$	33.97	34.08	34.06	34.15	34.21	34.47
$P_{shaft_{cr}}$ $[kW]$	17.08	17.08	17.11	17.17	17.24	17.45
$P_{shaft_{de}}$ $[kW]$	6.69	2.76	-0.78	-3.65	-5.99	-10.17
J_{cl} $[-]$	0.404	0.376	0.378	0.404	0.409	0.471
J_{cr} $[-]$	0.895	0.821	0.840	0.875	0.901	1.008
J_{de} $[-]$	1.130	1.357	1.411	0.948	0.723	0.614
$Pitch_{cl}$ $[degree]$	20.0	19.0	19.0	20.0	20.0	22.2
$Pitch_{cr}$ $[degree]$	30.0	28.0	29.0	29.0	30.0	32.0
$Pitch_{de}$ $[degree]$	34.0	35.0	27.0	14.0	8.0	5.0
η_{cl} $[-]$	73.16	72.98	73.12	73.15	73.23	73.20
η_{cr} $[-]$	88.32	88.38	88.34	88.31	88.23	87.78
η_{de} $[-]$	90.29	91.43	1.43	6.71	11.02	18.72

A.5. vRvP - Fixed Rate of Descent

Sizing Parameters

Table A.17: Aircraft sizing parameters of the descent analysis with fixed rate of descent and variable pitch propeller.

	v_{minP}	$1.2v_{stall}$	v_{minD}	v_{cr}
$W/S\ [N/m^2]$	568.9	568.9	568.9	568.9
$W/P_{EM}\ [N/W]$	0.0845	0.0845	0.0846	0.0844
$MTOM\ [kg]$	616.0	614.7	612.8	613.7
$M_{bat}\ [kg]$	131.2	130.3	129.2	129.7
$M_{EM}\ [kg]$	23.8	23.8	23.7	23.8
$M_{OEM}\ [kg]$	278.9	278.5	277.8	278.1
$M_{PL}\ [kg]$	182.0	182.0	182.0	182.0
$E_{bat}\ [MJ]$	94.45	93.84	93.02	93.38
$E_{TO}\ [MJ]$	2.46	2.44	2.42	2.43
$E_{cl}\ [MJ]$	12.80	12.94	12.90	12.98
$E_{cr}\ [MJ]$	59.35	58.73	57.84	57.34
$E_{de}\ [MJ]$	-0.56	-0.54	-0.24	0.47
$E_{L}\ [MJ]$	1.51	1.50	1.49	1.49
$E_{res}\ [MJ]$	18.89	18.77	18.60	18.68

Mission Parameters

Table A.18: Aircraft mission parameters of the descent analysis with fixed rate of descent and variable pitch propeller.

	v_{minP}	$1.2v_{stall}$	v_{minD}	v_{cr}
t_{cl} $[s]$	355.6	359.7	359.7	359.7
t_{cr} $[s]$	3274.2	3249.3	3211.0	3178.5
t_{de} $[s]$	336.2	334.2	327.8	321.0
v_{cl} $[m/s]$	25.2	25.2	25.2	25.2
v_{cr} $[m/s]$	37.1	37.1	37.1	37.1
v_{de} $[m/s]$	25.2	27.8	32.7	37.1
c_{cl} $[ft/min]$	433	433	433	433
c_{de} $[ft/min]$	-460	-460	-460	-460
Θ_{cl} $[degree]$	5.0	5.0	5.0	5.0
Θ_{de} $[degree]$	-5.3	-4.8	-4.1	-3.6
R_{cl} $[km]$	9.0	9.0	9.0	9.0
R_{cr} $[km]$	121.5	120.6	119.2	118.0
R_{de} $[km]$	8.4	9.3	10.7	11.9

Performance Parameters

Table A.19: Aircraft performance parameters of the descent analysis with fixed rate of descent and variable pitch propeller.

	v_{minP}	$1.2v_{stall}$	v_{minD}	v_{cr}
CL_{cl} $[-]$	1.504	1.504	1.504	1.504
CL_{cr} $[-]$	0.725	0.725	0.725	0.725
CL_{de} $[-]$	1.517	1.247	0.904	0.698
CD_{cl} $[-]$	0.116	0.116	0.116	0.116
CD_{cr} $[-]$	0.049	0.049	0.049	0.049
CD_{de} $[-]$	0.118	0.089	0.060	0.048

Propeller Parameters

Table A.20: Propeller performance parameters of the descent analysis with fixed rate of descent and variable pitch propeller.

	v_{minP}	$1.2v_{stall}$	v_{minD}	v_{cr}
T_{cl} $[N]$	992.6	990.4	987.3	988.8
T_{cr} $[N]$	409.5	408.6	407.3	407.9
T_{de} $[N]$	-93.7	-79.7	-30.5	31.5
$P_{shaft_{cl}}$ $[kW]$	34.18	34.16	34.06	34.26
$P_{shaft_{cr}}$ $[kW]$	17.22	17.17	17.11	17.14
$P_{shaft_{de}}$ $[kW]$	-1.84	-1.78	-0.78	1.37
J_{cl} $[-]$	0.408	0.404	0.378	0.391
J_{cr} $[-]$	0.899	0.875	0.840	0.890
J_{de} $[-]$	0.894	1.054	1.411	1.564
$Pitch_{cl}$ $[degree]$	20.0	20.0	19.0	19.0
$Pitch_{cr}$ $[degree]$	30.0	29.0	29.0	30.0
$Pitch_{de}$ $[degree]$	12.7	16.7	27.0	34.1
η_{cl} $[-]$	73.25	73.13	73.12	72.81
η_{cr} $[-]$	88.25	88.31	88.34	88.34
η_{de} $[-]$	7.36	5.33	1.43	85.19

A.6. vRvP - Fixed Descent Angle

Sizing Parameters

Table A.21: Aircraft sizing parameters of the descent analysis with fixed descent angle and variable pitch propeller.

	$0.8v_{minD}$	$0.9v_{minD}$	$1.0v_{minD}$	$1.1v_{minD}$
$W/S\ [N/m^2]$	568.9	568.9	568.9	568.9
$W/P_{EM}\ [N/W]$	0.0844	0.0845	0.0846	0.0845
$MTOM\ [kg]$	615.3	613.2	612.8	613.5
$M_{bat}\ [kg]$	130.7	129.4	129.2	129.6
$M_{EM}\ [kg]$	23.8	23.7	23.7	23.7
$M_{OEM}\ [kg]$	278.7	277.9	277.8	278.0
$M_{PL}\ [kg]$	182.0	182.0	182.0	182.0
$E_{bat}\ [MJ]$	94.08	93.18	93.02	93.32
$E_{TO}\ [MJ]$	2.45	2.42	2.42	2.43
$E_{cl}\ [MJ]$	13.06	12.90	12.90	12.91
$E_{cr}\ [MJ]$	58.00	57.84	57.84	58.01
$E_{de}\ [MJ]$	0.26	-0.11	-0.24	-0.19
$E_{L}\ [MJ]$	1.51	1.49	1.49	1.49
$E_{res}\ [MJ]$	18.82	18.64	18.60	18.66

Mission Parameters

Table A.22: Aircraft mission parameters of the descent analysis with fixed descent angle and variable pitch propeller.

	$0.8v_{minD}$	$0.9v_{minD}$	$\underline{1.0v_{minD}}$	$1.1v_{minD}$
t_{cl} $[s]$	359.7	359.7	359.7	359.7
t_{cr} $[s]$	3206.6	3208.0	3211.0	3215.3
t_{de} $[s]$	416.0	368.0	327.8	293.6
v_{cl} $[m/s]$	25.2	25.2	25.2	25.2
v_{cr} $[m/s]$	37.1	37.1	37.1	37.1
v_{de} $[m/s]$	26.1	29.4	32.7	35.9
c_{cl} $[ft/min]$	433	433	433	433
c_{de} $[ft/min]$	-368	-414	-460	-506
Θ_{cl} $[degree$	5.0	5.0	5.0	5.0
Θ_{de} $[degree]$	-4.1	-4.1	-4.1	-4.1
R_{cl} $[km]$	9.0	9.0	9.0	9.0
R_{cr} $[km]$	119.0	119.1	119.2	119.3
R_{de} $[km]$	10.8	10.8	10.7	10.5

Performance Parameters

Table A.23: Aircraft performance parameters of the descent analysis with fixed descent angle and variable pitch propeller.

	$0.8v_{minD}$	$0.9v_{minD}$	$\underline{1.0v_{minD}}$	$1.1v_{minD}$
CL_{cl} $[-]$	1.504	1.504	1.504	1.504
CL_{cr} $[-]$	0.725	0.725	0.725	0.725
CL_{de} $[-]$	1.409	1.115	0.904	0.747
CD_{cl} $[-]$	0.116	0.116	0.116	0.116
CD_{cr} $[-]$	0.049	0.049	0.049	0.049
CD_{de} $[-]$	0.106	0.077	0.060	0.050

Propeller Parameters

Table A.24: Propeller performance parameters of the descent analysis with fixed descent angle and variable pitch propeller.

	$0.8v_{minD}$	$0.9v_{minD}$	$\underline{1.0v_{minD}}$	$1.1v_{minD}$
T_{cl} $[N]$	991.4	988.0	987.3	988.5
T_{cr} $[N]$	409.0	407.6	407.3	407.8
T_{de} $[N]$	18.9	-18.2	-30.5	-25.5
$P_{shaft_{cl}}$ $[kW]$	34.47	34.06	34.06	34.08
$P_{shaft_{cr}}$ $[kW]$	17.18	17.13	17.11	17.14
$P_{shaft_{de}}$ $[kW]$	0.61	-0.34	-0.78	-0.67
J_{cl} $[-]$	0.358	0.403	0.378	0.404
J_{cr} $[-]$	0.821	0.893	0.840	0.893
J_{de} $[-]$	1.141	1.231	1.411	1.550
$Pitch_{cl}$ $[degree]$	17.0	20.0	19.0	20.0
$Pitch_{cr}$ $[degree]$	28.0	30.0	29.0	30.0
$Pitch_{de}$ $[degree]$	25.5	24.5	27.0	30.1
η_{cl} $[-]$	72.55	73.16	73.12	73.16
η_{cr} $[-]$	88.35	88.31	88.34	88.30
η_{de} $[-]$	79.97	0.86	1.43	0.93

B

Appendix B: Detailed Propeller Analysis Results

Below are all the results presented for the performed simulations within the propeller airfoil camber analysis, as presented in section 7.2

B.1. vR - Shallow Descent

Sizing Parameters

Table B.1: Aircraft sizing parameters of the propeller analysis for the shallow descent and fixed pitch propeller.

	100%	**75%**	**50%**	**25%**	**0%**
$W/S\ [N/m^2]$	568.9	568.9	568.9	568.9	568.9
$W/P_{EM}\ [N/W]$	0.0844	0.0844	0.0842	0.0838	0.0827
$MTOM\ [kg]$	615.7	616.0	617.4	619.6	623.5
$M_{bat}\ [kg]$	130.9	131.1	131.8	133.0	134.8
$M_{EM}\ [kg]$	23.9	23.9	24.0	24.2	24.7
$M_{OEM}\ [kg]$	278.9	279.0	279.5	280.4	282.0
$M_{PL}\ [kg]$	182.0	182.0	182.0	182.0	182.0
$E_{bat}\ [MJ]$	94.25	94.41	94.93	95.74	97.07
$E_{TO}\ [MJ]$	2.45	2.46	2.47	2.49	2.52
$E_{cl}\ [MJ]$	13.24	13.26	13.40	13.62	13.89
$E_{cr}\ [MJ]$	58.42	58.53	58.79	59.17	59.90
$E_{de}\ [MJ]$	-0.22	-0.22	-0.22	-0.22	-0.21
$E_{L}\ [MJ]$	1.51	1.51	1.52	1.53	1.55
$E_{res}\ [MJ]$	18.85	18.88	18.99	19.15	19.41

Mission Parameters

Table B.2: Aircraft mission parameters of the propeller analysis for the shallow descent and fixed pitch propeller.

	100%	**75%**	**50%**	**25%**	**0%**
t_{cl} $[s]$	359.7	359.7	359.7	359.7	359.7
t_{cr} $[s]$	3211.0	3211.0	3211.0	3211.0	3211.0
t_{de} $[s]$	327.8	327.8	327.8	327.8	327.8
v_{cl} $[m/s]$	25.2	25.2	25.2	25.2	25.2
v_{cr} $[m/s]$	37.1	37.1	37.1	37.1	37.1
v_{de} $[m/s]$	32.7	32.7	32.7	32.7	32.7
c_{cl} $[ft/min]$	433.0	433.0	433.0	433.0	433.0
c_{de} $[ft/min]$	-460	-460	-460	-460	-460
Θ_{cl} $[degree]$	5.0	5.0	5.0	5.0	5.0
Θ_{de} $[degree]$	-4.1	-4.1	-4.1	-4.1	-4.1
R_{cl} $[km]$	9.0	9.0	9.0	9.0	9.0
R_{cr} $[km]$	119.2	119.2	119.2	119.2	119.2
R_{de} $[km]$	10.7	10.7	10.7	10.7	10.7

Performance Parameters

Table B.3: Aircraft performance parameters of the propeller analysis for the shallow descent and fixed pitch propeller.

	100%	**75%**	**50%**	**25%**	**0%**
CL_{cl} $[-]$	1.504	1.504	1.504	1.504	1.504
CL_{cr} $[-]$	0.725	0.725	0.725	0.725	0.725
CL_{de} $[-]$	0.904	0.904	0.904	0.904	0.904
CD_{cl} $[-]$	0.116	0.116	0.116	0.116	0.116
CD_{cr} $[-]$	0.049	0.049	0.049	0.049	0.049
CD_{de} $[-]$	0.060	0.060	0.060	0.060	0.060

Propeller Parameters

Table B.4: Propeller performance parameters of the propeller analysis for the shallow descent and fixed pitch propeller.

	100%	**75%**	**50%**	**25%**	**0%**
T_{cl} $[N]$	992.0	992.6	994.7	998.3	1004.7
T_{cr} $[N]$	409.3	409.5	410.4	411.8	414.5
T_{de} $[N]$	-30.6	-30.7	-30.7	-30.8	-31.0
$P_{shaft_{cl}}$ $[kW]$	34.95	35.00	35.37	35.96	36.67
$P_{shaft_{cr}}$ $[kW]$	17.28	17.32	17.39	17.51	17.72
$P_{shaft_{de}}$ $[kW]$	-0.72	-0.74	-0.74	-0.73	-0.70
J_{cl} $[-]$	0.440	0.424	0.432	0.441	0.475
J_{cr} $[-]$	0.791	0.759	0.770	0.781	0.830
J_{de} $[-]$	1.263	1.202	1.191	1.181	1.208
$Pitch_{cl}$ $[degree]$	25.0	24.8	25.3	26.0	27.4
$Pitch_{cr}$ $[degree]$	25.0	24.8	25.3	26.0	27.4
$Pitch_{de}$ $[degree]$	25.0	24.8	25.3	26.0	27.4
η_{cl} $[-]$	71.60	71.53	70.94	70.02	69.11
η_{cr} $[-]$	87.88	87.77	87.57	87.32	86.80
η_{de} $[-]$	1.33	1.36	1.36	1.34	1.28

B.2. vR - Steep Descent

Sizing Parameters

Table B.5: Aircraft sizing parameters of the propeller analysis for the steep descent and fixed pitch propeller.

	100%	**75%**	**50%**	**25%**	**0%**
$W/S\ [N/m^2]$	568.9	568.9	568.9	568.9	568.9
$W/P_{EM}\ [N/W]$	0.0823	0.0826	0.0827	0.0826	0.0824
$MTOM\ [kg]$	637.3	634.8	634.1	634.0	635.2
$M_{bat}\ [kg]$	143.1	141.8	141.4	141.3	141.9
$M_{EM}\ [kg]$	25.3	25.1	25.1	25.1	25.2
$M_{OEM}\ [kg]$	286.9	286.0	285.7	285.7	286.2
$M_{PL}\ [kg]$	182.0	182.0	182.0	182.0	182.0
$E_{bat}\ [MJ]$	103.04	102.06	101.80	101.75	102.17
$E_{TO}\ [MJ]$	2.68	2.65	2.65	2.65	2.66
$E_{cl}\ [MJ]$	13.74	13.64	13.62	13.63	13.76
$E_{cr}\ [MJ]$	65.64	65.04	64.89	64.87	65.08
$E_{de}\ [MJ]$	-1.28	-1.31	-1.34	-1.37	-1.39
$E_{L}\ [MJ]$	1.65	1.63	1.63	1.63	1.63
$E_{res}\ [MJ]$	20.61	20.41	20.36	20.35	20.43

Mission Parameters

Table B.6: Aircraft mission parameters of the propeller analysis for the steep descent and fixed pitch propeller.

	100%	**75%**	**50%**	**25%**	**0%**
t_{cl} $[s]$	359.7	359.7	359.7	359.7	359.7
t_{cr} $[s]$	3305.6	3305.6	3305.6	3305.6	3305.6
t_{de} $[s]$	220.8	220.8	220.8	220.8	220.8
v_{cl} $[m/s]$	25.2	25.2	25.2	25.2	25.2
v_{cr} $[m/s]$	37.1	37.1	37.1	37.1	37.1
v_{de} $[m/s]$	32.7	32.7	32.7	32.7	32.7
c_{cl} $[ft/min]$	433.0	433.0	433.0	433.0	433.0
c_{de} $[ft/min]$	-690	-690	-690	-690	-690
Θ_{cl} $[degree]$	5.0	5.0	5.0	5.0	5.0
Θ_{de} $[degree]$	-6.2	-6.2	-6.2	-6.2	-6.2
R_{cl} $[km]$	9.0	9.0	9.0	9.0	9.0
R_{cr} $[km]$	122.7	122.7	122.7	122.7	122.7
R_{de} $[km]$	7.2	7.2	7.2	7.2	7.2

Performance Parameters

Table B.7: Aircraft performance parameters of the propeller analysis for the steep descent and fixed pitch propeller.

	100%	**75%**	**50%**	**25%**	**0%**
CL_{cl} $[-]$	1.504	1.504	1.504	1.504	1.504
CL_{cr} $[-]$	0.725	0.725	0.725	0.725	0.725
CL_{de} $[-]$	0.901	0.901	0.901	0.901	0.901
CD_{cl} $[-]$	0.116	0.116	0.116	0.116	0.116
CD_{cr} $[-]$	0.049	0.049	0.049	0.049	0.049
CD_{de} $[-]$	0.060	0.060	0.060	0.060	0.060

Propeller Parameters

Table B.8: Propeller performance parameters of the propeller analysis for the steep descent and fixed pitch propeller.

	100%	**75%**	**50%**	**25%**	**0%**
T_{cl} $[N]$	1026.8	1022.7	1021.7	1021.6	1023.4
T_{cr} $[N]$	423.6	421.9	421.5	421.4	422.2
T_{de} $[N]$	-256.7	-255.7	-255.4	-255.4	-255.8
$P_{shaft_{cl}}$ $[kW]$	36.27	36.00	35.96	35.98	36.31
$P_{shaft_{cr}}$ $[kW]$	18.86	18.69	18.65	18.64	18.70
$P_{shaft_{de}}$ $[kW]$	-6.31	-6.50	-6.63	-6.75	-6.88
J_{cl} $[-]$	0.506	0.486	0.476	0.476	0.475
J_{cr} $[-]$	0.782	0.755	0.743	0.742	0.742
J_{de} $[-]$	1.431	1.431	1.432	1.432	1.424
$Pitch_{cl}$ $[degree]$	21.6	21.9	22.5	23.1	23.6
$Pitch_{cr}$ $[degree]$	21.6	21.9	22.5	23.1	23.6
$Pitch_{de}$ $[degree]$	21.6	21.9	22.5	23.1	23.6
η_{cl} $[-]$	71.41	71.66	71.67	71.63	71.09
η_{cr} $[-]$	83.34	83.77	83.89	83.90	83.78
η_{de} $[-]$	11.61	11.96	12.20	12.43	12.66

B.3. vRvP - Shallow Descent

Sizing Parameters

Table B.9: Aircraft sizing parameters of the propeller analysis for the shallow descent and variable pitch propeller.

	100%	**75%**	**50%**	**25%**	**0%**
$W/S\ [N/m^2]$	568.9	568.9	568.9	568.9	568.9
$W/P_{EM}\ [N/W]$	0.0846	0.0846	0.0843	0.0840	0.0833
$MTOM\ [kg]$	612.8	612.9	613.7	615.4	618.0
$M_{bat}\ [kg]$	129.2	129.2	129.6	130.5	131.7
$M_{EM}\ [kg]$	23.7	23.7	23.8	24.0	24.3
$M_{OEM}\ [kg]$	277.8	277.8	278.2	278.8	279.9
$M_{PL}\ [kg]$	182.0	182.0	182.0	182.0	182.0
$E_{bat}\ [MJ]$	93.02	93.05	93.33	93.94	94.86
$E_{TO}\ [MJ]$	2.42	2.42	2.43	2.44	2.47
$E_{cl}\ [MJ]$	12.90	12.90	12.97	13.08	13.29
$E_{cr}\ [MJ]$	57.84	57.87	58.02	58.37	58.86
$E_{de}\ [MJ]$	-0.24	-0.24	-0.25	-0.24	-0.25
$E_{L}\ [MJ]$	1.49	1.49	1.49	1.50	1.52
$E_{res}\ [MJ]$	18.60	18.61	18.67	18.79	18.97

Mission Parameters

Table B.10: Aircraft mission parameters of the propeller analysis for the shallow descent and variable pitch propeller.

	100%	**75%**	**50%**	**25%**	**0%**
t_{cl} $[s]$	359.7	359.7	359.7	359.7	359.7
t_{cr} $[s]$	3211.0	3211.0	3211.0	3211.0	3211.0
t_{de} $[s]$	327.8	327.8	327.8	327.8	327.8
v_{cl} $[m/s]$	25.2	25.2	25.2	25.2	25.2
v_{cr} $[m/s]$	37.1	37.1	37.1	37.1	37.1
v_{de} $[m/s]$	32.7	32.7	32.7	32.7	32.7
c_{cl} $[ft/min]$	433.0	433.0	433.0	433.0	433.0
c_{de} $[ft/min]$	-460	-460	-460	-460	-460
Θ_{cl} $[degree]$	5.0	5.0	5.0	5.0	5.0
Θ_{de} $[degree]$	-4.1	-4.1	-4.1	-4.1	-4.1
R_{cl} $[km]$	9.0	9.0	9.0	9.0	9.0
R_{cr} $[km]$	119.2	119.2	119.2	119.2	119.2
R_{de} $[km]$	10.7	10.7	10.7	10.7	10.7

Performance Parameters

Table B.11: Aircraft performance parameters of the propeller analysis for the shallow descent and variable pitch propeller.

	100%	**75%**	**50%**	**25%**	**0%**
CL_{cl} $[-]$	1.504	1.504	1.504	1.504	1.504
CL_{cr} $[-]$	0.725	0.725	0.725	0.725	0.725
CL_{de} $[-]$	0.904	0.904	0.904	0.904	0.904
CD_{cl} $[-]$	0.116	0.116	0.116	0.116	0.116
CD_{cr} $[-]$	0.049	0.049	0.049	0.049	0.049
CD_{de} $[-]$	0.060	0.060	0.060	0.060	0.060

Propeller Parameters

Table B.12: Propeller performance parameters of the propeller analysis for the shallow descent and variable pitch propeller.

	100%	**75%**	**50%**	**25%**	**0%**
T_{cl} $[N]$	987.3	987.5	988.8	991.5	995.8
T_{cr} $[N]$	407.3	407.4	407.9	409.0	410.8
T_{de} $[N]$	-30.5	-30.5	-30.5	-30.6	-30.8
$P_{shaft_{cl}}$ $[kW]$	34.06	34.05	34.23	34.53	35.08
$P_{shaft_{cr}}$ $[kW]$	17.11	17.12	17.17	17.27	17.41
$P_{shaft_{de}}$ $[kW]$	-0.78	-0.80	-0.82	-0.81	-0.82
J_{cl} $[-]$	0.378	0.388	0.387	0.410	0.386
J_{cr} $[-]$	0.840	0.859	0.857	0.904	0.854
J_{de} $[-]$	1.411	1.408	1.421	1.437	1.450
$Pitch_{cl}$ $[degree]$	19.0	20.0	20.0	21.0	20.0
$Pitch_{cr}$ $[degree]$	29.0	30.0	30.0	31.0	30.0
$Pitch_{de}$ $[degree]$	27.0	28.0	29.0	30.0	31.0
η_{cl} $[-]$	73.12	73.14	72.87	72.43	71.60
η_{cr} $[-]$	88.34	88.31	88.19	87.90	87.55
η_{de} $[-]$	1.43	1.48	1.51	1.49	1.51

B.4. vRvP - Steep Descent

Sizing Parameters

Table B.13: Aircraft sizing parameters of the propeller analysis for the steep descent and variable pitch propeller.

	100%	**75%**	**50%**	**25%**	**0%**
$W/S\ [N/m^2]$	568.9	568.9	568.9	568.9	568.9
$W/P_{EM}\ [N/W]$	0.0842	0.0843	0.0843	0.0839	0.0831
$MTOM\ [kg]$	620.8	620.1	620.0	621.4	624.8
$M_{bat}\ [kg]$	133.9	133.5	133.5	134.1	135.8
$M_{EM}\ [kg]$	24.1	24.1	24.1	24.2	24.6
$M_{OEM}\ [kg]$	280.7	280.4	280.4	280.9	282.3
$M_{PL}\ [kg]$	182.0	182.0	182.0	182.0	182.0
$E_{bat}\ [MJ]$	96.43	96.13	96.09	96.58	97.79
$E_{TO}\ [MJ]$	2.51	2.50	2.50	2.51	2.54
$E_{cl}\ [MJ]$	13.06	13.03	13.07	13.22	13.49
$E_{cr}\ [MJ]$	61.57	61.37	61.30	61.54	62.20
$E_{de}\ [MJ]$	-1.55	-1.69	-1.74	-1.77	-1.84
$E_{L}\ [MJ]$	1.54	1.54	1.54	1.55	1.56
$E_{res}\ [MJ]$	19.29	19.38	19.42	19.55	19.83

Mission Parameters

Table B.14: Aircraft mission parameters of the propeller analysis for the steep descent and variable pitch propeller.

	100%	**75%**	**50%**	**25%**	**0%**
t_{cl} $[s]$	359.7	359.7	359.7	359.7	359.7
t_{cr} $[s]$	3353.0	3353.0	3353.0	3353.0	3353.0
t_{de} $[s]$	167.4	167.4	167.4	167.4	167.4
v_{cl} $[m/s]$	25.2	25.2	25.2	25.2	25.2
v_{cr} $[m/s]$	37.1	37.1	37.1	37.1	37.1
v_{de} $[m/s]$	32.7	32.7	32.7	32.7	32.7
c_{cl} $[ft/min]$	433.0	433.0	433.0	433.0	433.0
c_{de} $[ft/min]$	-920	-920	-920	-920	-920
Θ_{cl} $[degree]$	5.0	5.0	5.0	5.0	5.0
Θ_{de} $[degree]$	-8.2	-8.2	-8.2	-8.2	-8.2
R_{cl} $[km]$	9.0	9.0	9.0	9.0	9.0
R_{cr} $[km]$	124.4	124.4	124.4	124.4	124.4
R_{de} $[km]$	5.4	5.4	5.4	5.4	5.4

Performance Parameters

Table B.15: Aircraft performance parameters of the propeller analysis for the steep descent and variable pitch propeller.

	100%	**75%**	**50%**	**25%**	**0%**
CL_{cl} $[-]$	1.504	1.504	1.504	1.504	1.504
CL_{cr} $[-]$	0.725	0.725	0.725	0.725	0.725
CL_{de} $[-]$	0.897	0.897	0.897	0.897	0.897
CD_{cl} $[-]$	0.116	0.116	0.116	0.116	0.116
CD_{cr} $[-]$	0.049	0.049	0.049	0.049	0.049
CD_{de} $[-]$	0.060	0.060	0.060	0.060	0.060

Propeller Parameters

Table B.16: Propeller performance parameters of the propeller analysis for the steep descent and variable pitch propeller.

	100%	**75%**	**50%**	**25%**	**0%**
T_{cl} $[N]$	1000.2	999.1	998.9	1001.2	1006.6
T_{cr} $[N]$	412.6	412.2	412.1	413.0	415.3
T_{de} $[N]$	-469.7	-469.2	-469.2	-470.2	-472.8
$P_{shaft_{cl}}$ $[kW]$	34.47	34.41	34.51	34.89	35.61
$P_{shaft_{cr}}$ $[kW]$	17.45	17.39	17.37	17.44	17.62
$P_{shaft_{de}}$ $[kW]$	-10.17	-11.10	-11.43	-11.64	-12.07
J_{cl} $[-]$	0.471	0.450	0.413	0.386	0.376
J_{cr} $[-]$	1.008	0.976	0.886	0.853	0.834
J_{de} $[-]$	0.614	0.601	0.544	0.532	0.573
$Pitch_{cl}$ $[degree]$	22.2	22.0	22.0	20.0	19.0
$Pitch_{cr}$ $[degree]$	32.0	32.0	31.0	30.0	29.0
$Pitch_{de}$ $[degree]$	5.0	5.0	5.0	5.0	6.0
η_{cl} $[-]$	73.20	73.24	73.01	72.39	71.32
η_{cr} $[-]$	87.78	87.98	88.07	87.92	87.45
η_{de} $[-]$	18.72	20.42	21.03	21.42	22.21

C

Appendix C: Detailed Mission Analysis Results

Below are all the results presented for the performed simulations within the flight mission profile analysis, as presented in section 8.2.

C.1. Final Traffic Pattern Descent

Sizing Parameters

Table C.1: Aircraft sizing parameters of the final traffic pattern analysis with a variable pitch propeller.

	RoD 230	**RoD 345**	**RoD 460**	**RoD 575**	**RoD 690**	**RoD 920**
$W/S\ [N/m^2]$	568.9	568.9	568.9	568.9	568.9	568.9
$W/P_{EM}\ [N/W]$	0.0836	0.0842	0.0846	0.0847	0.0848	0.0847
$MTOM\ [kg]$	665.2	628.6	612.8	605.0	600.2	596.6
$M_{bat}\ [kg]$	160.9	138.8	129.2	124.4	121.6	119.3
$M_{EM}\ [kg]$	26.0	24.4	23.7	23.4	23.1	23.0
$M_{OEM}\ [kg]$	296.5	283.4	277.8	275.0	273.3	272.1
$M_{PL}\ [kg]$	182.0	182.0	182.0	182.0	182.0	182.0
$E_{bat}\ [MJ]$	115.83	99.93	93.02	89.59	87.52	85.89
$E_{TO}\ [MJ]$	3.01	2.60	2.42	2.33	2.28	2.23
$E_{cl}\ [MJ]$	14.20	13.32	12.90	12.70	12.56	12.46
$E_{cr}\ [MJ]$	68.67	61.15	57.84	56.08	54.96	54.02
$E_{de}\ [MJ]$	4.93	1.28	-0.24	-0.87	-1.18	-1.49
$E_{L}\ [MJ]$	1.85	1.60	1.49	1.43	1.40	1.37
$E_{res}\ [MJ]$	23.17	19.99	18.60	17.92	17.50	17.30

Mission Parameters

Table C.2: Aircraft mission parameters of the final traffic pattern analysis with a variable pitch propeller.

	RoD 230	**RoD 345**	**RoD 460**	**RoD 575**	**RoD 690**	**RoD 920**
t_{cl} $[s]$	359.7	359.7	359.7	359.7	359.7	359.7
t_{cr} $[s]$	3493.9	3305.4	3211.0	3154.4	3116.5	3069.1
t_{de} $[s]$	648.7	434.7	327.8	263.6	220.8	167.4
v_{cl} $[m/s]$	25.2	25.2	25.2	25.2	25.2	25.2
v_{cr} $[m/s]$	37.1	37.1	37.1	37.1	37.1	37.1
v_{de} $[m/s]$	32.7	32.7	32.7	32.7	32.7	32.7
c_{cl} $[ft/min]$	433.0	433.0	433.0	433.0	433.0	433.0
c_{de} $[ft/min]$	-230.0	-345.0	-460.0	-575.0	-690.0	-920.0
Θ_{cl} $[degree]$	5.0	5.0	5.0	5.0	5.0	5.0
Θ_{de} $[degree]$	-2.0	-3.1	-4.1	-5.1	-6.2	-8.2
R_{cl} $[km]$	9.0	9.0	9.0	9.0	9.0	9.0
R_{cr} $[km]$	129.7	122.7	119.2	117.1	115.7	113.9
R_{de} $[km]$	21.2	14.2	10.7	8.6	7.2	5.4

Performance Parameters

Table C.3: Aircraft performance parameters of the final traffic pattern analysis with a variable pitch propeller.

	RoD 230	**RoD 345**	**RoD 460**	**RoD 575**	**RoD 690**	**RoD 920**
CL_{cl} $[-]$	1.504	1.504	1.504	1.504	1.504	1.504
CL_{cr} $[-]$	0.725	0.725	0.725	0.725	0.725	0.725
CL_{de} $[-]$	0.903	0.903	0.904	0.904	0.901	0.897
CD_{cl} $[-]$	0.116	0.116	0.116	0.116	0.116	0.116
CD_{cr} $[-]$	0.049	0.049	0.049	0.049	0.049	0.049
CD_{de} $[-]$	0.060	0.060	0.060	0.060	0.060	0.060

Propeller Parameters

Table C.4: Propeller performance parameters of the final traffic pattern analysis with a variable pitch propeller.

	RoD 230	**RoD 345**	**RoD 460**	**RoD 575**	**RoD 690**	**RoD 920**
T_{cl} $[N]$	1071.8	1012.8	987.3	974.8	967.1	961.2
T_{cr} $[N]$	442.2	417.8	407.3	402.1	399.0	396.5
T_{de} $[N]$	201.2	79.5	-30.5	-136.8	-241.8	-451.4
$P_{shaft_{cl}}$ $[kW]$	37.49	35.16	34.06	33.53	33.16	32.89
$P_{shaft_{cr}}$ $[kW]$	18.67	17.57	17.11	16.89	16.75	16.72
$P_{shaft_{de}}$ $[kW]$	7.30	2.84	-0.78	-3.58	-5.83	-9.81
J_{cl} $[-]$	0.376	0.374	0.378	0.406	0.409	0.469
J_{cr} $[-]$	0.837	0.818	0.840	0.897	0.900	1.007
J_{de} $[-]$	1.058	1.353	1.411	0.939	0.722	0.612
$Pitch_{cl}$ $[degree]$	19.0	19.0	19.0	20.0	20.0	22.1
$Pitch_{cr}$ $[degree]$	29.0	28.0	29.0	30.0	30.0	32.0
$Pitch_{de}$ $[degree]$	33.0	35.0	27.0	14.0	8.0	5.0
η_{cl} $[-]$	72.12	72.66	73.12	73.34	73.57	73.71
η_{cr} $[-]$	87.89	88.24	88.34	88.37	88.38	88.03
η_{de} $[-]$	90.04	91.43	1.43	6.59	10.73	18.06

C.2. Regen on vs. off

Sizing Parameters

Table C.5: Aircraft sizing parameters of the air-brake analysis with a variable pitch propeller.

	Regenerative	**Air-brake**
$W/S\ [N/m^2]$	568.9	568.9
$W/P_{EM}\ [N/W]$	0.0842	0.0843
$MTOM\ [kg]$	620.8	626.9
$M_{bat}\ [kg]$	133.9	137.8
$M_{EM}\ [kg]$	24.1	24.3
$M_{OEM}\ [kg]$	280.7	282.8
$M_{PL}\ [kg]$	182.0	182.0
$E_{bat}\ [MJ]$	96.43	99.19
$E_{TO}\ [MJ]$	2.51	2.58
$E_{cl}\ [MJ]$	13.06	13.24
$E_{cr}\ [MJ]$	61.57	61.90
$E_{de}\ [MJ]$	-1.55	0.05
$E_{L}\ [MJ]$	1.54	1.59
$E_{res}\ [MJ]$	19.29	19.84

Mission Parameters

Table C.6: Aircraft mission parameters of the air-brake analysis with a variable pitch propeller.

	Regen	**Air-brake**
t_{cl} $[s]$	359.7	359.7
t_{cr} $[s]$	3353.0	3353.0
t_{de} $[s]$	167.4	167.4
v_{cl} $[m/s]$	25.2	25.2
v_{cr} $[m/s]$	37.1	37.1
v_{de} $[m/s]$	32.7	32.7
c_{cl} $[ft/min]$	433	433
c_{de} $[ft/min]$	-920	-920
Θ_{cl} $[degree]$	5.0	5.0
Θ_{de} $[degree]$	-8.2	-8.2
R_{cl} $[km]$	9.0	9.0
R_{cr} $[km]$	124.4	124.4
R_{de} $[km]$	5.4	5.4

Performance Parameters

Table C.7: Aircraft performance parameters of the air-brake analysis with a variable pitch propeller.

	Regen	**Air-brake**
CL_{cl} $[-]$	1.504	1.504
CL_{cr} $[-]$	0.725	0.725
CL_{de} $[-]$	0.897	0.897
CD_{cl} $[-]$	0.116	0.116
CD_{cr} $[-]$	0.049	0.049
CD_{de} $[-]$	0.060	0.060

Propeller Parameters

Table C.8: Propeller performance parameters of the air-brake analysis with a variable pitch propeller.

	Regen	**Air-brake**
T_{cl} $[N]$	1000.2	1010.1
T_{cr} $[N]$	412.6	416.7
T_{de} $[N]$	-469.7	-
$P_{shaft_{cl}}$ $[kW]$	34.47	34.95
$P_{shaft_{cr}}$ $[kW]$	17.45	17.54
$P_{shaft_{de}}$ $[kW]$	-10.17	-
J_{cl} $[-]$	0.471	0.403
J_{cr} $[-]$	1.008	0.892
J_{de} $[-]$	0.614	-
$Pitch_{cl}$ $[degree]$	22.2	20.0
$Pitch_{cr}$ $[degree]$	32.0	30.0
$Pitch_{de}$ $[degree]$	5.0	-
η_{cl} $[-]$	73.20	72.91
η_{cr} $[-]$	87.78	88.18
η_{de} $[-]$	18.72	-

C.3. Long vs. Short Mission

Sizing Parameters

Table C.9: Aircraft sizing parameters of the aircraft mission type analysis with a variable pitch propeller.

	Long Shallow	**Long Steep**	**Short shallow**	**Short Steep**
$W/S\ [N/m^2]$	568.9	568.9	568.9	568.9
$W/P_{EM}\ [N/W]$	0.0846	0.0842	0.0852	0.0836
$MTOM\ [kg]$	612.8	620.8	584.7	616.1
$M_{bat}\ [kg]$	129.2	133.9	112.2	130.7
$M_{EM}\ [kg]$	23.7	24.1	22.4	24.1
$M_{OEM}\ [kg]$	277.8	280.7	267.9	279.1
$M_{PL}\ [kg]$	182.0	182.0	182.0	182.0
$E_{bat}\ [MJ]$	93.02	96.43	80.82	94.11
$E_{TO}\ [MJ]$	2.42	2.51	2.10	2.45
$E_{cl}\ [MJ]$	12.90	13.06	12.17	13.01
$E_{cr}\ [MJ]$	57.84	61.57	0.13	2.75
$E_{de}\ [MJ]$	-0.24	-1.55	-0.22	-1.66
$E_{L}\ [MJ]$	1.49	1.54	1.29	1.51
$E_{res}\ [MJ]$	18.60	19.29	65.35	76.05

Mission Parameters

Table C.10: Aircraft mission parameters of the aircraft mission type analysis with a variable pitch propeller.

	Long Shallow	**Long Steep**	**Short shallow**	**Short Steep**
t_{cl} $[s]$	359.7	359.7	359.7	359.7
t_{cr} $[s]$	3211.0	3353.0	7.4	149.3
t_{de} $[s]$	327.8	167.4	327.8	167.4
v_{cl} $[m/s]$	25.2	25.2	25.2	25.2
v_{cr} $[m/s]$	37.1	37.1	37.1	37.1
v_{de} $[m/s]$	32.7	32.7	32.7	32.7
c_{cl} $[ft/min]$	433	433	433	433
c_{de} $[ft/min]$	-460	-920	-460	-920
Θ_{cl} $[degree]$	5.0	5.0	5.0	5.0
Θ_{de} $[degree]$	-4.1	-8.2	-4.1	-8.2
R_{cl} $[km]$	9.0	9.0	9.0	9.0
R_{cr} $[km]$	119.2	124.4	0.3	5.5
R_{de} $[km]$	10.7	5.4	10.7	5.4

Performance Parameters

Table C.11: Aircraft performance parameters of the aircraft mission type analysis with a variable pitch propeller.

	Long Shallow	**Long Steep**	**Short shallow**	**Short Steep**
CL_{cl} $[-]$	1.504	1.504	1.504	1.504
CL_{cr} $[-]$	0.725	0.725	0.725	0.725
CL_{de} $[-]$	0.904	0.897	0.904	0.897
CD_{cl} $[-]$	0.116	0.116	0.116	0.116
CD_{cr} $[-]$	0.049	0.049	0.049	0.049
CD_{de} $[-]$	0.060	0.060	0.060	0.060

Propeller Parameters

Table C.12: Propeller performance parameters of the aircraft mission type analysis with a variable pitch propeller.

	Long Shallow	**Long Steep**	**Short shallow**	**Short Steep**
T_{cl} $[N]$	987.3	1000.2	942.1	992.6
T_{cr} $[N]$	407.3	412.6	388.7	409.5
T_{de} $[N]$	-30.5	-469.7	-29.1	-466.2
$P_{shaft_{cl}}$ $[kW]$	34.06	34.47	32.12	34.34
$P_{shaft_{cr}}$ $[kW]$	17.11	17.45	16.31	17.52
$P_{shaft_{de}}$ $[kW]$	-0.78	-10.17	-0.72	-10.94
J_{cl} $[-]$	0.378	0.471	0.409	0.519
J_{cr} $[-]$	0.840	1.008	0.875	1.146
J_{de} $[-]$	1.411	0.614	1.439	0.768
$Pitch_{cl}$ $[degree]$	19.0	22.2	20.0	22.5
$Pitch_{cr}$ $[degree]$	27.0	5.0	28.0	9.0 0
$Pitch_{de}$ $[degree]$	24.8	25.6	25.0	25.4
η_{cl} $[-]$	73.12	73.20	74.00	72.92
η_{cr} $[-]$	88.34	87.78	88.46	86.73
η_{de} $[-]$	1.43	18.72	1.32	20.14

D

Appendix D: Simulation Results Using the New Optimisation Function

Below are the simulations results presented for the performed simulations with the new defined optimisation objective function, as presented in section 6.3.3.

D.1. Baseline Mission

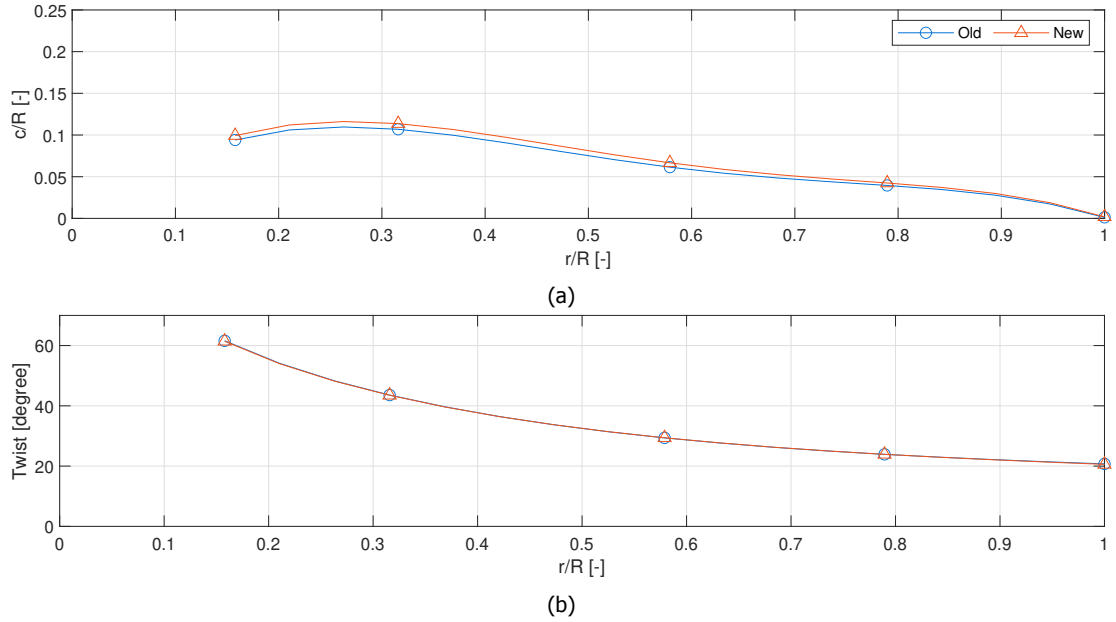

Figure D.1: Propeller blade chord (a) and twist distribution (b) of the new and old optimisation objective function for the baseline mission with a fixed pitch propeller.

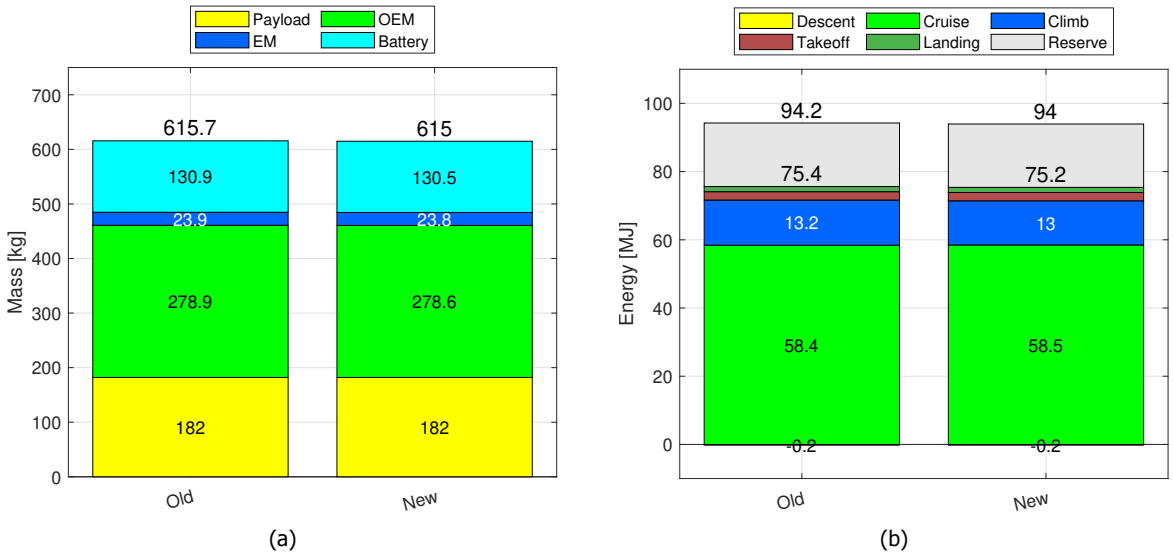

Figure D.2: Mass (a) and energy (b) per fight phase breakdown of the new and old optimisation objective function for the baseline mission with a fixed pitch propeller.

D.2. Steep Descent Mission

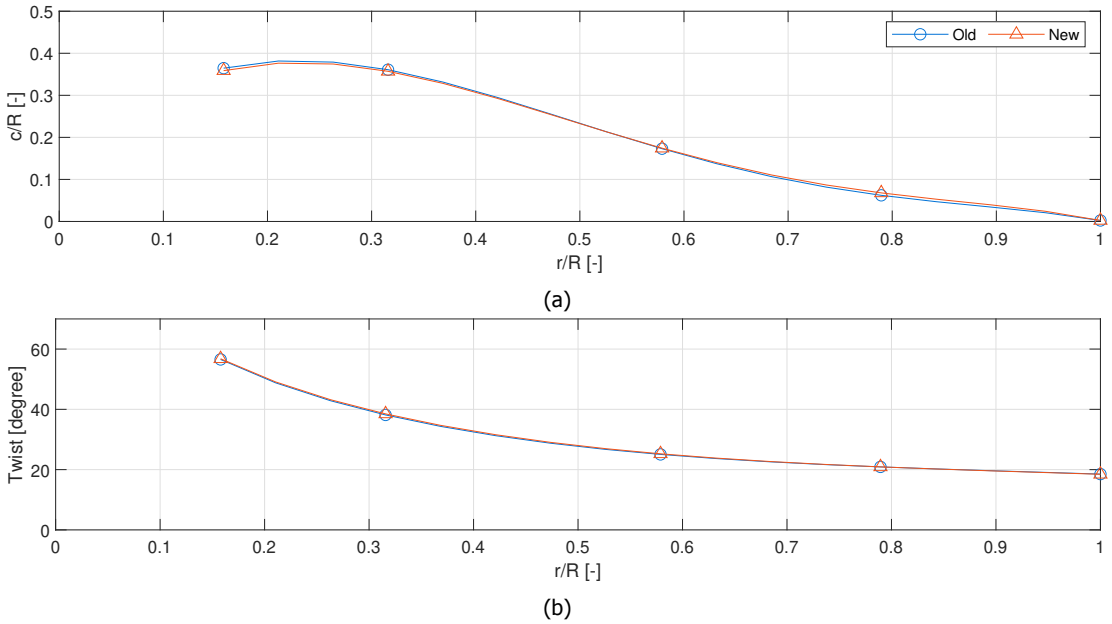

Figure D.3: Propeller blade chord (a) and twist (b) distribution of the new and old optimisation objective function for the steep descent strategy ($690 ft/min$) mission with a fixed pitch propeller.

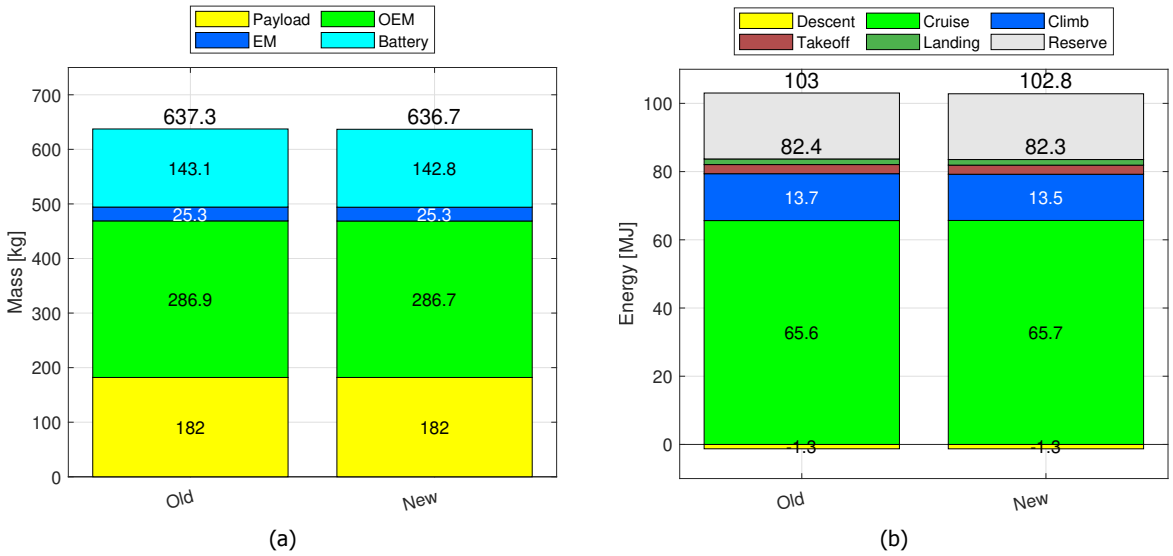

Figure D.4: Mass (a) and energy (b) per fight phase breakdown of the new and old optimisation objective function for the steep descent strategy ($690 ft/min$) mission with a fixed pitch propeller.

D.3. Fixed Descent Angle, Reduced Flight Speed Descent

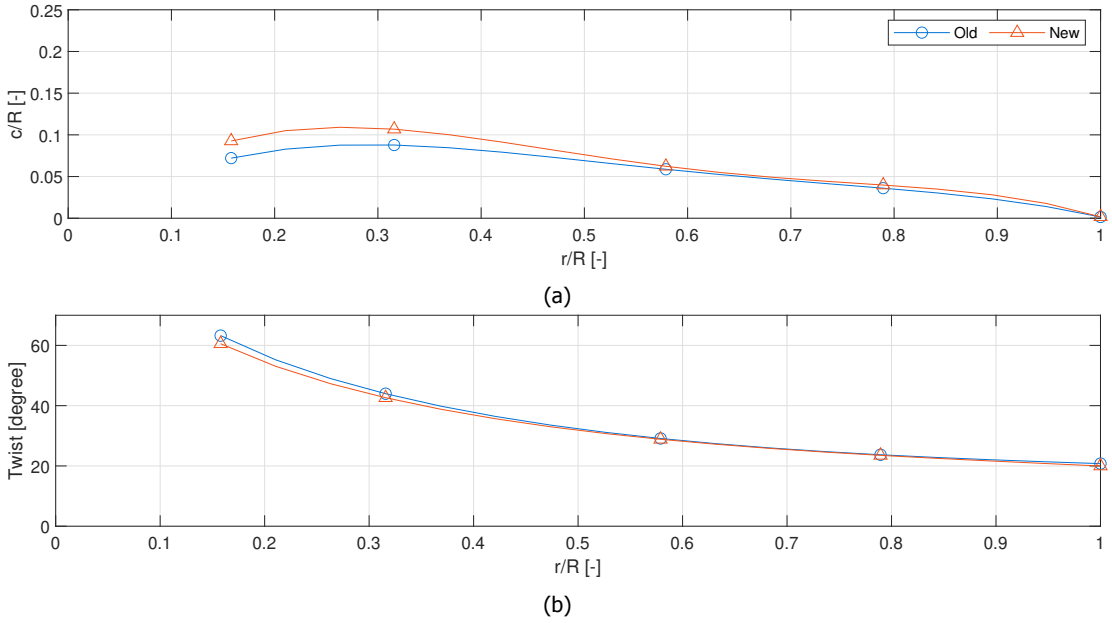

Figure D.5: Propeller blade chord (a) and twist (b) distribution of the new and old optimisation objective function for the same descent angle as the baseline mission, but with a reduced flight speed ($0.8v_{minD}$) mission with a fixed pitch propeller.

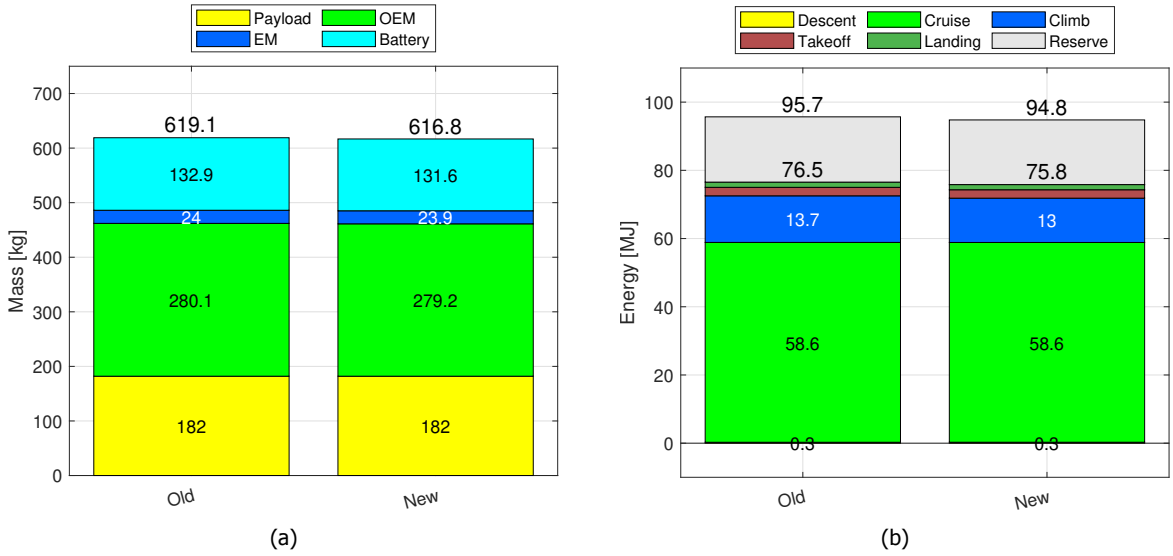

Figure D.6: Mass (a) and energy (b) per fight phase breakdown of the new and old optimisation objective function for the same descent angle as the baseline mission, but with a reduced flight speed ($0.8v_{minD}$) mission with a fixed pitch propeller.